

Alma Mater Studiorum – Università di Bologna

DOTTORATO DI RICERCA IN
INGEGNERIA CHIMICA, DELL'AMBIENTE E DELLA
SICUREZZA
Ciclo XXVII

Settore Concorsuale di afferenza: 09/D3

Settore Scientifico disciplinare: ING-IND/25

AEROBIC BIODEGRADATION OF CHLORINATED
SOLVENTS AND PLASTICS IN BATCH AND
CONTINUOUS-FLOW BIOREACTORS: PROCESS
DEVELOPMENT AND IDENTIFICATION OF
SUITABLE CHEMICAL PRE-TREATMENTS

Presentata da: Nasrin Tavanaie

Coordinatore del Dottorato di Ricerca

Prof. Serena Bandini

Relatore

Dr. Dario Frascari

Dario Frascari

Correlatore

Prof. Davide Pinelli

Esame finale anno 2015

Dedication

This document is dedicated to my parents for the bestowal of a beautiful life to me.

Acknowledgments

I would like to take this opportunity to thank the variety of people who have contributed significantly to the thesis and made it a success. First of all, I would like to thank my advisor, Dr. Dario Frascari whose expert guidance has led to the realization of this thesis. I would like to acknowledge the constant motivation and encouragement of Professor Davide Pinelli who was my co-advisor in this project. Next, I would like to acknowledge Professor Philippe Corvini (University of Applied Sciences and Arts Northwestern Switzerland) who gave me the opportunity to do part of my research in his group and his periodic comments have immensely helped me improve on the thesis.

I would then like to extend my heartfelt gratitude to Dr. Roberta Ciavy, Dr. Giacomo Bucchi, Miss Antonella Rosato (University of Bologna), Dr. Nora Corvini, Dr. Boris Kolvenbach and Dr. Jan Svojitka (University of Applied Sciences and Arts Northwestern Switzerland) for their support in numerous important aspects related to the project and the thesis. They were always available to help me whenever there were impediments in the way. Thanks to my parents for always being my source of inspiration.

Table of Contents

1	Aim of this study	1
2	Biodegradation of chlorinated solvents.....	6
2.1	Chlorinated solvents	6
2.1.1	Structure and chemical properties	6
2.1.2	Applications	11
2.1.3	Dispersion of chlorinated solvents in the environment.....	12
2.1.4	Effect of chlorinated solvents on human beings	14
2.2	Groundwater contamination.....	16
2.2.1	Factors determining the pollution of aquifers	16
2.2.2	Treatment of contaminated aquifers.....	19
2.2.3	Biodegradation	20
2.2.4	Degradation of chlorinated solvents.....	22
2.2.5	Suitable Reactor for aerobic co-metabolic biodegradation	27
3	Biofilm reactors	30
3.1	Factors affecting the production of biofilms	30
3.2	Structure of the biofilm	31
3.2.1	Exocellular polymeric substances (EPS).....	31
3.2.2	Architecture of the biofilm	32
3.3	Biofilm formation.....	33
3.4	Detachment of biofilm	35

3.5	Biofilm reactors.....	35
4	Materials and Methods.....	38
4.1	Analytical methods.....	38
4.1.1	Gas-chromatographic analysis	38
4.1.2	Biomass analysis	45
5	Growth substrate and carrier selection for aerobic co- metabolic biodegradation of CAH	47
5.1	Selection of the best performing growth substrate.....	47
5.2	Evaluation of the abiotic pre-treatment step to convert TCE to TeCA... 54	54
5.3	Selection of the best biofilm carrier	55
5.3.1	Performance of biofilm carriers in batch test at 30 °C.....	57
5.3.2	Performance of biofilm carriers in batch test at 15°C.....	60
5.3.3	Performance of biofilm carriers in continuous flow test at 30°C....	62
6	Kinetic study of TCE and butane biodegradation by the selected consortium.....	66
6.1	Kinetic study of substrate uptake in suspended cell batch tests at 30°C. 69	69
6.1.1	Kinetic study of butane uptake in the suspended cell batch test	69
6.1.2	Kinetic study of TCE uptake in the suspended cell batch test	72
6.1.3	Kinetic study of butane uptake in the presence of TCE in the suspended cell batch test	74

6.1.4	Kinetic study of TCE biodegradation in the presence of butane in the suspended cell batch test	75
6.2	Kinetic study of substrates uptake in the attached cell batch tests at 30°C.	77
6.2.1	Kinetic study of butane uptake in the attached cell batch test	77
6.2.2	Kinetic study of TCE biodegradation in the attached cell batch test ..	80
6.2.3	Kinetic study of butane degradation in the presence of TCE in the attached cell batch test.....	82
6.2.4	Kinetic study of TCE biodegradation in the presence of butane in the attached cell batch test.....	84
7	Design procedure for biofilm reactor scale-up.....	87
7.1	Pulsed feed of oxygen and growth substrate	87
7.2	Fluid-dynamic characterization of a packing of the selected biofilm carrier	90
7.3	Sizing of the PBR and preliminary design of the schedule of pulsed oxygen/substrate supply.....	91
8	Conclusions, part 1.....	97
	The conclusions from the first part of this work can be summarized as follows:	97
9	Polymer biodegradation	100

9.1 The diffusion of plastics and the possible chemical/biodegradation treatment approaches	100
---	-----

10 Materials and methods for the evaluation of plastic (bio)degradation..... 104

10.1 Experimental setup for chemical treatment of plastics	104
10.1.1 Materials.....	105
10.1.2 Ozonation procedure	107
10.1.3 UV/ozonation procedure	108
10.2 Experimental setup for biological treatment test of plastics	110
10.2.1 Experimental setup of biodegradation test of plastics by bacterial cultures	110
10.2.2 Experimental setup for co-metabolic biodegradation test of PS by fungal culture.....	111
10.2.3 Disinfection procedure	112
10.2.4 Mineral salt medium.....	112
10.2.5 Removing the biofilm from taken plastic samples for analysis	114
10.3 Analytical methods for the evaluation of plastic (bio)degradation	114
10.3.1 Melt rheology analysis	115
10.3.2 Fourier transform infrared analysis (FTIR).....	116
10.3.3 Differential scanning calorimetry (DSC)	118
10.3.4 Thermogravimetric Analysis (TGA).....	120

10.3.5	Microscopic pictures of polymer's surfaces	121
10.3.6	Colony forming unit (CFU) of bacterial growth	122
10.4	Advantages/disadvantages of analytical methods	122
11	Chemical treatment of polymers	124
11.1	Results of analytical methods.....	124
11.1.1	FTIR analysis of LLDPE film and powder in gaseous phase ozonation	124
11.1.2	Carbonyl index of gaseous phase ozonated LLDPE	125
11.1.3	FTIR analysis of PP film and powder in gaseous phase ozonation	126
11.1.4	Carbonyl index of gaseous phase ozonated PP	128
11.1.5	FTIR analysis of PS film and powder in gaseous phase ozonation	129
11.1.6	Carbonyl index of gaseous phase ozonated PS	131
11.1.7	FTIR analysis of PVC film and powder in gaseous phase ozonation	131
11.1.8	Carbonyl index of gaseous phase ozonated PVC	133
11.1.9	Effect of different treatment on carbonyl groups generation	134
11.1.10	Ozone and UV/ozone treatment of LLDPE in gaseous and aqueous phases	134
11.1.11	Ozone and UV/ozone treatment of PP in gaseous and aqueous phases	135
11.1.12	Ozone and UV/ozone treatment of PS in gaseous and aqueous phases	136

11.1.13	Effect of longer exposure time to UV/ozone	137
11.2	Aging test on the treated polymer films	139
11.2.1	Carbonyl groups stability of UV/ozonated LLDPE films.....	140
11.2.2	Carbonyl groups stability of UV/ozonated PP films.....	141
11.2.3	Carbonyl groups stability of UV/ozonated PS films.....	143
12	Plastic biodegradation with pure or mixed bacterial cultures	145
12.1	Results of biological treatment of PS films with <i>Rhodococcus ruber</i> ..	145
12.1.1	FTIR analysis of incubated PS with <i>Rhodococcus ruber</i>	145
12.1.2	Bacterial growth of <i>Rhodococcus ruber</i> on ozonated and non-ozonated PS	146
12.1.3	Effect of chemical and biotic treatment on melt rheology analysis of PS	147
12.2	Biological treatment of PVC powder with <i>Rhodococcus ruber</i>	149
12.2.1	FTIR analysis of incubated PVC with <i>Rhodococcus ruber</i>	149
12.2.2	Bacterial growth of <i>Rhodococcus ruber</i> on ozonated and non-ozonated PVC.....	150
12.3	Biological treatment of LLDPE films with <i>Rhodococcus ruber</i>	151
12.3.1	FTIR analysis of incubated LLDPE with <i>Rhodococcus ruber</i>	152
12.3.2	Bacterial growth of <i>Rhodococcus ruber</i> on ozonated and non-ozonated LLDPE	152

12.3.3	Effect of chemical and biotic treatment on melt rheology analysis of LLDPE	153
12.3.4	Microscopic analysis of chemically and biologically treated LLDPE	155
12.4	Biological treatment of PP films with <i>Rhodococcus ruber</i>	157
12.4.1	FTIR analysis of incubated PP with <i>Rhodococcus ruber</i>	157
12.4.2	Bacterial growth of <i>Rhodococcus ruber</i> on ozonated and non-ozonated PP	158
12.4.3	Microscopic analysis of chemically and biologically treated PP ..	159
12.4.4	Biofilm formation on PP films incubated with <i>Rhodococcus ruber</i>	161
12.4.5	TGA analysis of incubated PP with <i>Rhodococcus ruber</i>	162
12.5	Biological treatment of PP films with mixed bacterial culture	163
12.5.1	FTIR analysis of incubated PP with the mixed bacterial culture ..	163
12.5.2	Bacterial growth of mixed culture on ozonated and non-ozonated PP	164
12.5.3	DSC analysis of incubated PP with mixed bacterial culture	165
12.5.4	Weight loss measurement of PP film incubate with mixed bacterial culture	166
12.5.5	TGA analysis of incubated PP with mixed bacterial culture	167
13	Plastic biodegradation with a pure fungal culture	169

13.1 Evaluation of the biodegradation of PS incubated with pure fungal culture	169
13.1.1 FTIR analysis of incubated PS with <i>Penicillium variable</i>	169
13.1.2 Weight loss measurement of PS film incubate with <i>Penicillium variable</i>	170
13.1.3 Evaluation of <i>Penicillium variable</i> growth on PS films	171
14 Conclusions, part 2.....	173
Appendix I.....	175
References.....	179

List of tables

Table 2.1 Classifications and formulae of the major chlorinated solvents	9
Table 2.2 Physico-chemical properties of some chlorinated solvents at 25°C	10
Table 2.3 Environmental threshold limits value TLV-TWA of chlorinated solvents	15
Table 2.4 Degradation reactions of chlorinated compounds	24
Table 4.1 Standard butane samples for calibration	41
Table 4.2 TCE and TeCA standard solutions for calibration.....	43
Table 4.3 Calibration coefficients of butane and chlorinated solvents	44
Table 5.1 Chemical characterization of studied groundwater	48
Table 5.2 Selected biofilm carrier for the test.....	56
Table 5.3 Degradation rates of TCE at 30 °C in the biofim batch test	59
Table 5.4 Degradation rate of TCE at 15 °C in the biofim batch test.....	62
Table 6.1 Best estimate kinetic parameters relative to butane uptake and TCE biodegradation in suspended or attached cell tests with 95% confidence intervals	86
Table 9.1 Global market share of plastics by volume produced [51].	100
Table 10.1 Characterization of studied polymers	106
Table 10.2 Ozone and oxygen properties	106
Table 10.3 Description of the treatment conditions relative to ozonation and UV/ozonation of plastics in gaseous and aqueous phases.	109
Table 10.4 4 Mineral salt medium composition	113
Table 10.5 Composition of sugar free Czapek Dox medium.....	114

List of figures:

Figure 2.1 Structural formulae of the main chlorinated solvents.....	7
Figure 2.2 NAPL balance in four phases	13
Figure 2.3 Example of transport of chlorinated solvents in the subsoil.....	14
Figure 2.4 Schematic representation of the microbial oxidation of a primary substrate (left) and of a non-growth substrate such as a CAH (right).....	26
Figure 3.1 Biofilms grown on stainless steel	32
Figure 3.2 Different stages in formation of biofilm.....	34
Figure 4.1 Calibration line of butane: chromatographic area vs. concentration of standard	42
Figure 4.2 Calibration line of TEC	44
Figure 4.3 Calibration line of TeCA.....	45
Figure 5.1 Batch test for growth substrate selection: concentrations in the aqueous phase versus time for substrate (butane), TCE and TeCA, for a representative case	51
Figure 5.2 First-order kinetic constant of substrates, TCE and TeCA at 30°C	52
Figure 5.3 First-order kinetic constants of butane and TCE at 15°C.....	54
Figure 5.4 depletion rate of TeCA to TCE in an abiotic reaction.....	55
Figure 5.5 performance of biofilm carrier Biomax in a batch test at 30°C	57
Figure 5.6 performance of biofilm carrier Biomech in a batch test at 30°C.....	58
Figure 5.7 performance of biofilm carrier Biopearl in a batch test at 30°C	58
Figure 5.8 Performance of biofilm carrier Cerambios in a batch test at 30°C.....	59
Figure 5.9 Performance of biofilm carrier Biomax in a batch test at 15°C	60
Figure 5.10 Performance of biofilm carrier Biomech in a batch test at 15°C	61

Figure 5.11 Performance of biofilm carrier Biopearl in a batch test at 15°C	61
Figure 5.12 Performance of biofilm carrier Cerambios in a batch test at 15°C.....	62
Figure 5.13 diagram of columns in a continuous flow test for carrier selection	63
Figure 5.14 Performance of four different carriers in terms of normalized TCE degradation rate.....	64
Figure 5.15 Concentration of attached cells formed on four different carriers	65
Figure 6.1 Initial specific depletion rate of butane versus initial concentration of butane in a suspended cell batch reactor at 30°C	71
Figure 6.2 Initial specific depletion rate of TCE versus initial concentration of butane in the suspended cell batch reactor at 30 °C	73
Figure 6.3 Effect of TCE inhibition on butane uptake.....	75
Figure 6.4 Effect of butane inhibition on TCE uptake in suspended cell batch test.....	76
Figure 6.5 Initial specific depletion of butane ($\text{mg}_{\text{butane}}\text{mg}_{\text{prot}}^{-1}\text{d}^{-1}$) vs. initial concentration of butane present in the liquid phase (mg/L) in the attached cell batch test.....	79
Figure 6.6 Initial specific degradation rate vs. the initial concentration of TCE in attached cell test	82
Figure 6.7 Effect of TCE inhibition on butane uptake in attached cell test.....	84
Figure 6.8 Effect of butane inhibition on TCE biodegradation in attached cell test.	85
Figure 7.1 Flow-sheet of an on-site PBR process for the aerobic co-metabolic treatment of CAHs with pulsed supply of oxygen and growth substrate.....	89
Figure 7.2 Schematic picture of designed up-scaled packed bed bioreactor for aerobic co-metabolism biodegradation of chlorinated solvents	96
Figure 7.3 View of the 31-L lab-scale PBR.....	96
Figure 10.1 Typical DSC curve	120
Figure 10.2 Typical thermogram curve	120

Figure 11.1 FTIR spectra of LLDPE film.....	124
Figure 11.2 FTIR spectra of LLDPE powder	125
Figure 11.3 carbonyl index versus different ozonation time	126
Figure 11.4 FTIR spectra of PP film.....	127
Figure 11.5 FTIR spectra of PP powder	128
Figure 11.6 carbonyl index versus different ozonation time	129
Figure 11.7 FTIR spectra of PS film.....	130
Figure 11.8 FTIR spectra of PS powder	130
Figure 11.9 carbonyl index of PS versus different ozonation time.....	131
Figure 11.10 FTIR spectra of PVC film	132
Figure 11.11 FTIR spectra of PVC powder	133
Figure 11.12 Carbonyl index versus different ozonation time of PVC film.....	134
Figure 11.13 Carbonyl index versus treatment time of LLDPE film	135
Figure 11.14 Carbonyl index versus treatment time of PP film	136
Figure 11.15 Carbonyl index versus treatment time of PS film	137
Figure 11.16 Carbonyl index versus gaseous UV/ozonation time of LLDPE film	138
Figure 11.17 Carbonyl index versus gaseous UV/ozonation time of PP film	139
Figure 11.18 carbonyl index versus aging time of gaseous phase UV/O ₃ LLDPE.....	140
Figure 11.19 carbonyl index versus aging time of aqueous phase UV/O ₃ LLDPE.....	141
Figure 11.20 carbonyl index versus aging time of gaseous phase UV/O ₃ PP	142
Figure 11.21 carbonyl index versus aging time of aqueous phase UV/ozonated PP.....	142
Figure 11.22 carbonyl index versus aging time of gaseous phase UV/ozonated PS	143
Figure 11.23 Carbonyl index versus aging time of aqueous phase UV/O ₃ PS.....	144
Figure 12.1 Carbonyl index versus incubation time of PS with R.ruber	146
Figure 12.2 growth of pure bacterial culture versus incubation time with PS.....	147

Figure 12.3 Tangent of the loss angle of PS versus oscillatory frequency	148
Figure 12.4 Complex viscosity of PS versus oscillatory frequency	149
Figure 12.5 FTIR spectra of ozonated PVC powder after incubation	150
Figure 12.6 growth of pure bacterial culture versus incubation time with PVC	151
Figure 12.7 Carbonyl index versus incubation time of LLDPE with <i>R.ruber</i>	152
Figure 12.8 Growth of pure bacterial culture versus incubation time with LLDPE.....	153
Figure 12.9 Tangent of the loss angle of LLDPE versus oscillatory frequency	154
Figure 12.10 Complex viscosity of LLDPE versus oscillatory frequency	155
Figure 12.11 AFM images of LLDPE films	156
Figure 12.12 SEM images of LLDPE film	156
Figure 12.13 Carbonyl index versus incubation time of PP with <i>R.ruber</i>	158
Figure 12.14 Growth of pure bacterial culture versus incubation time with PP.....	159
Figure 12.15 AFM images of PP films	160
Figure 12.16 SEM images of PP film	160
Figure 12.17 Fluorescence microscope images of biofilm formation on PP film samples	161
Figure 12.18 Decomposition temperature of PP film versus incubation time with <i>R.ruber</i>	162
Figure 12.19 Carbonyl index versus incubation time of PP with mixed bacterial culture	164
Figure 12.20 Growth of mixed bacterial culture versus incubation time with PP.....	165
Figure 12.21 Melting temperature of PP film versus incubation time with mixed bacterial culture	166
Figure 12.22 Weight loss measurements of PP films incubated with mixed bacterial culture	167

Figure 12.23 Decomposition temperature of PP film versus incubation time with Mixed bacterial culture.....	168
Figure 13.1 Carbonyl index versus incubation time of PS with fungal culture	170
Figure 13.2 Weight loss measurements of PS films incubated with pure fungal culture.	171
Figure 13.3 Dry weight of fungal culture versus incubation time with PS.....	172

1 Aim of this study

This work deals with the development of aerobic processes for the biodegradation of recalcitrant synthetic compounds until recently considered non-biodegradable: chlorinated solvents, studied in the first part of the thesis, and plastics in the second part.

Since the 1980s, widespread use of chlorinated compounds such as organic solvents, pesticides, additives, drugs and antiseptics has led to the gradual release of these substances into the environment, particularly resulting in contamination of soil and groundwater. Among these compounds, chlorinated solvents are a main source of groundwater contamination, due to their widespread use and high water-solubility. All chlorinated solvents have a xenobiotic nature and are toxic and irritant. Most of them, including vinyl chloride and trichloroethylene (TCE), are proven or suspected carcinogens.

There are three groups of technologies for remediating chlorinated solvents in groundwater: physical, chemical and biological processes. Bioremediation is gaining much current attention for groundwater decontamination: it has the advantage of reducing both costs and environmental impact. While the aerobic biodegradation of chlorinated solvents in the absence of a co-substrate presents poor results because the biomass cannot restore the redox energy needed to continue the process of degradation, the addition of a co-metabolic substrate as a source of carbon and energy greatly improves results. In this process—aerobic co-metabolic biodegradation—a growth substrate (the primary substrate) acts as a source of carbon and energy (ATP), inducing the cells to produce the enzymes required for degradation of the pollutant (metabolic substrate).

On-site aerobic co-metabolic biodegradation of contaminated aquifers is a particularly interesting option, capable of taking place either in suspended cell bioreactors or in packed bed bioreactors (PBRs). PBRs in particular present such interesting advantages as higher cell retention times and biomass concentrations, the elimination of the biomass settling step, and a partial protection of cells against toxic substances. Thus, the first part of this study develops an on-site PBR process for the aerobic co-metabolic biodegradation of chlorinated aliphatic hydrocarbons (CAHs) contained in a real contaminated aquifer located in the north of Italy. The goals of this section of the thesis are:

- 1) to select the best growth substrate for the AC process, and to develop an effective CAH-degrading microbial consortium from the site's indigenous biomass in the presence of the selected substrate
- 2) to evaluate the possible need for a chemical pre-treatment aimed at the degradation of the CAHs present in the studied site and not biodegradable via AC
- 3) to select the best biofilm carrier for the PBR process, and to evaluate the process performances attainable with the selected growth substrate and biofilm carrier in a continuous flow PBR
- 4) to perform a kinetic study of CAH biodegradation with the selected growth substrate and biofilm carrier
- 5) to perform a model-based scale-up of the process, aimed at designing and implementing a 31-L PBR

Another class of xenobiotic compounds representing an extremely relevant source of environmental pollution is synthetic polymers and plastics in particular. Polymers are applied widely, from medical applications to the food and agriculture industries: the

demand for polymers has rapidly increased due to their low cost of production and versatility of application. Due to the high level of polymer production and consumption, accumulation of polymers has become a major concern and environmental threat. Plastics, plasticizers, other plastic additives and constitutional monomers can leach from disposal sites into groundwater and surface water and therefore marine ecosystems. As a consequence, microscopic particles are able to enter the food chain and threaten marine biodiversity.

It is generally understood that plastics are non-degradable, mainly due to their high molecular weight and hydrophobic nature. Recently, however, several lines of research have been developed to understand possible physical, chemical or biological processes for degrading plastics. One of the proposed mechanisms is exposure of the polymer to physico-chemical processes followed by biological processes. In this approach, the physico-chemical treatment leads to a decrease in polymer molecular weight as well as to the generation of some hydrophilic groups on the surface of the polymer. These physico-chemical approaches may well facilitate the biodegradation of polymers. However, finding the right biological approaches is the next challenging step, since knowledge of the possible biodegradation pathways and the microorganisms capable of using polymers as carbon sources is still very limited. Thus, in the second part of this study, different combinations of physico-chemical pretreatments and biodegradation approaches were tested on four polymers—polyethylene (PE), polypropylene (PP), polyvinyl chloride (PVC), and polystyrene (PS)—with the following goals:

- 1) development of effective pre-treatments for improving plastic biodegradability
 - a) ozone treatment
 - b) combined UV/ozone treatment

2) assessment of the impact of pre-treatments on plastic biodegradability:

- a) pure culture tests
- b) mixed culture tests
- c) fungal culture tests

Part 1:

Aerobic co-metabolic biodegradation of chlorinated solvents in biofilm reactors

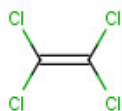
2 Biodegradation of chlorinated solvents

2.1 Chlorinated solvents

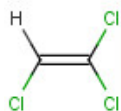
2.1.1 Structure and chemical properties

Chlorinated solvents are compounds derived from aliphatic or cyclic hydrocarbons, in which one or more hydrogen atoms are replaced by four chlorine atoms. These substances have properties such as good solvent power, low flammability and can be used as fuel or coolant . Names and molecular formulae are shown in Figure 2.1.

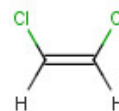
Chlorinated ethylene



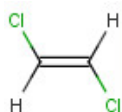
Tetrachloroethylene



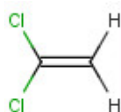
Trichloroethane



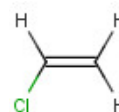
Cis-1,2-dichloroethane



Trans-1,2-Dichloroethane

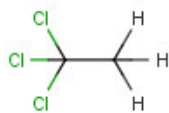


1,1-Dichloroethene

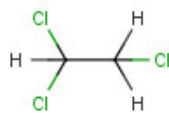


Chloroethene

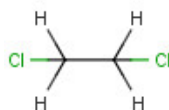
Chlorinated ethane



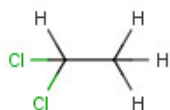
1,1,1-Trichloroethane



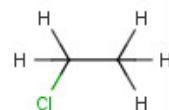
1,1,2-Trichloroethane



1,2-Dichloroethane



1,1-Dichloroethane

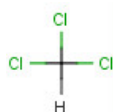


Chloroethane

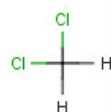
Chlorinated methane



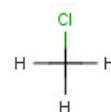
Tetrachloromethane



Trichloromethane



Dichloromethane



Chloromethane

Figure 2.1 Structural formulae of the main chlorinated solvents [1]¹.

¹ Modified from reference [1].

The physico-chemical properties of the chlorinated solvents determine the effect of these components on the environment. The properties of chlorinated solvents are listed in Table 2.1 and described here:

- There is a positive correlation between the molecular weight of chlorinated solvents and density. However, the vapor pressure and water solubility decrease with an increase of the number atoms of these molecules.
- All compounds are liquid and denser than water (with the exception of chloroethane and vinyl chloride, which are gaseous). In the presence of an aqueous phase, the chlorinated solvents tend to migrate downwards until they reach impermeable soil layers. This obviously makes it more difficult to identify and treat them.
- The compounds have a high solubility at 25°C on the order of g/L: for example, the solubility of dichloromethane is 20 g/L, which is a very high amount, especially when compared to legislation, which provides a maximum concentration of 1µg/L.
- The vapor pressures at 25°C range from a minimum of 30 mmHg for 1,1,2-trichloroethane to a maximum of 600 mmHg for 1,1-dichloroethylene.
- The logarithm to base ten of the octanol/water coefficient is in the range 0.48-2.64. This means that, within the contaminated groundwater, the chlorinated solvent will be mainly present in the aqueous phase rather than in the ground.

Table 2.1 Classifications and formulae of the major chlorinated solvents [1].

Chlorinated methanes		Abbreviation	Formula
Tetrachloromethane	-	CT	CCl_4
Trichloromethane	Chloroform	CF	CHCl_3
Dichloromethane	-	DCM	CH_2Cl_2
Chloromethane	-	CM	CH_3Cl
Chlorinated Ethanes			
Hexachloroethane	Perchloroethane	HCA	C_2Cl_6
Pentachloroethane	-	PCA	C_2HCl_5
1,1,1,2-Tetrachloroethane	-	1,1,1,2-TeCA	$\text{C}_2\text{H}_2\text{Cl}_4$
1,1,2,2-Tetrachloroethane	-	1,1,2,2-TeCA	$\text{C}_2\text{H}_2\text{Cl}_4$
1,1,2-Trichloroethane	-	1,1,2-TCA	$\text{C}_2\text{H}_3\text{Cl}_3$
1,1,1-Trichloroethane	Methyl chloroform	1,1,1-TCA	$\text{C}_2\text{H}_3\text{Cl}_3$
1,2-Dichloroethane	-	1,2-DCA	$\text{C}_2\text{H}_4\text{Cl}_2$
1,1-Dichloroethane	-	1,1-DCA	$\text{C}_2\text{H}_4\text{Cl}_2$
Chloroethane	-	CA	$\text{C}_2\text{H}_5\text{Cl}$
Chlorinated Ethene			
Tetrachloroethylene	Perchloroethylene	PCE	C_2Cl_4

Trichloroethylene	-	TCE	C_2HCl_3
<i>Cis</i> -1,2-Dichloroethene	-	<i>cis</i> -DCE	$C_2H_2Cl_2$
<i>Trans</i> -1,2-Dichloroethene	-	trans-DCE	$C_2H_2Cl_2$
1,1-Dichloroethene	-	1,1-DCE	$C_2H_2Cl_2$
Chloroethylene	Vinyl chloride	VC	C_2H_3Cl

Table 2.2 Physico-chemical properties of some chlorinated solvents at 25°C [1]

Type	Molecular weight (g/mol)	Liquid density (g/mL)	Aqueous solubility (mg/L)	Vapor pressure (mmHg)	Henry's law constant (atm·m ³ /mol)
CT	153.8	1.595	757	90	0.0304
CF	119.4	1.485	8200	151	0.00435
DCM	84.9	1.325	20000	362	0.00268
1,1,1-TCA	133.4	1.325	1500	123	0.008
1,1,2-TCA	133.4	1.440	4500	30	0.0012
1,1-DCA	99.0	1.175	5500	182	0.0059
1,2-DCA	99.0	1.253	8520	64	0.00098

CA	64.5	Gas	5700	1064	0.0085
PCE	165.8	1.620	150	17.8	0.0153
TCE	131.4	1.460	1100	57.9	0.0091
c-DCE	96.9	1.280	3500	208	0.0037
t-DCE	96.9	1.280	6300	324	0.0072
1,1-DCE	96.9	1.210	2250	600	0.018
VC	62.5	Gas	2670	2660	0.315

2.1.2 Applications

Chlorinated solvents are widely used in the chemical, textile, rubber and plastics industries; in fire extinguishers and coolants; and for degreasing and cleaning of metals, leather and fabrics.

Among the most widely used are methylene chloride (MC), chloroform (CF), carbon tetrachloride (CT), trichlorethylene (TCE) and tetrachlorethylene (TeCA). Their main features are summarized below.

Methylene chloride: Its volatility and the ability to dissolve a wide spectrum of organic compounds are such that dichloromethane is an excellent solvent for many chemical processes. In fact it is used in the removal of paint and fats, in the food industry (e.g. among others the extraction of caffeine from coffee, the preparation of hop extracts), and is used as a foaming agent in the production of polyurethane foams and as a propellant for aerosol spray.

Chloroform: In the past this was used as an anesthetic in surgery and as a syrup antitussive, but it has been replaced by less toxic substances. Chloroform was then mainly used in the production of Freon R-22 (refrigerant)—now banned and replaced with less hazardous materials due to its destructive effect on the ozone layer in the stratosphere. Chloroform is also used as laboratory solvent for the extraction and purification of drugs, dyes and pesticides, as well as an adhesive in the production of certain plastics. Deuterated chloroform (CDCl_3) is used as a solvent in nuclear magnetic resonance spectroscopy (NMR).

Carbon tetrachloride: In the past this was used for dry cleaning, for the synthesis of refrigerants (Freon R-11 and Freon R-12) and in fire extinguishers. Now it is used largely as a solvent on a laboratory scale.

Trichloroethylene: Known by the commercial name of trichlor, this is used to extract vegetable oils in exotic plants (coconut and palm), to clean (degrease) metal parts, to produce adhesives, as a substitute for CFCs and as a solvent in dry cleaning in the textile industry.

Tetrachloroethylene: This type of compound is used mainly in the dry cleaning of garments in the textile industry. Also, it can be exploited as a starting point for the synthesis of CFC less destructively, or for cleaning (degreasing) of metal parts.

2.1.3 Dispersion of chlorinated solvents in the environment

Current accumulation of chlorinated solvents in groundwater and soil is significant due to mismanagement of the waste in the past. This problem has spread throughout Europe and the United States and there is a need for remediation of these components.

In general, a solvent contaminant is normally released as pure liquid (indicated by the acronym NAPL for Non Aqueous Phase Liquid). Underground, once it has reached equilibrium, the solvent is present divided into four distinct phases: in part as a pure liquid (NAPL), in part dissolved in underground water, in part adsorbed onto the soil and in part evaporated in the gases present in the soil (in cases where the aquifer is not saturated). This situation is shown in Figure 2.2, providing a schematic explanation of the balance established between the four phases. As can be seen, the balance between the pure liquid, the adsorbed phase on the ground and the dissolved phase in water is determined by the solubility in water and the octanol/water coefficient of the specific contaminant. The vapor pressure regulates the balance between the pure liquid phase, the adsorbed phase in the ground and the gas phase present in the subsoil. The equilibrium established between the dissolved phase in water and the gas phase present in the subsoil is defined by the Henry constant.

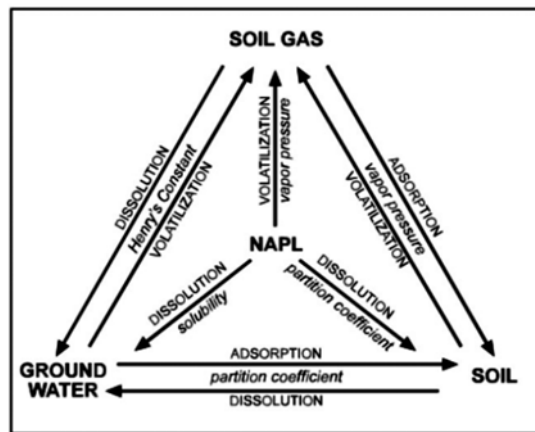


Figure 2.2 NAPL balance in four phases [1]

For chlorinated solvents with a higher density than water, the term Dense Non Aqueous Phase Liquid (DNAPL) can be used. These compounds perfectly reflect the balance described above. Due to their high density, these compounds tend to settle on the bottom

of the aquifer, so they pass over unsaturated zones located at the saturated subsoil, until reaching the impermeable layer delimiting the aquifer in height.

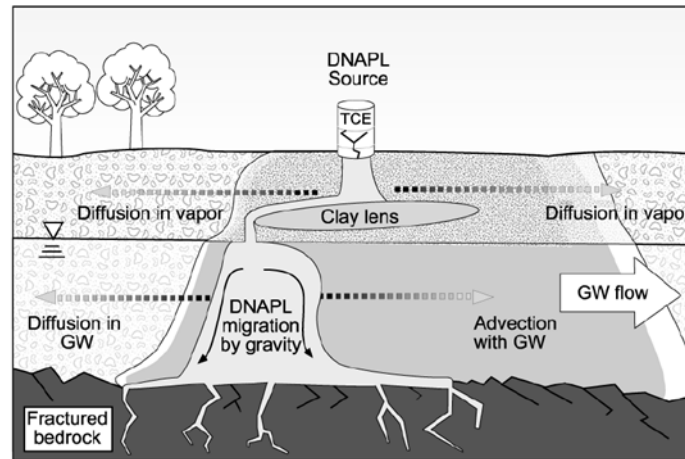


Figure 2.3 Example of transport of chlorinated solvents in the subsoil [1]

Since DNAPL are located in the deepest area of a water body, it is very difficult to recognize and remediate them. In addition to the transfer of material seen previously, chlorinated solvents can move in the subsoil both by convection and by diffusion due to the flow of the aquifer itself, as shown in Figure 2.3.

2.1.4 Effect of chlorinated solvents on human beings

The absorption of chlorinated solvents is carried out mainly by the respiratory route, but it can be also introduced through the skin or digestive system. Toxic effects of chlorinated solvents mainly concern the liver, kidneys and central nervous system. Exposure of humans to high concentrations of chlorinated solvents leads to intoxication, followed by physiological depression and narcosis to coma; chronic exposure usually leads to disequilibrium (headache, fatigue, irritability). Severe liver injury and acute kidney character may occur in the event of massive intoxication; continuous exposure

over time can be observed usually through manifestations of chronic liver disease. The greatest potential detriments among chlorinated aliphatic compounds are associated with carbon tetrachloride and tetrachloroethane (nephro-hepato-neurotoxicity), followed by chloroform and 1,2-dichloroethane. Trichlorethylene, widely used in various sectors, on the other hand presents a greater risk of chronic toxicity (possible liver disease). The toxicity of the cyclic compounds (monochlorobenzene and dichlorobenzene) is similar to that of carbon tetrachloride. In addition, some aliphatic compounds (such as trichlorethylene) may cause cardiac arrhythmia and, upon contact, irritant dermatitis or allergic reaction. In the presence of fire or surfaces at high temperature, aliphatic chlorinated solvents may decompose into toxic vapours, also containing phosgene, with serious effects on the respiratory system (such as lung edema). The environmental threshold limits value TLV-TWA of chlorinated solvents, as recommended by the American Conference of Government Industrial Hygienists (ACGIH) in 2001, are shown in Table 2.3 together with the carcinogen classification under the ACGIH.

Table 2.3 Environmental threshold limits value TLV-TWA of chlorinated solvents [2]

TLV-TWA	ppm	mg/m ³	CAS No.
Chloromethane	50	103	74-87-3
Dichloromethane	50	174	75-09-2
Chloroform	10	49	67-66-3
Carbon tetrachloride	5	31	56-23-5
Chloroethane	100	264	75-00-3
1,1-Dichloroethane	100	405	75-34-3
1,2-Dichloroethane	10	40	107-06-2
1,1,1-Trichloroethane	350	1910	71-55-6

1,1,2-Trichloroethane	10	55	79-00-5
1,1,2,2-Tetrachloroethane	1	6.9	79-34-5
Vinyl chloride	1	2.6	75-01-4
Dichloroethylene	5	20	75-35-4
Trichloroethylene	50	269	79-01-6
Perchloroethylene	25	170	127-18-4
Chlorobenzene	10	46	108-90-7
Ortho-dichlorobenzene	25	150	95-50-1
Paradichlorobenzene	10	60	106-46-7

2.2 Groundwater contamination

2.2.1 Factors determining the pollution of aquifers

The term groundwater refers to the mass of water contained in the aquifer, where the aquifer is a permeable rock or soil that can contain water and allow flow with a speed compatible with the possibilities of normal use. The flow can be free, or limited only by the lower permeable soils; confined, and bounded below the surface by impermeable layers; or suspended, supported by a waterproof level of reduced extension.

The contaminated groundwater can be divided to three zones in a vertical direction from top to bottom of the ground:

- unsaturated zone or vadose zone
- capillary fringe
- saturated zone or aquifer

Most groundwater contaminations originate from the release of pollutants in the soil. The movement of these substances in the unsaturated zone is controlled by the characteristics of the soil, the composition of the contaminant and the phase in which it is located. Generally, the contaminant is conveyed in solution by the flow of water seepage so that its solubility in water is fundamental; but transport can also be due to a gas flow. Once reaching groundwater, the contaminant is transported by a saturated stream, undergoing further modifications linked to its chemical characteristics, solubility and density, controlling the delay, degradation, and behaviour in the water table: whether the contaminant has a tendency to float in the water table, dissolve in it or deepen towards the base.

Water pollution can be chemical, physical or microbiological and the consequences can compromise the health of plants and animals including humanity, and damage to ecosystems and water supplies for food. There are two main routes by which the pollutants reach the water: directly and indirectly. The direct means is when pollutants are poured directly into waterways, without any purification treatment. The indirect route, instead, is when pollutants reach watercourses through air and soil (such as the washing away of soil containing harmful substances).

The main sources of water pollution can be classified into:

- industrial pollution
- urban pollution
- agricultural pollution
- natural pollution
- waste waters containing organic materials

The most common water pollutants are:

- Fecal pollutants: derived from animal excrement and food residues. Aerobically these consume O_2 to form CO_2 , NO_3^- , PO_3^{4-} , SO_2 , while anaerobically CH_4 , NH_3 , H_2S , and PH_3 are formed. Cases with strong fecal pollution can also demonstrate the presence of pathogenic microorganisms in the water (e.g. typhoid, cholera, hepatitis).
- Inorganic toxic substances: formed by heavy metal ions (such as Cr^{6+} , Hg^{2+} , Cd^{2+} , Cu^{2+} , CN^-) that can block the catalytic action of the enzymes of an organism, resulting in poisoning or death.
- Inorganic harmful substances: phosphates and polyphosphates in fertilizers, detergents, and nitrogen and phosphorus compounds in some industrial discharges. These cause eutrophication: a huge development of the aquatic flora which largely dies, settling on the bottom to decompose and therefore consume considerable amounts of oxygen. When the water mass is deficient in oxygen, the products of anaerobic decomposition increase, resulting in the death of animal life by asphyxiation. The water then becomes cloudy, limiting light penetration depth, further worsening the situation.
- Unnatural organic substances: herbicides, pesticides and insecticides bring benefits to agriculture but can pollute water.
- Free oils and emulsifiers: insoluble because of their low density, these rest on the surface, creating an oily film preventing oxygen from being soluble in water.

- Suspended solids: substances of a different nature, which make the water turbid and intercept sunlight. Also, once deposited on the bottom, these prevent the development of the vegetation.
- Heat, strong acids and bases: mostly due to industrial wastes, may decrease the solubility of oxygen and alter the temperature and pH of the environment causing pathological alterations or disappearance of some species or even the development of others normally absent.

2.2.2 Treatment of contaminated aquifers

As described above, the heterogeneity and the high number of pollutants affecting aquifers requires the use of cleaning treatment as diverse and numerous as the pollutants. However, they can be combined together. There are three different classes of treatment:

- immobilization: the pollutants are transformed into products of low solubility or embedded in the matrix, preventing physical movement.
- separation: pollutants are separated by extraction or volatile action, concentrated and sent to a final treatment.
- transformation: the pollutants are transformed into different products less harmful or harmless.

These treatments can be conducted via two modes: *in situ* remediation done directly on the site of the contamination, and *ex situ* remediation processes, performed after the excavation of contaminated soil or sediment. In *ex situ* work, the process can be done on-site, on the site of the excavation, or off-site, with the sediment transported to a plant or a laboratory.

Heterogeneous classes of treatments mainly use chemical and physical principles for the removal of contaminants from the soil from the aquifer. In particular, for treatments removing pollutants from the water, mainly the following are used: pump and treat, soil vapor extraction, and air sparging.

2.2.3 Biodegradation

One of the novel techniques that have recently been developed for the removal of pollutants is biodegradation of contaminants. Biodegradation consists of a series of chemical and biological processes that lead, by the action of microorganisms, to the decomposition of the substances. The organisms degrade the organic substance (and therefore the contaminant) for three main reasons:

- They use the organic contaminant as a growth substrate.
- The degradation reactions are the source of energy for their development.
- The organic contaminants share their source of nutrients for growth.

Bioremediation can be conducted *in situ* directly to remove the contamination from the site, or by an *ex situ* method. There are many different contaminants that can be subjected to biodegradation for removal from soil or aquifer environments. According to a ranking prepared by the Environmental Protection Agency, among the most hazardous compounds chlorinated aliphatic solvents are a major cause of contamination of groundwater and industrial wastewater and were considered for a long time non-biodegradable compounds. In fact, since the mid-eighties, studies have shown that it is possible to transform chlorinated solvents by processes mediated by microorganisms. In general, the advancement of knowledge on the mechanisms of degradation is used to

determine the optimal conditions for the biological process. It is often necessary to maintain relatively low levels of concentration of the substance to be biodegraded, in order to minimize the toxic effects upon the microbial consortium. It is also very important to verify that the biodegradation process not result in the formation of intermediate compounds more toxic for the microorganisms degrading the natural environment as compared to those of departure. In our case, it is also important to evaluate if the degradation of chlorinated solvents by the selected consortium has as a final result the production of chloride ions, and not of other compounds as metabolic intermediates.

Despite this, the degradation processes are preferred to traditional purification treatments, as well as providing cost advantages, and the environmental impact can transform the contaminant rather than simply transferring it from one phase to another, which would require subsequent treatment for its definitive elimination from the environment. The process of degradation by the microorganisms can be conducted both under anaerobic conditions and in conditions requiring the presence of oxygen. In general, however, for chlorinated solvents which have a chlorination degree of medium or high, the processes of biodegradation most effective are those that take place in anaerobic conditions.

Anaerobic processes, besides being slow and in some cases difficult to implement, are not easily to be controlled. Also, sometimes, the processes cannot achieve complete dechlorination of the compounds (as in the case of chloroethene). An alternative, applicable in the case of compounds having a lower degree of chlorination, is to develop processes in aerobic conditions. However, most of the microorganisms are not able to benefit from energy directly, so co-metabolic degradation is an alternative. Co-metabolic

degradation of chlorinated solvents, requires of a growth substrate as a source of energy (ATP) and carbon.

In the present work we studied the process of co-metabolic biodegradation of trichlorethylene (TCE) and 1,1,2,2-tetrachloroethane (TeCA) under aerobic conditions. In particular, this chapter explains the basic transformation reactions of organic and non-chlorinated solvents, focusing particular attention on the processes of aerobic co-metabolic degradation.

2.2.4 Degradation of chlorinated solvents

The degradation of chlorinated solvents can occur in the absence of micro-organisms; in this case we speak of abiotic degradation. Alternatively, it may be mediated by biological processes, and known as biotic degradation [1].

In general, the degradation reactions can be classified into two main categories:

- reactions without the exchange of electrons
- reactions with electron transfer

Table 2.4 shows degradation reactions of chlorinated solvents for these two groups.

2.2.4.1 Reactions without the exchange of electrons

This kind of reaction takes place predominantly in abiotic systems and does not require the presence of organic or biochemical catalysts. Compared to redox reactions, these are rather slow, but not negligible with respect to motion in the water of the subsoil. Such reactions are divided into two main classes: substitution and elimination. In the substitution reaction, chlorine is replaced by another chemical functionality to form a second compound. The most common substitution reaction is hydrolysis, in which the chlorinated solvent replaces the chlorine atom with water to form an alcohol; this reaction

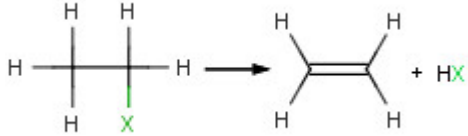
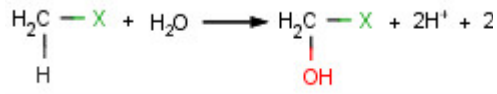
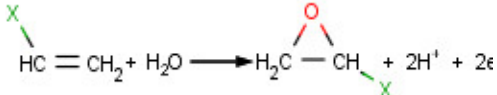
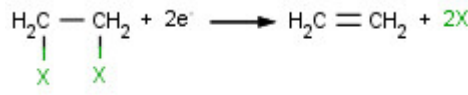
is characterized by pseudo-first-order kinetics. The most common elimination reaction is dehydrohalogenation, in which the chlorine bonds with a hydrogen atom of the adjacent carbon leading to the formation of a double bond in the solvent and elimination of hydrochloric acid (HCl).

2.2.4.2 Reactions with electron transfer

Reactions with electron transfer occur predominantly in biological systems and can be classified into two main categories: oxidations and reductions.

Unlike reactions in the first category, oxidation and reduction reactions require the presence of, respectively, external donors and acceptors of electrons. In general, organic compounds act as electron donors (oxidization). However, the characteristic electronegative atom of chlorine makes chlorinated compounds also good electron acceptors. Chlorinated aliphatic compounds, therefore, can behave both as donors and acceptors of electrons, respectively being oxidized or reduced, depending on the number of chlorine atoms present in the molecule. In particular, the increase of this number also increases the electronegative character of the compound and therefore the possibility that it behaves as an oxidizing agent (electron acceptor), rather than reducing agent (electron donor).

Table 2.4 Degradation reactions of chlorinated compounds

	Reactions	Classification of the reactions	Reaction mechanism
Reactions without exchange of electrons	Substitution	Hydrolysis	$R - X + H_2O \longrightarrow ROH + HX$
	Elimination	Dehydrohalogenation (saturated CAH)	
		α -hydroxylation	
Reaction with electron transfer	Oxidation	Halo-oxidation	$H_3C - X + H_2O \longrightarrow H_3C - X^+ O^- + 2H^+ + 2e^-$
		Epoxidation (unsaturated CAH)	
		Hydrogenolysis	$R - X + 2H^+ + 2e^- \longrightarrow R - H + X^-$
	Reduction	Coupling	$2R - X + 2e^- \longrightarrow R - R + 2X^-$
		Double elimination (saturated CAH)	

2.2.4.3 Aerobic biodegradation with co-metabolism

Among the biological processes that can be utilized for CAH degradation, aerobic co-metabolism (AC) plays an important role. AC can lead to the rapid and full dechlorination of a wide range of CAHs, including some high-chlorinated ones [3, 4]. Methane [5], toluene [6], phenol [7], ammonia [8], propane [9, 10], butane [11], n-pentane, n-hexane [12] and vinyl chloride [9] can be effectively utilized as growth substrates. In particular, methane, propane and butane present the advantages of the absence of toxicity and of the possibility to inject hydrocarbon/air gaseous mixtures directly in the groundwater or in the bioreactor, a technology known as co-metabolic air sparging [13].

The first published study on aerobic co-metabolism was by Wilson and Wilson, who observed that the simultaneous supply of methane and oxygen stimulated the aerobic biodegradation of TCE [6]. During the aerobic co-metabolism, the chlorinated compound is "incidentally" oxidized by an enzyme normally produced during the metabolism of another substrate. In fact, the microorganisms are able to derive the energy and carbon which are necessary for their growth by the oxidation of a substrate, catalysed by a monooxygenase enzyme, and are also able to oxidize most of the chlorinated compounds [5].

In an oxidation reaction catalysed by monooxygenases, molecular oxygen acts as electron accepting (decreasing), while the growth substrate or alternatively the chlorinated compound are the electron donors (oxidizing). The oxidative process depends upon the growth substrate, which serves co-metabolic coenzyme NADH (nicotinamide adenine dinucleotide) as a reducing agent, which in both oxidative processes oxidizes the reduced form NADH to the oxidized form NAD^+ . Only the products resulting from oxidation of

the growth substrate allow regeneration of the cofactor in its reduced form (NADH). During the oxidation of chlorinated compounds, microorganisms cannot produce energy, NADH cannot be regenerated, and degradation continues until the energy runs out. In addition, the chlorinated compounds may convert to very toxic intermediate products resulting in inactivation of the microorganisms [14]. Figure 2.4 gives the schematic of oxidation of growth substrate and co-metabolic substrate.

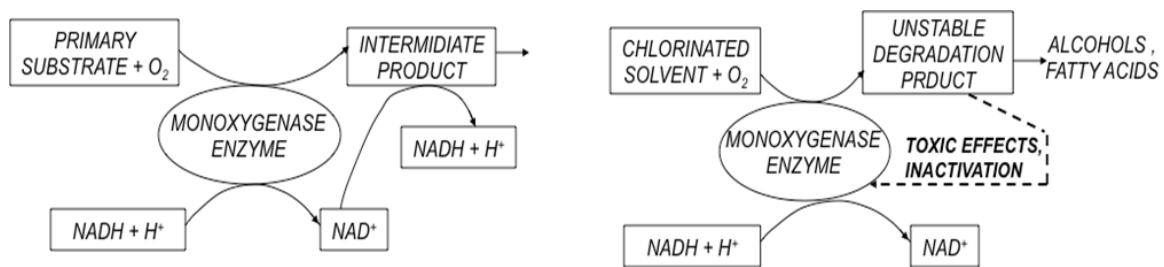


Figure 2.4 Schematic representation of the microbial oxidation of a primary substrate (left) and of a non-growth substrate such as a CAH (right)

Thus the bioremediation of a CAH-contaminated site requires in most cases the supply of a suitable primary substrate whose function is to stimulate the selection and growth of a microbial consortium able to perform the degradation of the target contaminants. Research on the aerobic co-metabolic degradation of chlorinated solvents [3, 4, 5, 8, 9, 11, 12, 15, 16] showed that:

- With the exception of carbon tetrachloride, all chlorinated methanes, ethenes and ethanes with up to 4 chlorines can be degraded via aerobic co-metabolism, the higher-chlorinated compounds being typically characterized by lower degradation rates.
- CAHs with higher chlorine content exert a higher toxicity when oxidized.

- Saturated growth substrates, such as methane, propane and butane, usually induce the growth of consortia able to transform both saturated (methanes and ethanes) and unsaturated (ethanes) chlorinated hydrocarbons, whereas aromatic growth substrates, such as phenol and toluene, usually induce the growth of consortia able to transform only unsaturated CAHs.

It is therefore of primary importance to perform a correct choice of the growth substrate utilized, on the basis of the characteristics of the site's indigenous biomass and of the target contaminants.

2.2.5 Suitable Reactor for aerobic co-metabolic biodegradation

An important first step for implementation of aerobic co-metabolic biodegradation in a contaminated aquifer is to choose the suitable bioreactor for this process. Frequently, in CAH-contaminated sites it is necessary to protect downstream targets and to prevent the widening of the plume; this determines the choice of a "pump and treat" remediation approach. In these cases, groundwater is treated on-site typically by means of adsorption, which concentrates the contaminants in the adsorbing medium without destroying them. On the other hand, on-site AC in bioreactors represents an interesting alternative, thanks to its potential to completely transform CAHs into non-toxic end products. Numerous bioreactor solutions can be implemented. Among these, packed bed reactors (PBRs) present important advantages, such as the removal of the biomass settling step and a higher cell resistance in the presence of toxic compounds [17]. In addition, they display a high tolerance to very high and variable organic loads [18]. In particular, they represent an interesting solution for the biodegradation of recalcitrant and toxic compounds, since biomass grown in the form of biofilm is partially protected against toxic substances and

inhibition phenomena due to high substrate concentrations [19]. In this respect, PBRs inoculated with selected pure cultures or mixed consortia have been shown to be very promising both for the metabolic and the co-metabolic degradation of several recalcitrant and toxic compounds, such as polychlorinated biphenyls [20], polyethoxylated nonyl phenols [21, 22], nitrophenols [23] and chlorinated solvents [11].

A relevant step in the development of a PBR process for the on-site bioremediation of CAH-contaminated groundwater is the selection of the biofilm carrier. Numerous types of biofilm carriers were investigated in the studies of CAH aerobic co-metabolism (or CAH AC): stainless steel cylinders, glass beads, diatomaceous earth or activated carbon pellets, anthracite or polyethylene packings [11, 24, 25, 26, 27, 28, 29, 30 and 31]. However, these PBR studies were characterized by the following limitations:

- a) conducted in small-scale laboratory reactors
- b) did not include a formal procedure for the rational selection of the best-performing biofilm carrier
- c) in most cases, tested carriers were not specifically designed for biofilm reactors.

The first part of this Ph.D. program was carried out in the framework of the EU-funded research program MINOTAURUS (Microorganism and enzyme Immobilization: NOvel Techniques and Approaches for Upgraded Remediation of Underground-, wastewater and Soil) [32]. This part of the thesis presents the progress made in the framework of the MINOTAURUS project with regard to the development of a PBR process specifically designed for CAH AC, with specific focus on the following aims:

- to select the best growth substrate for the AC process, and develop an effective CAH-degrading microbial consortium from the site's indigenous biomass in the presence of the selected substrate
- to evaluate the possible need for a chemical pre-treatment aimed at the degradation of CAHs present in the studied site and not biodegradable via AC
- to select the best biofilm carrier for the PBR process, and evaluate the process performances attainable with the selected growth substrate and biofilm carrier in a continuous flow PBR
- to perform a kinetic study of CAH biodegradation with the selected growth substrate and biofilm carrier
- to perform a model-based scale-up of the process, aimed at designing and implementing a 30 L PBR

3 Biofilm reactors

Microorganisms play a key role in the bioremediation processes. In the environment they are mainly found in two types of aggregates, as suspended biomass and attached biofilm, which differ in that the suspended cells form in the liquid media, while the formation of biofilm is dependent on the adhesion of aggregate to a solid surface.

This chapter takes an overall view on the conditions for biofilm formation and reviews its main characteristics and its most important application in the bioremediation process.

3.1 Factors affecting the production of biofilms

The interface between a surface and an aqueous medium provides a favourable environment for the development of biofilms. Important factors promoting the formation of biofilm on the surface, include the physico-chemical characterization of the solid surface, the properties of the liquid medium, and the properties of the microbial cells. The adhesion of microorganisms to a surface is a very complex process, with many variables influencing the results, but in general, biofilm formation is easier on surfaces which are very rough, hydrophobic and covered with a film of organic molecules. An increase in flow rate, temperature, and nutrient status may also promote adhesion, providing these factors do not exceed critical values. The presence of fimbriae, flagella, polysaccharides and proteins are also important in promoting adhesion.

3.2 Structure of the biofilm

3.2.1 Exocellular polymeric substances (EPS)

Biofilm is composed mainly of microbial cells and extra-cellular polymeric substances (EPS). The latter may comprise 50 to 90 percent of the total organic carbon of biofilms and are therefore considered the primary matrix of biofilm. Extra-cellular polymeric substances may exhibit different physico-chemical properties while maintaining a basic structure consisting mainly of polysaccharides and proteins. Their composition and their structure determine the shape of the primary biofilms. An EPS can be neutral or polyanionic—as with an EPS of gram-negative bacteria. In this case, the presence of uronic acid (such as D-glucuronic acid, D-mannuronic acid and galacturonic) or pyruvates allows the creation of links with divalent cations such as calcium and magnesium, which are fundamental to cell adhesion on the surfaces of solids. The EPS may be highly hydrated and able to accumulate a significant amount of water in their structure through the implementation of hydrogen bridge bonds, but in some cases can also be hydrophobic [33].

The composition of an EPS is generally not uniform but can vary in space and time; the amount of exocellular polymeric substances varies depending on the organism and the amount increases with the age of the biofilm. The EPS, in addition to being associated with metal ions (such as divalent cations), may also be associated with macromolecules such as proteins, DNA, lipids and humic substances. The production of EPS is influenced by the state of the nutrients in the growth medium: their synthesis is promoted by an excess of carbon and small amounts of nitrogen, potassium and phosphate.

Extracellular polymeric substances may also contribute to resistance to antibiotics, by binding directly to their molecules and thus preventing mass transport through the biofilm.

3.2.2 Architecture of the biofilm

Some researchers suggest the term biofilm is not really suitable: it is not a surface deposit realized as a single continuous layer but is typically a heterogeneous structure containing microcolonies of bacterial cells encapsulated in a matrix of EPS and separated from each other by means of interstitial voids as water channels [34]. Figure 3.1 shows the biofilm of *Pseudomonas aeruginosa*, *Klebsiella pneumoniae* and *Flavobacterium* developed on a steel surface. This image shows the presence of water channels and the characteristics of heterogeneity mentioned above.

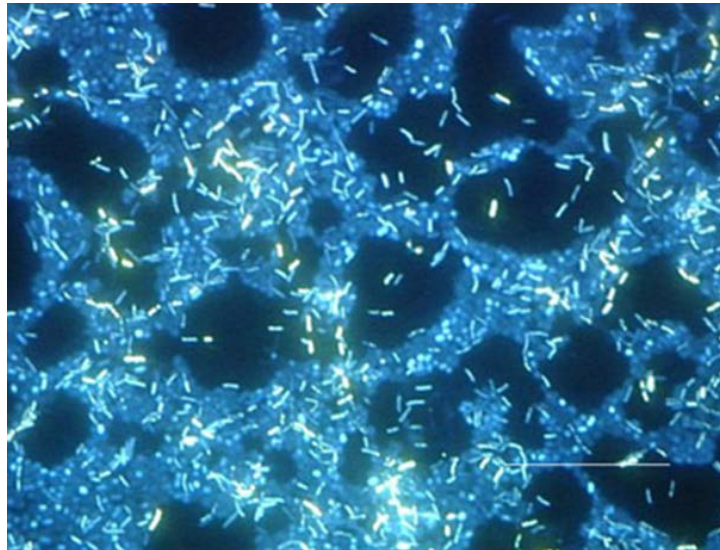


Figure 3.1 Biofilms grown on stainless steel [35]

Surface of a reactor exposed to drinking water for 14 days and observed with a fluorescence microscope.

The flow of liquid occurs in the water channels, allowing the spread of nutrients and oxygen. The concept of heterogeneity not only applies to biofilm made from mixed

cultures but also for biofilm deriving from pure cultures. The presence of EPS is important for the development and architecture of the biofilm, stabilizing interactions with the bacterial surface and contributing to the formation of its architecture.

3.3 Biofilm formation

The formation of biofilms is not the result of a random process but on the contrary is a well-defined sequence of steps constituting a complex process controlled by several factors. Figure 3.2 shows the cyclic process leading to the formation of an active biofilm: the cells initially bind to the surface due to chemical-physical interactions or through the secretion of extracellular proteins carrying out a cell monolayer. This leads to the formation of cells in a monolayer, while other microbes adhere to it to form a biofilm. The biofilm's development and its distortion are influenced by environmental factors such as hydrodynamic and mechanical stress. In mature biofilm, cells are mobile and exhibit chemotaxis, leading to the diffusion of nutrients and biomass and accelerating the horizontal transmission of genetic material. Dead cells undergo detachment from biofilms, denoting active bioconversion processes and biodegradation, which occur cyclically. The approximate period for each of these phases is shown to the left side of Figure 3.2.

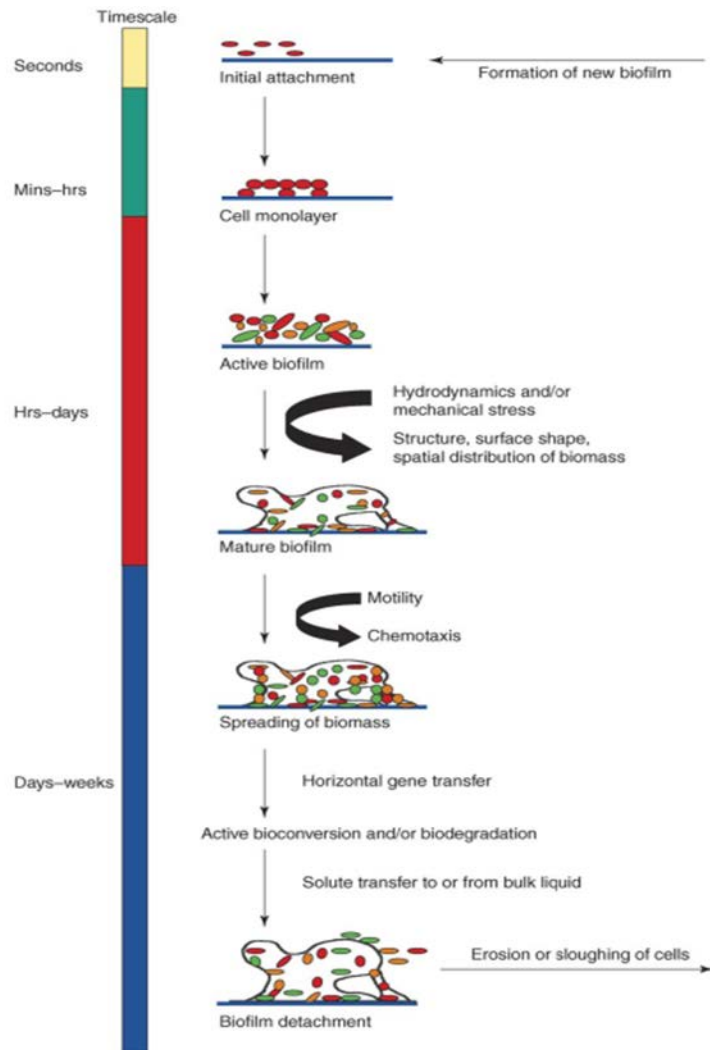


Figure 3.2 Different stages in formation of biofilm [36].

Substrate and oxygen are transported in the biofilm by diffusion and convection. Through the same mechanisms, metabolic products are transported from the biofilm. Oxygen could reach only the outside of the biofilm, thus determining the growth of aerobic microorganisms such as nitrifying bacteria and protozoa. The nitrates and nitrites produced in this layer are reduced by means of the anoxic metabolism in a second intermediate layer. This leads to the formation of a third layer characterized by anaerobic

conditions in direct contact with the solid surface, where acetic acid and sulphates undergo reduction [36].

3.4 Detachment of biofilm

Parts of the biofilm can be dispersed either because of the separation of daughter cells reproduced from the mass of cells or due to the effect of the flow. Detachment due to physical forces has been studied in great detail, providing three main processes through which the cells are separated from the biofilm: erosion—the continuous removal of small portions of the biofilm; sloughing—rapid and massive removal; and abrasion—detachment due to the collision of particles from the bulk of the fluid phase against the biofilm.

The rate of erosion increases with increased thickness of the biofilm and increased shear at the interface of biofilm and fluid. Sloughing is rarer, and is due to the decrease of nutrients or oxygen in the structure of the biofilm. It is commonly observed with thick biofilms made from environments rich in nutrients. Abrasion occurs when the biofilm is used in fluidized beds or filters for bioremediation operations.

3.5 Biofilm reactors

Aggregates of microbial cells, such biofilms, are of great interest in biotechnology and in bioremediation. They offer significant advantages compared to suspended cells. A biofilm, as previously mentioned, is a complex structure and consistent set of cells and cell products [37], realized spontaneously on a solid surface static (static biofilms) or on a carrier (biofilm supported by particles) [38].

Microbial aggregates in the form of biofilm have some key features:

- Separation of the biomass from the effluent is easier in biofilm reactors and the operations of sedimentation and filtration can be eliminated.
- Biofilms (both static biofilms and particle-supported biofilms) have a higher specific surface area than the individual cells suspended.
- The substrates present in a medium (such as oxygen, source carbon and nitrogen) must pass the interface liquid-aggregates and be transported to their site. In an aggregate, the concentration gradient causing transportation is mainly through diffusion. The depth of penetration of the substrates in biofilms depends mainly on the porosity of the biofilm, the substrate concentration in the bulk of the liquid, the transport of substrate through the biofilm-liquid interface and the rate of reaction in the biofilm. For poorly soluble substrates, such as oxygen, the depth of penetration is low (typically 100-150 μM) [39].

The concentration gradient of the substrate leads to a gradient in the speed of growth in the aggregate. In multi-species biofilm this will lead to a biofilm with a layered structure, where bodies with the highest rate of growth will occupy the outer layers of the biofilm, and slower-growing organisms occupy the inner layers [40]. As a result of this organization, organisms that growing slowly will be protected from shear forces, and are thus less prone to detachment and wash-out. Thanks to the small size (typically between 10 and 150 μm) and the high porosity of biofilm supports, transport circulation is generally faster than with suspended cells, (ranging in size usually between 0.5-3 mm). The concentration gradients of the substrate, therefore, are less important in flakes, as compared to biofilms. Reactors based on biofilms are commonly used to treat large volumes of dilute aqueous solutions such as groundwater, municipal water and industrial

water. Among the major biofilm reactors, conventional biofilm systems can be identified as trickling filters or biodisks (DRC), upflow sludge blanket (USB), fluidized bed biofilm reactors (FBR), expanded granular sludge blanket (EGSB), biofilm air lift suspension (BAS) or internal circulation (IC). These reactors include both types of biofilms mentioned above: trickling filters and biodisks use static biofilms, while fluidized bed reactors, upflow anaerobic sludge blanket biofilm reactors and air lift suspension reactors rely upon biofilms supported by particles. In USB, BFB and EGSB reactors, particles supporting the biofilm are fluidized by a stream of liquid rising to the top. BAS refers to a type of suspension obtained through pumping air into the system. In an IC reactor, the product gas drives the circulation and mixing of the liquid and solids as in an air-lift reactor. In the trickling filter and biodisks (DRC), biofilms adhere to support materials invested from the process stream [41].

Considering the important role of formation of biofilm for biodegradation process, selection of the right biofilm support is critical. As mentioned in section 2.2.5, the packed bed reactor (PBR) has been chosen in this study for implementation of aerobic co-metabolic biodegradation of contaminated site due to its advantages.

4 Materials and Methods

This chapter shows experimental and analytical procedures used for the monitoring of the primary substrate and chlorinated solvents, for the analysis of the concentration of biomass and for the determination of chloride ions released upon the biodegradation of the chlorinated solvents.

4.1 Analytical methods

4.1.1 Gas-chromatographic analysis

Measurement of the concentration of the growth substrate and of chlorinated solvents in the liquid phase was carried out by gas chromatographic techniques. Since the compounds have a different nature, two different detectors were used: a flame ionization detector (FID) and an electron capture detector (ECD). The FID is used for compounds in which carbon-hydrogen bonds are present: the compound to be analysed is substantially burned by combining a stream of hydrogen and oxygen and the passage of a flame. The ions contained in the vapours of combustion are discharged on an electrode generating an electric current, which translates into a signal to the instrument. In our case, the FID was used for the measurement of the growth substrate.

For the determination of chlorinated solvents the ECD was used. This detector uses a radioactive isotope of nickel (^{63}Ni) deposited on a gold foil, which emits β radiation ionizing the carrier gas (N_2) and producing electrons and then an electric current. In our case this detector was used for the measurement of chlorinated solvents and oxygen.

In general, gas chromatography measures the concentration of the substrate or of chlorinated solvents in the gas phase. The analysis is carried out upon the head space of a vial within which is inserted the sample liquid; the concentration of solutes in the liquid phase and the total mass of the substrate and chlorinated solvent present in the vial can be traced by means of the following relations, which are valid in the hypothesis of equilibrium between the phases:

$$C_g = H \cdot C_l \quad (4.1)$$

$$m_T = C_l \cdot V_l + C_g \cdot V_g \quad (4.2)$$

where:

m_T = total amount of substrate or solvent [mg or mmol];

C_l and C_g = concentration in the liquid phase and in the gaseous phase [mg/L or mmol/L];

V_l and V_g = volume of the liquid phase and the gas phase [L];

H = dimensionless Henry's constant at 30°C.

For the determination of the compounds, the following methods were used:

For sampling in a manual mode, samples were taken from the headspace of the vials containing the suspension cells and the concentration of chlorinated solvents in gas phase was measured. To make the analysis more accurate, the condition of equilibrium between the liquid phase and the gas phase inside the vial was assured by placing the vials under stirring conditions. The temperature was set at 30°C or 15°C, depending upon the condition of the experiment. To collect the gas from the head space of the vials, a gas-

tight syringe with a volume of 100 μL was used. The volume of the gas taken was negligible compared to the total volume of head space, which approximated 50 to 60 ml.

For this study a HP 6890 gas chromatograph was used.

For automatic sampling, a head space analyzer Agilent 7694E connected to the gas chromatograph was used. This analyzer, connected to the gas chromatograph, is able to withdraw reproducible volumes of the gas in the head space created in the sampling vial. The operation of the analyzer required the preparation of twenty 10 mL vials in a basket. The vials were moved to a heating chamber at the desired temperature and maintained there for a fixed period ("equilibrium time") sufficient to establish equilibrium between the phases. Following injection into the gas chromatograph, the instrument pressurized the vial to successively load a valve. The conditions of temperature and equilibrium time are parameters set by the operator and are of fundamental importance as they may affect the sensitivity and the accuracy of the analysis. The sampling procedure in this study involved the injection of 1 mL of the sample through a syringe into a 10 mL vial closed with a Teflon plug. The vial was then left to equilibrate in a chamber for 15 minutes; the sample was then placed in the analyzer head space, set at a temperature of 40°C with an equilibration time of 30s. Analysis was performed in the manual mode on the headspace of the vial with the inner cell suspension and concentration of the compound in gas phase measured.

4.1.1.1 Calibration of the gas chromatograph

The known and standard concentration of chlorinated solvents were prepared and analyzed with the gas chromatograph. The areas under the peaks related to each standard concentration were evaluated and the correlation coefficient calculated. The analysis was performed twice for each concentration to evaluate the accuracy of the method through

statistic deviation. Calibration of the gas chromatograph (GC) for measuring the growth substrates was carried out by preparing standard and known concentrations. The different volume of gas (growth substrate) was injected into sealed 119 mL vials. Table 4.1 presents the volume and concentration of butane for calibrating the gas chromatograph.

Table 4.1 Standard butane samples for calibration

	V_{butane}	C_{gas}	Area
	(mL)	($\mu\text{mol/L}$)	
A	0.5	173	168
B	2	692	630
C	6	2075	1986
D	20	6916	6475
E	40	13832	12139

Figure 4.1 presents the calibration curve obtained from measuring the standard and known concentration samples. This graph shows the concentration of standards versus measured area under the peaks related to butane.

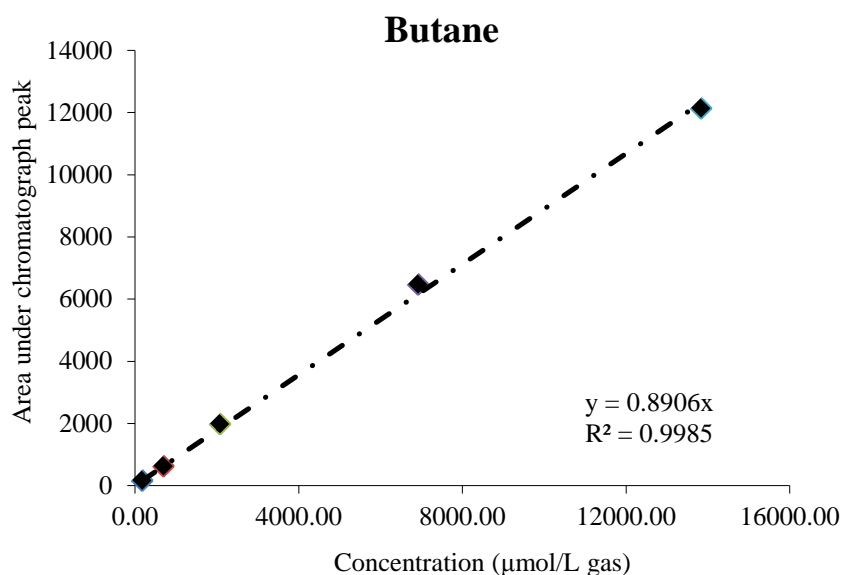


Figure 4.1 Calibration line of butane: chromatographic area vs. concentration of standard

The calibration coefficient is determined through linear regression of the straight line.

The gas chromatograph was also calibrated for the two chlorinated solvents trichlorethylene and 1,1,2,2-tetrachloroethane. Standard solutions with known concentration of these two components were prepared in hexane. First, 500 µL of pure TCE were inserted in a 125 mL flask, and diluted with hexane up to a final concentration of 4.55×10^{-2} mol/L. Next, 60 L of pure TCeA were injected in a 250 mL flask with hexane: the final solution had therefore a concentration of 2.27×10^{-3} mol/L. These samples were used as a stock solutions and different samples with various concentrations were prepared. **Table 4.2** shows the standard concentration of TCE and TeCA and the areas under the peaks related to them.

Table 4.2 TCE and TeCA standard solutions for calibration

Standard TCE				Standard TeCA			
	V_{TCE} (uL)	C_{gas} ($\mu\text{mol/L}$)	Area		V_{TeCA} (uL)	C_{gas} ($\mu\text{mol/L}$)	Area
A	5	1.87	21157	A	5	0.095	891.7
B	10	3.74	41167	B	10	0.191	1598.9
C	20	7.47	82101	C	30	0.572	3918.5
D	30	11.21	122398	D	40	0.762	5272.3
E	40	14.94	165770	E	60	1.143	7981.5

The calibration lines obtained from the calibration of the TEC and TeCA are shown in Figure 4.2 and Figure 4.3. Also in this case, calibration coefficients were calculated from linear regression of the straight lines.

Table 4.3 summarizes the results obtained in the calibration of the growth substrate and chlorinated solvents.

Table 4.3 Calibration coefficients of butane and chlorinated solvents

	Molar mass (g/mol)	Calib. Coeff. (Area $\text{mmol}^{-1} \text{L}^{-1}$) 1)	Calib. Coeff. (Area $\text{mg}^{-1} \text{L}^{-1}$)
BUTANE	58	8906	14.85
TCE	131,35	11026	83947
TeCA	167.85	6978.0	41573

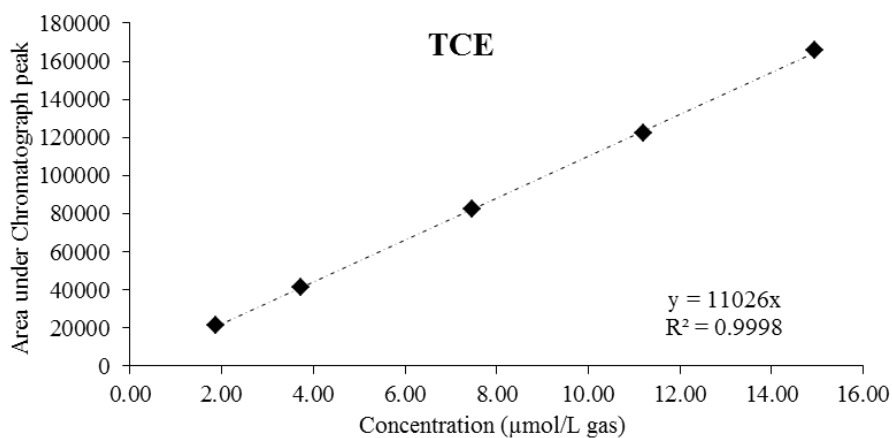


Figure 4.2 Calibration line of TEC

Chromatographic area vs. gas concentration in mol/L

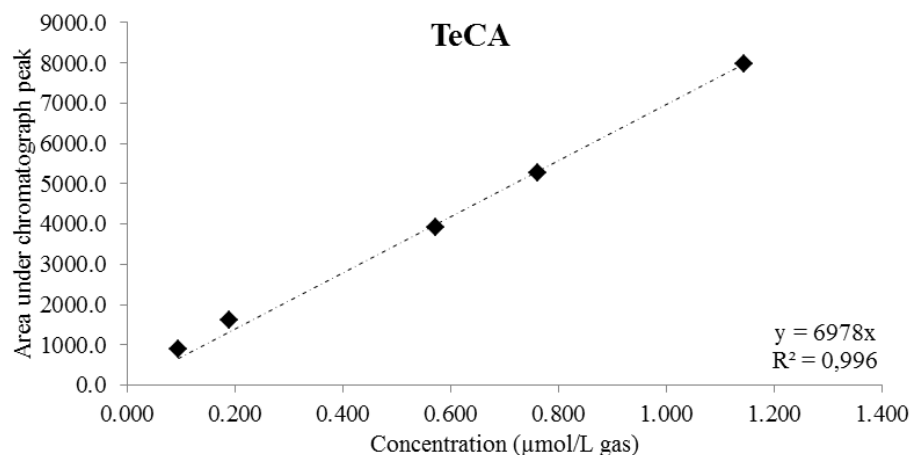


Figure 4.3 Calibration line of TeCA

Chromatographic area vs. gas concentration in mol/L

4.1.2 Biomass analysis

The measurement of biomass formed during the process was a monitoring method in this study: the formation of biomass in the form of suspended cells and those attached to the porous as biofilm was analyzed.

The Lowry method [42] was used for measurement of suspended cells. In this method the amount of cells is determined by measuring the total protein concentration; distinguishing between dead and live cells is therefore not possible in this method.

The Lowry assay is a colorimetric method, effective in determining protein concentrations comprised in a range of 0.01 to 1.0 mg/mL, which combines the reaction of the ion branches with peptide bonds (under alkaline conditions) with the oxidation of aromatic protein residues. It starts from a denaturation of the cells in a basic environment (pH 10-10.5), which leads to disruption of the cell membrane and to the consequent release of the protein content, which reacts with citrate or tartrate of copper (CuII). In the presence of bivalent copper, the peptide bond of the protein complex with the ion reduces it to monovalent copper (CuI). At this point, the copper in its reduced form is capable of

reacting with Folin-Ciocalteu reagent (reactive-phospho-tungstic molybdic acid salified with sodium and potassium, of yellow color, which in an alkaline medium is capable of oxidizing soluble proteins) to produce a complex unstable molecule of blue color, which can be analyzed by the UV-Vis spectrophotometer at a wavelength of 750 nm. The standards for the calibration of the instrument must be prepared each time the analysis is carried out and are composed of different solutions to increasing concentrations of BSA (bovine serum albumin).

For quantification of the attached cells, a certain number of biofilm carriers were taken and washed with water to remove the suspended cells. The carriers were then placed in 1M NaOH and kept under shaking conditions at 77°C. The separated biofilms from carriers were analyzed by the Lowry method as described above.

5 Growth substrate and carrier selection for aerobic co-metabolic biodegradation of CAH

This chapter describes the tests aimed at selecting a suitable bacterial consortium, the best growth substrate and the best performing carrier for the aerobic co-metabolic biodegradation of the two target chlorinated solvents.

5.1 Selection of the best performing growth substrate

The selection of the best substrate and groundwater was articulated in two sub-steps.

- An initial screening extending to five substrates and all the available groundwater was performed at 30°C
- The performance evaluation of the selected consortium at 15°C (annual average temperature of the site)

In the first step, groundwater samples were taken from different locations of the site of Rho, which was contaminated with TCE and TeCA. Five different consortia were chosen from this sample's groundwater. Chemical characterization of the sampled groundwater as well as the concentration of TCE and TeCA is shown in Table 5.1.

Table 5.1 Chemical characterization of studied groundwater

Chemical compound	Concentration (mg/L)
Cl ⁻	27-57
NO ²⁻	0.1-0.8
PO ₄ ³⁻	33-53
NO ²⁻	1.3-2.5
SO ₄ ²⁻	56-274
Suspended solids	54-93
TCE	0.04-5.8
TeCA	0.2-4

The high concentration of TCE and TeCA confirms that this contaminated site is a good case study for aerobic co-metabolic biodegradation.

As reported in the literature [43], chlorinated aliphatic solvents can be biodegraded by a large number of microorganisms which express the enzyme monooxygenase. The synthesis of these enzymes is induced by the presence of a growth substrate, used as a source of carbon and energy. Among these, bacterial species are able to exploit methane [5], toluene [6], phenol [7], ammonia [8], propane [9, 10], butane [11], n-pentane, n-hexane [12] and vinyl chloride [9].

In this study, a set of twenty-five microcosms was set up exposing four samples of groundwater from the contaminated site to five different growth substrates: methane (M), propane (PR), butane (B), pentane (PE) and phenol (F). Samples 1-4 of the groundwater were also mixed to create sample 5.

To reach the goal of selecting the consortium best able to degrade CAH from samples of groundwater, 60 mL of water directly from the contaminated site was placed in a sterile 119 mL glass at 30°C and stirred at 125 rpm. The vials were initially enriched with 2 mg L⁻¹ of growth substrate (methane, propane, butane, pentane or phenol). For 60 days, oxygen, substrate, TCE and TeCA were re-supplied each time their concentration decreased below 1 percent of the initial value. The concentration of TCE, TeCA and growth substrates was monitored for 60 days. Figure 5.1 presents the typical monitoring graph of contaminant and substrate concentration over incubation time.

The substances present or introduced into the microcosm are in equilibrium with the aqueous phase and the gas phase. It is therefore possible to calculate the mass of a generic substance through the following equation:

$$m_i = m_{i,g} + m_{i,l} \quad (5.1)$$

where:

m_i is the total mass

$m_{i,g}$ is the mass in the gas phase

$m_{i,l}$ is the mass is in the liquid phase

Thus, the analysis of the gas phase (via the head space of the vials) allows measurement of the concentration growth substrates in the head space, which is in equilibrium with the

liquid phase. The concentration of growth substrate can be monitored using the following equations:

$$m_{i,g} = C_{i,g} \cdot M_i \cdot V_g \quad (5.2)$$

Henry's law:

$$P_i = H_i \cdot C_{i,l} \quad (5.3)$$

Ideal gas law:

$$P_i = \frac{n_{i,g}}{V_g} \cdot RT \quad (5.4)$$

Therefore, it is possible to express the concentration of the substance in the gas phase as:

$$C_{i,g} = \frac{H_i}{RT} \cdot C_{i,l} \quad (5.5)$$

The Henry's law constant can be expressed in a dimensionless form as shown below:

$$H^{\circ}_i = \frac{C_{i,g}}{C_{i,l}} \quad (5.6)$$

$$H^{\circ}_i = \frac{H_i}{RT} \quad (5.7)$$

Furthermore, gas chromatographic analysis provides the following equation:

$$C_{i,g} = \frac{Area}{f_{cal}} \quad (5.8)$$

where:

$C_{i,g}$ is the molar concentration in the gas phase (mol/L)

$C_{i,l}$ is the molar concentration in the liquid phase (mol/L)

M_i is the molecular weight of the generic substance (g/mol)

V_g is the gas volume (L)

P_i is the partial pressure of the gas on the solution (atm)

H_i is the Henry's constant, typical of each gas, which correlates with the pressure of the gas

on the solution and its concentration (LATM/mol)

H°_i is the dimensionless Henry constant

f_{cal} is the calibration coefficient

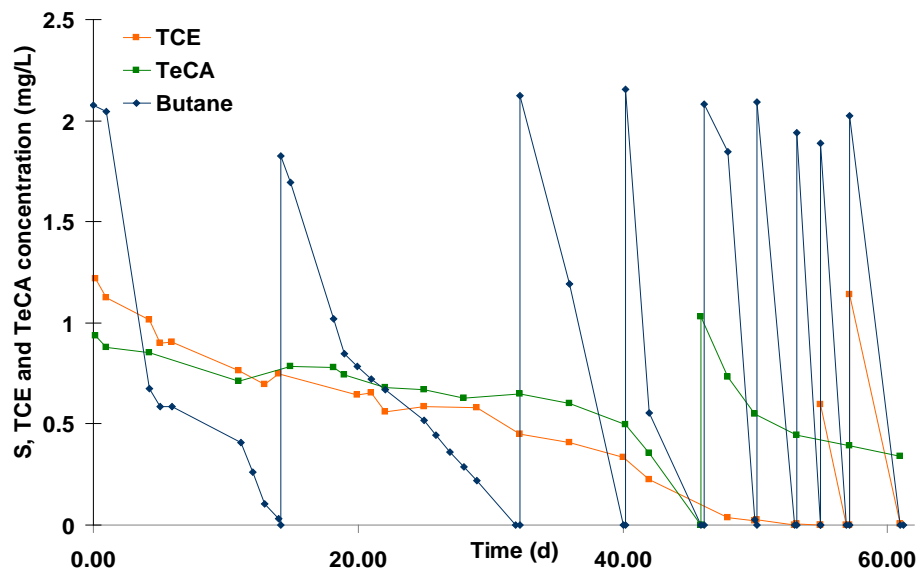


Figure 5.1 Batch test for growth substrate selection: concentrations in the aqueous phase versus time for substrate (butane), TCE and TeCA, for a representative case

For all microcosms, after a varied latency phase, the degradation rate of substrate consumption is increased after the first pulse, and then stabilizes to a threshold value. This increase in speed is due to a progressive increase of biomass in the relevant

consumer of the growth substrate, but also due to the selective pressures to which it is subjected in the microenvironment. The same trend is also found at this early pulse of chlorinated solvents (TCE and TeCA), although they did not follow the same behavior in all microcosms fed with different growth media.

On the basis of the normalized net biodegradation rates relative to the last TCE and TeCA pulse ($r_{TCE,30}/c_{TCE}$ $r_{TeCA,30}/c_{TeCA}$), the following substrate/groundwater combinations were selected and subjected to the standardized kinetic test described in the Materials and Methods section: M1, M4, PR2, PR4, B4, B5, PE1, PE4 —where the numbers represent the specific sample of groundwater and M, PR, B and PE represent methane, propane, butane and pentane (the growth substrate in each microcosm).

The substrate, TCE and TeCA first-order biodegradation constants $k_{1,S,30}$, $k_{1,TCE,30}$ and $k_{1,TeCA,30}$ relative to the eight selected combinations shown in Figure 5.2 were obtained by dividing the values of $r_{S,30}/c_S$, $r_{TCE,30}/c_{TCE}$ and $r_{TeCA,30}/c_{TeCA}$ relative to the kinetic tests by the biomass concentrations evaluated at the beginning of each pulse.

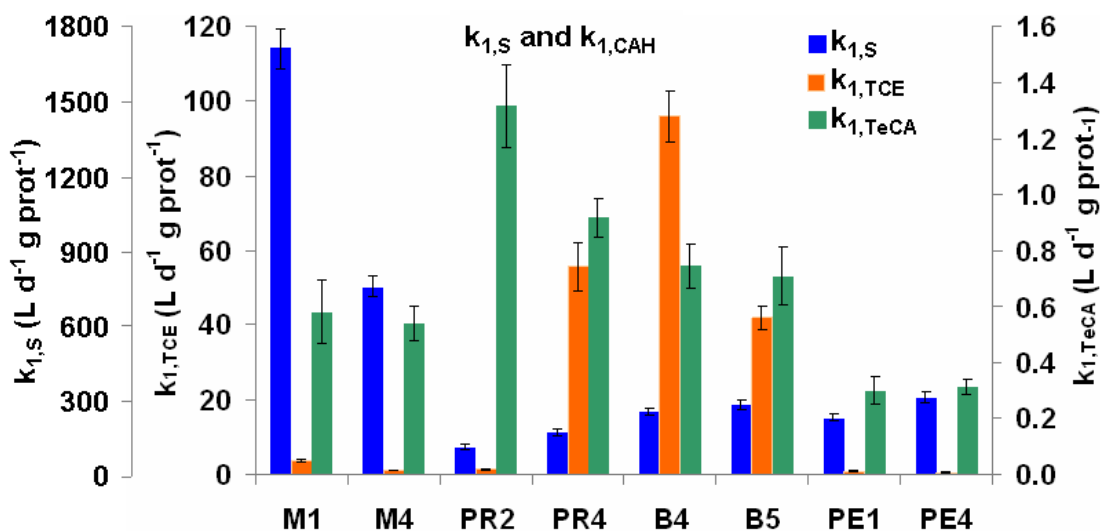


Figure 5.2 First-order kinetic constant of substrates, TCE and TeCA at 30°C

In agreement with most studies on CAH aerobic co-metabolism [10], in each consortium both $k_{1,TCE,30}$ and $k_{1,TeCA,30}$ were significantly lower than $k_{1,S,30}$. The substrate first-order constants $k_{1,S,30}$ were not considered in the selection of the best-performing consortium: indeed, a high $k_{1,S}$ is not necessarily a favourable condition in aerobic co-metabolic processes, as it might in a PBR lead to a complete substrate depletion in the first bioreactor portion, leaving the remaining portion inactive towards target CAHs. With the exception of consortium PR2, for all the other consortia $k_{1,TeCA,30}$ was significantly lower than $k_{1,TCE,30}$ (average $k_{1,TeCA,30}/k_{1,TCE,30} = 0.23$). Thus, $k_{1,TeCA}$ was not considered in the selection of the best-performing microbial consortium, and adding a pretreatment step to convert TeCA to TCE was evaluated. On the basis of the 30°C data, the coupling of butane and groundwater sample 4 (corresponding to consortium B4) was thus identified as best performing, thanks to its high $k_{1,TCE,30}$ ($96 \text{ L g}_{\text{protein}}^{-1} \text{ d}^{-1}$).

In the second step, the performance of the B4 consortium on uptake of TCE was tested at 15°C. The test procedure was repeated for another set of batch suspended cell bioreactors at 15°C. The pulses of oxygen, butane, TCE and TeCA were supplied for three months to the microcosm, and the standard kinetic study was repeated. The kinetic test conducted with the consortium B4 after three months of microbial growth at 15°C led to a $k_{1,TCE}$ equal to $22 \text{ d}^{-1} \text{ g}_{\text{prot}}^{-1} \text{ L}$. Thus, as presented in Figure 5.3, a decrease in temperature from 30°C to 15°C resulted in a drop in first-order constant ($k_{1,TEC}$) of more than four times, in studies conducted on cell suspension of the consortium selected.

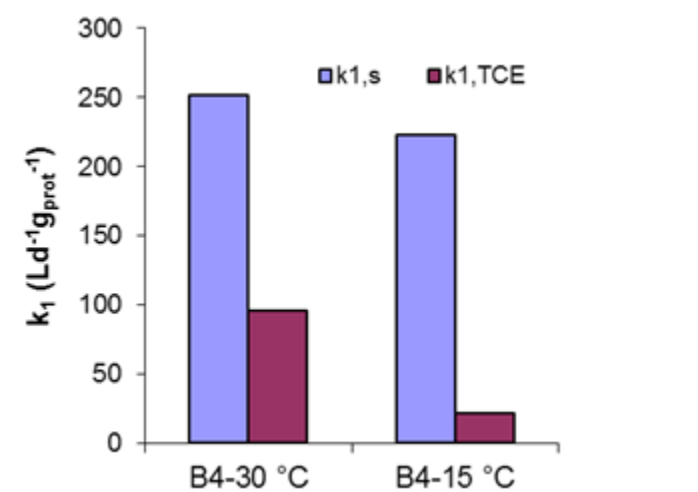


Figure 5.3 First-order kinetic constants of butane and TCE at 15°C

5.2 Evaluation of the abiotic pre-treatment step to convert TCE to TeCA

To evaluate the possible abiotic pre-treatment of TeCA to TCA, a new set of sterile glass vials was provided, and the depletion rate of TeCA to TCE at different pH was monitored. As shown in Figure 5.4a, the rates of TeCA depletion at pH 10.0 and 30°C were satisfactorily matched to a first-order model ($R^2 = 0.990$), in agreement with the indications of the literature [42]. Further, the first-order constants of TeCA elimination ($k_{1,TeCA,30,abio}$) obtained at 30°C at different pHs in the 6.5-10.1 range were in good agreement ($R^2 = 0.946$) with the corresponding theoretical values estimated on the basis of the model proposed by Joens *et al.* [42]. Joens' model was also used to evaluate the values of $k_{1,TeCA,15,abio}$ in the 6.5-10.1 pH range (Figure 5.4b). Further control tests indicated that neither the presence of biofilm carriers nor the replacement of the synthetic groundwater with site water (sample 1) had any effect on the first-order constant of TeCA conversion to TCE. The rates of TeCA abiotic depletion (calculated at each TeCA concentration tested in the viable microcosms from the values of $k_{1,TeCA,30,abio}$ and $k_{1,TeCA,15,abio}$ estimated at pH 7) varied between 1 and 8 percent of the TeCA rates

obtained in the viable tests. All TCE and TeCA biodegradation rates reported in this work are net biodegradation rates, calculated by subtracting the abiotic contribution to the depletion rates obtained in the tests with viable biomass.

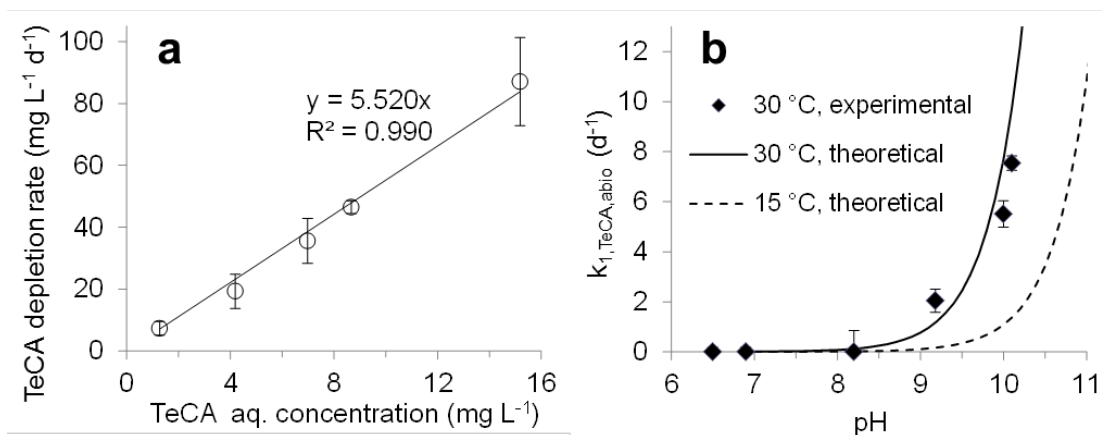



Figure 5.4 depletion rate of TeCA to TCE in an abiotic reaction

5.3 Selection of the best biofilm carrier

This step evaluates formation of biofilm on selected consortia. To this end, four commercially available biofilm carriers were chosen: Biomax®, Biopearl®, Cerambios® and Biomech®, all specifically designed to be biofilm carriers. Table 5.2 shows the characteristics of each carrier.

Table 5.2 Selected biofilm carrier for the test

Name	Biomax®	Biomech®	Cerambios®	Biomech®
Material	Ceramic	Ceramic	Ceramic	Sintered glass
Porosity(%)	60	64	74	58
Density (kg/L)	0.66	0.68	0.66	0.95
Image				

Three sets of experiment were performed to evaluate the performance of the selected carriers:

- Attached cells in batch test at 30°C
- Attached cells in batch test at 15°C
- Attached cells in a continuous flow test at 30 °C

TCE normalized degradation rates ($r_{TCE,15}/c_{TCE}$ and $r_{TCE,30}/c_{TCE}$) of the attached cell concentrations were measured and compared for each test.

5.3.1 Performance of biofilm carriers in batch test at 30 °C

The batch tests at 30°C were carried out by inoculating 10 percent of the selected consortium into four small bioreactors with batch volume of 119 mL, each containing 60 mL of one of the supports preselected, and 50 ml of consortium B4. To achieve a sufficient amount of biomass, a series of pulses of butane, each equal to a concentration in the liquid phase of 2 mg/L, were injected. Furthermore, in order to reduce the suspended biomass to a negligible level, before each pulse the substrate media were washed in saline (NaCl 9 g/L in de-ionized water) and supplied with 50 mL of sterilized water, always in the presence of TCE and TeCA (with a concentration in the liquid phase of 1 mg/L). Figures 5.5, Figure 5.6, Figure 5.7 and Figure 5.8 show the concentrations of butane as a growth substrate, TCE, and TECA for each carrier tested, conducted at 30°C.

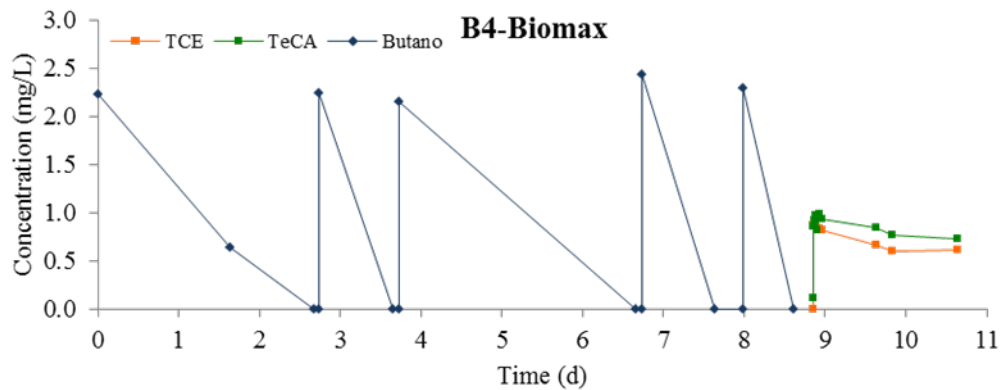


Figure 5.5 performance of biofilm carrier Biomax in a batch test at 30°C

Concentrations in the aqueous phase versus time for substrate (butane), TCE and TeCA.

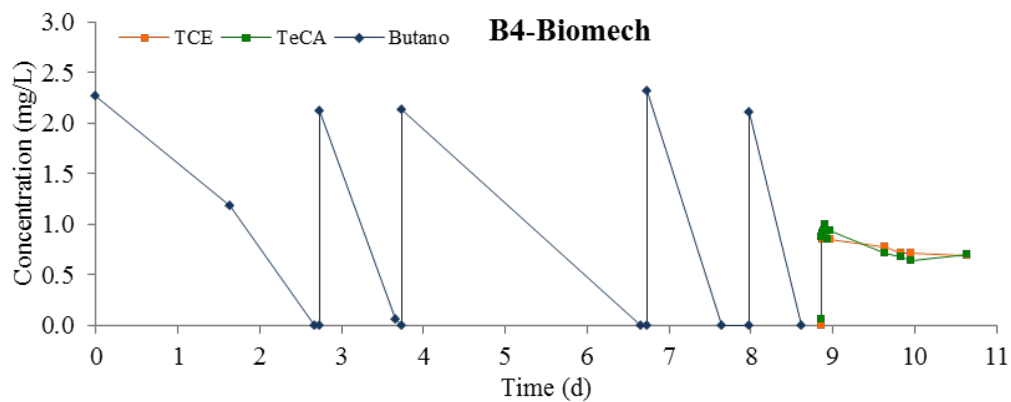


Figure 5.6 performance of biofilm carrier Biomech in a batch test at 30°C

Concentrations in the aqueous phase versus time for substrate (butane), TCE and TeCA.

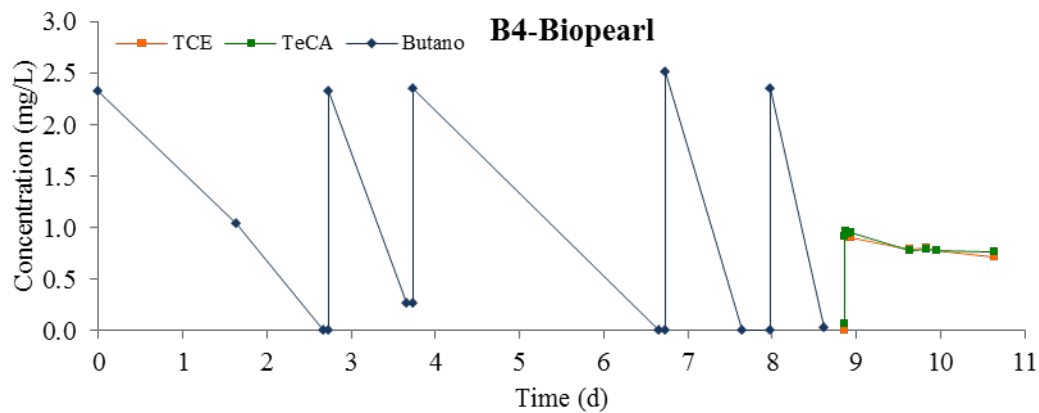


Figure 5.7 performance of biofilm carrier Biopearl in a batch test at 30°C

Concentrations in the aqueous phase versus time for substrate (butane), TCE and TeCA.

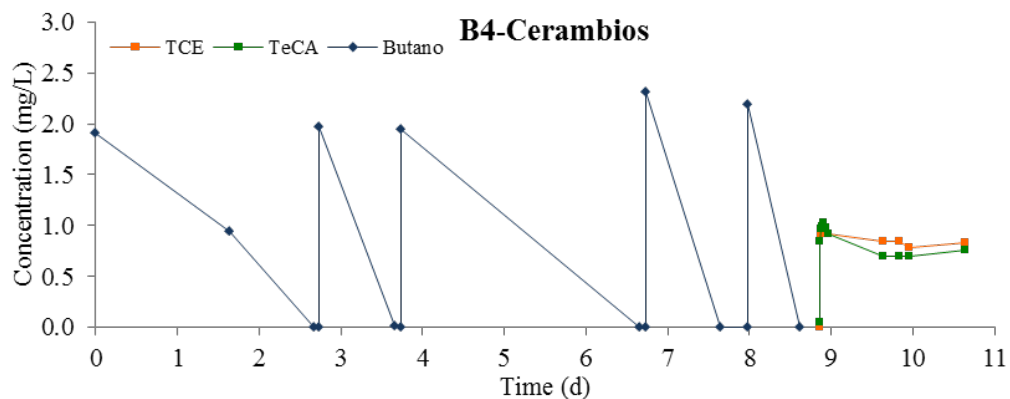


Figure 5.8 Performance of biofilm carrier Cerambios in a batch test at 30°C

Concentrations in the aqueous phase versus time for substrate (butane), TCE and TeCA.

Based on the concentration of TCE over time, the TCE normalized degradation rate ($r_{TCE,15}/c_{TCE}$ and $r_{TCE,30}/c_{TCE}$) was calculated. Table 5.3 presents the results.

Table 5.3 Degradation rates of TCE at 30 °C in the biofim batch test

Vial	r_{TCE} (mg/L ⁻¹ d ⁻¹)	c_{TCE} (mgL ⁻¹)	r_{CE}/c_{TCE} (d ⁻¹)
B4-Biomax	0.415	0.9	0.464
B4-Biomech	0.181	0.9	0.206
B4-Biopearl	0.183	0.9	0.200
B4-Cerambios	0.122	0.9	0.131

5.3.2 Performance of biofilm carriers in batch test at 15°C

The set of batch reactors was prepared as explained in section 5.3.1. In these tests the initial inoculum was withdrawn from the bioreactor containing the selected consortium at 15°C.

Figures 5.9, 5.10, 5.11 and 5.12, below, show the concentrations of butane as a growth substrate, TCE and TECA for each type of tested carrier, conducted at 15°C.

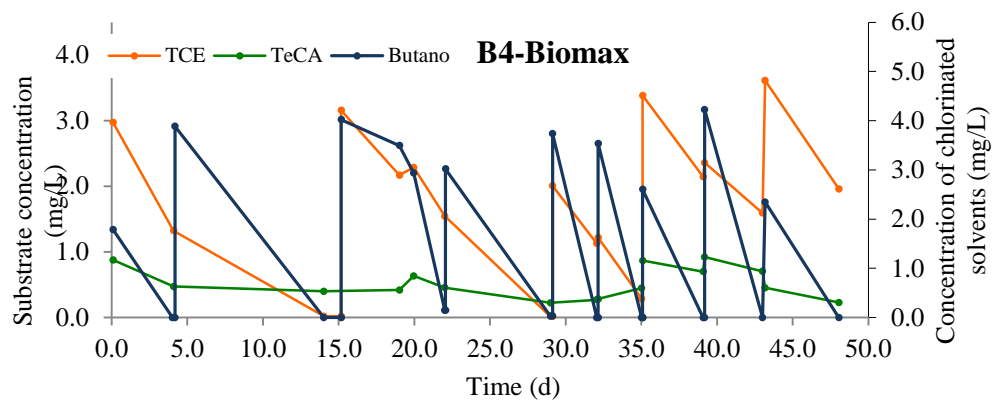


Figure 5.9 Performance of biofilm carrier Biomax in a batch test at 15°C

Concentrations in the aqueous phase versus time for substrate (butane), TCE and TeCA.

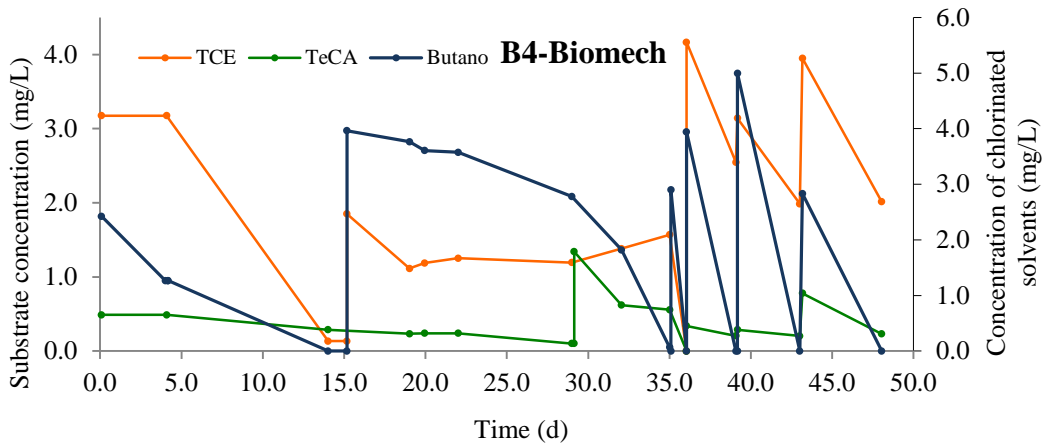


Figure 5.10 Performance of biofilm carrier Biomech in a batch test at 15°C

Concentrations in the aqueous phase versus time for substrate (butane), TCE and TeCA.

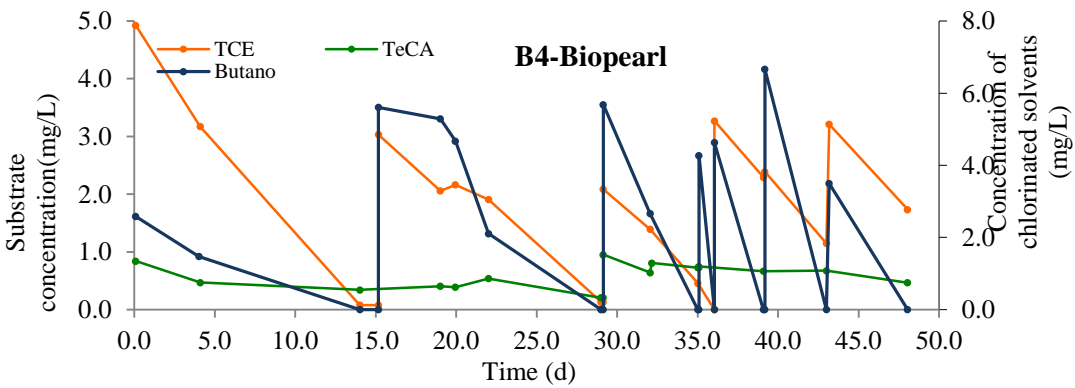


Figure 5.11 Performance of biofilm carrier Biopearl in a batch test at 15°C

Concentrations in the aqueous phase versus time for substrate (butane), TCE and TeCA.

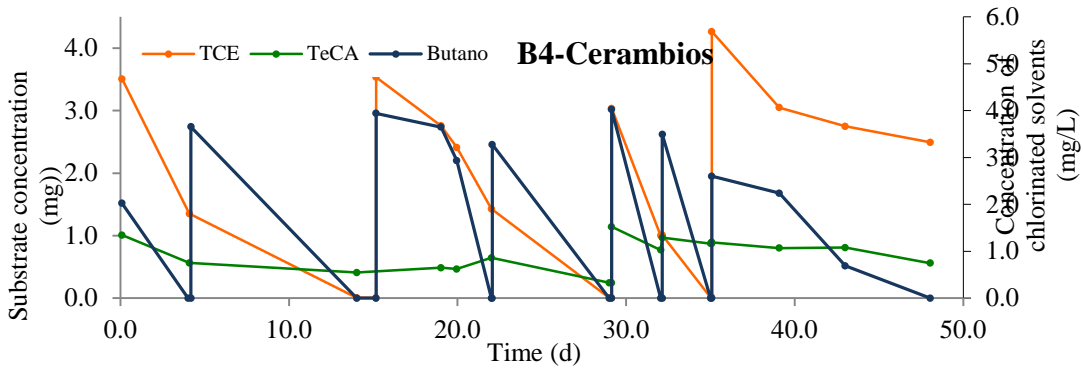


Figure 5.12 Performance of biofilm carrier Cerambios in a batch test at 15°C

Concentrations in the aqueous phase versus time for substrate (butane), TCE and TeCA.

Based on the concentration of TCE over time, the TCE normalized degradation rate ($r_{TCE,15}/c_{TCE}$ and $r_{TCE,30}/c_{TCE}$) was calculated. Table 5.4 presents the results.

Table 5.4 Degradation rate of TCE at 15 °C in the biofilm batch test

Vial	r_{TCE} (mg/L ⁻¹ d ⁻¹)	C_{TCE} (mgL ⁻¹)	r_{TCE}/C_{TCE} (d ⁻¹)
B4-Biomax	0.33	0.8	0.41
B4-Biomech	0.27	0.8	0.34
B4-Biopearl	0.18	0.8	0.23
B4-Cerambios	0.15	0.8	0.19

5.3.3 Performance of biofilm carriers in continuous flow test at 30°C

The performance of different carriers in terms of biofilm formation and normalized TCE degradation rate was also investigated under continuous flow conditions. To this end, four glass columns each with a volume of one liter were filled with different biofilm carriers. These columns were connected to pumps supplying oxygen and butane in separated pulses. Sampling valves were designed along each column to control the concentration of growth substrate and TCE along the column. The outlet of each column passed through glass vials filled with activated carbon before discharging the effluent.

Figure 5.13 shows a diagram of four columns used for testing biofilm formation on different carriers in a continuous flow test. Stainless steel was selected for the piping lines in order to avoid the absorption of substrates through the pipes. In order to minimize the competitive inhibition of the substrate on the chlorinated solvent and to distribute the growth of biomass as uniformly as possible along the columns, alternating pulses of oxygen and butane were fed into the columns. A flask containing a high concentration of biomass (prior to the test, biomass culture was produced in a fermenter) was connected and fed into the circulating mode of the columns hydraulically for two days to immobilize the cells on the carriers.

After immobilization of the cells, the columns were connected to a continuous flow of tap water mixed with TCE at a concentration of 1-3 mg/L and alternating pulses of oxygen and butane for 100 days. The test was performed at 30°C.

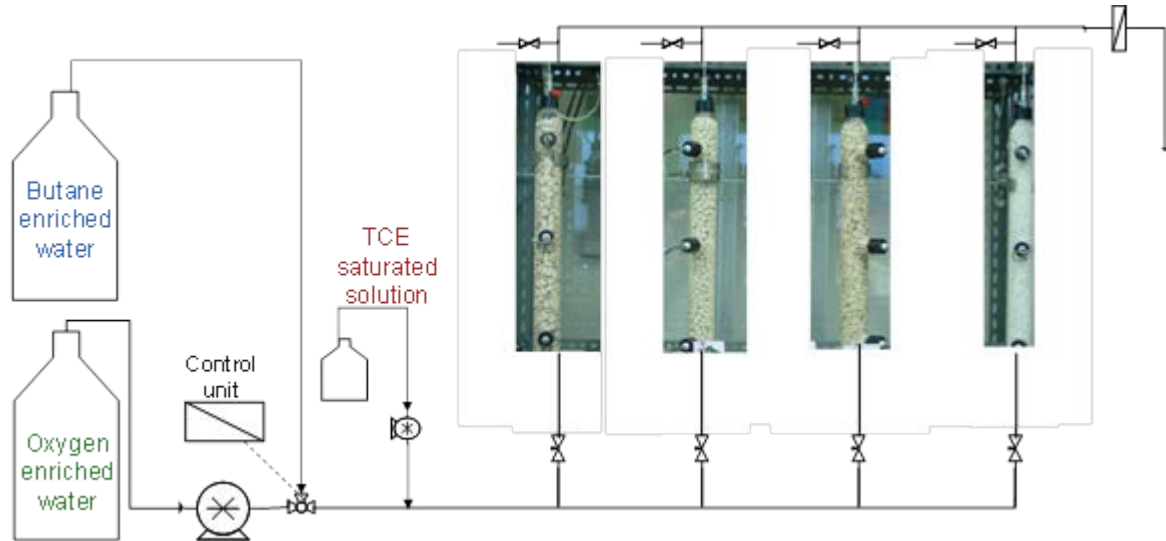


Figure 5.13 diagram of columns in a continuous flow test for carrier selection

This test was operated using normal tap water since at startup time the samples of water from the Rho site were not available in the lab.

The normalized TCE degradation rate and the concentration of biofilm attached to each type of carriers were calculated: Figure 5.14 compares the TCE normalized degradation rate ($r_{TCE,15}/c_{TCE}$ and $r_{TCE,30}/c_{TCE}$) obtained from batch tests at 30°C and 15°C, as well as the results of the continuous flow test at 30°C.

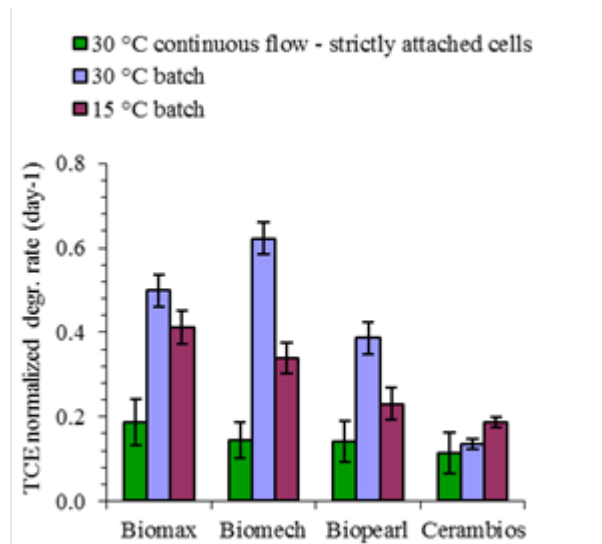


Figure 5.14 Performance of four different carriers in terms of normalized TCE degradation rate

The continuous flow test at 30°C (green), batch test at 30°C (blue) and batch test at 15°C (purple)

The values of r_{TCE}/c_{TCE} are highest for the batch test at 15 °C and the continuous flow test at 30°C when Biomax is used as the carrier of biofilms. For the batch test at 30°C the Biomech carrier had the highest value. Notably, the degradation rate of TCE in the continuous flow test is markedly lower than in the batch tests.

The performance of carriers in the formation of biofilm was also compared, with results shown in Figure 5.15. The concentration of attached cells on Biomax was highest in batch tests at 30°C and 15°C and second-highest in the continuous flow test. Again, the

formation of biofilm in the continuous flow test is significantly lower than in batch tests with the same carriers.

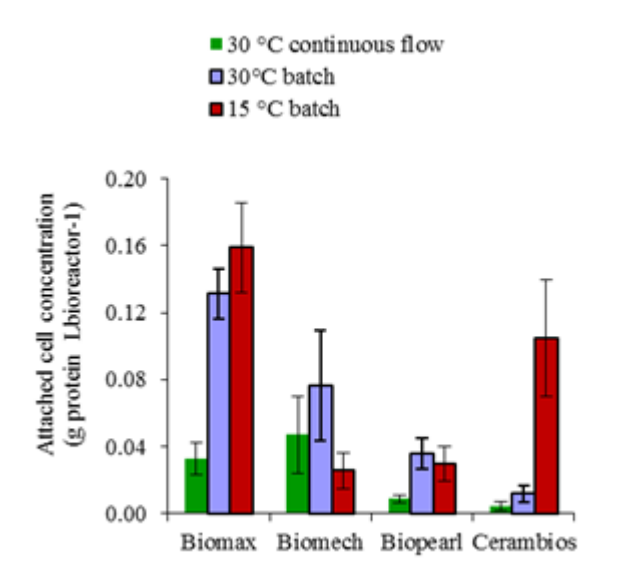


Figure 5.15 Concentration of attached cells formed on four different carriers

Based on a comparison of these results, the Biomax carrier was chosen as the carrier for the packed bed reactor (PBR).

6 Kinetic study of TCE and butane biodegradation by the selected consortium

The kinetic modelling of the aerobic co-metabolic biodegradation of chlorinated solvents is a crucial step to designing an on-site process for the bioremediation of contaminated groundwater sites. Different model types related to co-metabolic biodegradation of chlorinated solvents have been proposed in the literature [5, 10]. These models differ in the inhibition between growth substrate and the chlorinated solvent (or between different chlorinated solvents), the toxicity of the product of processing and the biodegradation of chlorinated solvents in the absence of growth substrate. Of particular note, the application of different inhibition models can lead to significantly different concentrations of contaminants in the process effluent [45, 46].

In this chapter, the kinetic study of TCE and butane uptake in presence of the selected consortium is described in both suspended cell batch tests at 30°C and attached cells on the selected biofilm carrier (Biomax) in batch tests at 30°C.

The results of these tests were used to evaluate the adaptability of the Michaelis-Menten kinetic model (equation 6.1) and identify a model to describe the phenomena of inhibition of the growth substrate (butane) and uptake of the co-metabolic substrate (TCE) in each test.

$$q = \frac{q_{\max} \cdot S}{K_s + S} \quad (6.1)$$

where:

q is the specific degradation rate

q_{max} is the maximum specific rate

S is the substrate concentration

K_s is the affinity constant of the substrate

Since the enzyme catalyzing the reaction of co-metabolism biodegradation can react with various substrates, there may be competition for uptaking primary and co-metabolic substrate during the biodegradation process. This phenomenon, called competitive inhibition (equation 6.2), causes a decrease in enzyme affinity for each substrate and ultimately a decrease in specific biodegradation of each substrate. The competitive inhibition between growth substrate and co-metabolic substrate has been observed in several microorganisms using monooxygenase.

$$q = \frac{q_{max} \cdot S}{K_s \left(1 + \frac{I}{K_i} \right) + S} \quad (6.2)$$

where:

q is the specific degradation rate

q_{max} is the maximum specific rate

S is the substrate concentration

K_s is the affinity constant of the substrate

I is the inhibitor concentration

K_i is the inhibition constant

However, other types of inhibitions may also occur during aerobic co-metabolic biodegradation of chlorinated solvents, such as non-competitive inhibition (equation 6.3) and a-competitive (or uncompetitive) inhibition (equation 6.4). Non-competitive inhibition causes a decrease in the maximum reaction rate without a decrease in the affinity of the substrate for the enzyme. A-competitive inhibition, by contrast, occurs when the inhibitor binds reversibly to the enzyme-substrate complex, forming an inactive complex enzyme-substrate-inhibitor. A-competitive inhibition is a reduction of the enzyme-substrate complex, adversely affecting both the maximum specific rate of degradation and the affinity of the enzyme for the substrates.

$$q = \frac{q_{\max} \cdot S}{K_s \left(1 + \frac{I}{K_i}\right) + S \left(1 + \frac{I}{K_i}\right)} \quad (6.3)$$

$$q = \frac{q_{\max} \cdot S}{K_s + S \left(1 + \frac{I}{K_i}\right)} \quad (6.4)$$

where:

q is the specific degradation rate

q_{\max} is the maximum specific rate

S is the substrate concentration

K_s is the affinity constant of the substrate

I is the inhibitor concentration

K_i is the inhibition constant

6.1 Kinetic study of substrate uptake in suspended cell batch tests at 30°C

Kinetic studies of the consortium in suspended form were conducted in a batch bioreactor with a volume of either 11 or 119 mL. Each experimental condition was studied in triplicate. Tests were conducted in the presence of only the growth substrate (butane) or co-metabolic substrate (TCE). The effect of inhibition was then evaluated when the growth substrate and the co-metabolic substrate are simultaneously present in the growth medium.

6.1.1 Kinetic study of butane uptake in the suspended cell batch test

This test was conducted in 11 mL glass vials containing 5 mL of suspended cell consortium with a defined biomass concentration in each vial. The vials were sealed and oxygen fluxed in each vial for 5 minutes to provide aerobic conditions. In order to evaluate the effects of butane concentration on its degradation, different amounts of butane were injected into the vials for varied concentrations of butane in the aqueous phase. Twelve experimental conditions with increasing initial concentrations of butane in the liquid phase were prepared in triplicate. These microcosms were kept at 30°C and stirred at 125 rpm, and subjected to continuous gas chromatographic analysis in order to detect the variation of the concentration of butane over time.

The Michaelis-Menten kinetic model was used to interpret the experimental data, and the following mass balance was used for the consumption of butane, in the absence of chlorinated solvent in the cell suspension, under the assumption of liquid/gas equilibrium:

$$-\frac{dC_{but}}{dt} \left(1 + H_{but,30} \cdot \frac{V_g}{V_l}\right) = R_{but, susp} \quad (6.5)$$

$$q_{but, susp} = \frac{R_{but, susp}}{X_0} = \frac{q_{max, but, susp} \cdot C_{but}}{K_{s, but, susp} + C_{but}} \quad (6.6)$$

where:

C_{but} is the initial concentration of butane in the liquid phase ($\text{mg}_{but}\text{L}^{-1}$).

$H_{but, 30}$ is the dimensionless constant for liquid/gas equilibrium of butane at 30°C.

V_g is the volume of the head space of the bioreactor batch (L).

V_l is the volume of the liquid phase of the batch bioreactor (L).

$R_{but,susp}$ is net consumption rate of butane in suspended cell test ($\text{mg}_{but}\text{L}^{-1}\text{d}^{-1}$).

X_0 is the concentration of the biomass ($\text{mg}_{prot}\text{L}^{-1}$) measured at the beginning of the pulse.

$q_{but, susp}$ is the initial specific butane uptake rate in the suspended cell test ($\text{mg}_{but}\text{mg}_{prot}^{-1}\text{d}^{-1}$).

$q_{max,but,susp}$ is the maximum specific depletion rate of butane in tests with suspended biomass ($\text{mg}_{but}\text{mg}_{prot}^{-1}\text{d}^{-1}$).

$K_{s, but, susp}$ is the affinity constant of the enzyme for butane in tests with suspended biomass ($\text{mg}_{but}\text{L}^{-1}$).

Therefore, the initial specific degradation rate of butane $q_{but,susp}$ as the ratio of net consumption rate of butane to the total concentration of biomass could be calculated.

Figure 6.1 shows the trend of the specific depletion rate of butane ($q_{but, susp}$) as a function of the initial concentration of butane aqueous phase (C_{but}).

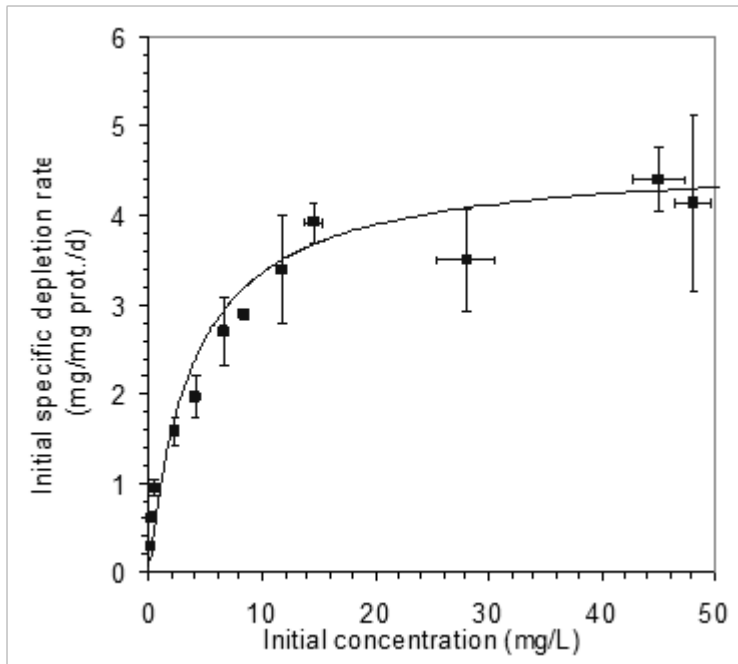


Figure 6.1 Initial specific depletion rate of butane versus initial concentration of butane in a suspended cell batch reactor at 30°C

As shown in Figure 6.1, the initial concentration of butane in the aqueous phase and the value of initial specific depletion rate of butane have a positive correlation. The maximum depletion rate of butane in suspended cell ($q_{max, but, susp}$) is equal to 4.5 $\text{mg}_{but}\text{mg}_{prot}^{-1}\text{d}^{-1}$. The affinity constant of the enzyme ($k_{s, but, susp}$), which represents the concentration of substrate necessary to ensure that the reaction takes a specific rate of biodegradation equal to half of the maximum speed, has been estimated at 4 mgL^{-1} . This trend is adaptable to the Michaelis-Menten kinetics described. These values are obtained by the method of least squares, by simulating the performance of specific rate versus the initial concentration of butane.

6.1.2 Kinetic study of TCE uptake in the suspended cell batch test

The kinetic study of TCE on the suspended biomass was carried out in batch bioreactors with a volume of 119 mL, containing 60 mL of suspended cell taken directly from the fermenter. The batch reactors were introduced to different concentrations of TCE in the aqueous phase. In order to evaluate the possible abiotic reactions (such as adsorption of TCE by the reactor's cap), negative control batch reactors containing sodium azide (NaN_3) were also prepared. The microcosms were maintained at 30°C, stirred at 125 rpm and subjected to continuous gas chromatographic analysis to detect the variation of concentration of the chlorinated solvent over time. The Michaelis-Menten model was used to interpret the experimental data, and as shown in equations 6.7 and 6.8 the following mass balance was used to study the reaction of biodegradation of TCE, under the assumption of liquid/gas equilibrium and in the absence of growth substrate:

$$-\frac{dC_{TCE}}{dt} \left(1 + H_{TCE,30} \cdot \frac{V_g}{V_l}\right) = R_{TCE, susp} \quad (6.7)$$

$$q_{TCE, susp} = \frac{R_{TCE, susp}}{X_0} = \frac{q_{\max, TCE, susp} \cdot C_{TCE}}{K_{s, TCE, susp} + C_{TCE}} \quad (6.8)$$

where:

C_{TCE} is the initial concentration of TCE in the liquid phase ($\text{mg}_{\text{TCE}}\text{L}^{-1}$).

$H_{TCE, 30}$ is the dimensionless liquid/gas equilibrium constant of TCE at 30°C.

V_g is the head space volume of the batch bioreactor (L).

V_l is the liquid phase volume of the batch bioreactor (L).

$R_{TCE, susp}$ is the net degradation rate of TCE ($\text{mg}_{\text{TCE}}\text{L}^{-1}$).

X_0 is the biomass concentration ($\text{mg}_{\text{prot}}\text{L}^{-1}$) measured at the beginning of the pulse.

$q_{TCE, \text{ susp}}$ is the specific degradation rate of TCE in the suspended cell batch test ($\text{mg}_{\text{TCE}}\text{mg}_{\text{prot}}^{-1}\text{d}^{-1}$).

$q_{\text{max}, TCE, \text{ susp}}$ is the maximum specific degradation rate of TCE in the suspended cell batch test ($\text{mg}_{\text{TCE}}\text{mg}_{\text{prot}}^{-1}\text{d}^{-1}$).

$K_s, TCE, \text{ susp}$ is the affinity constant of the enzyme for TCE in the suspended cell batch test ($\text{mg}_{\text{TCE}}\text{L}^{-1}$).

Based on the results of this experiment the specific initial degradation rate of TCE in suspended cell batch test at 30 °C ($q_{TCE, \text{ susp}}$) was calculated.

Figure 6.2 shows the trend of the specific degradation rate of TCE versus the initial concentration of TCE in the aqueous phase in different experimental conditions.

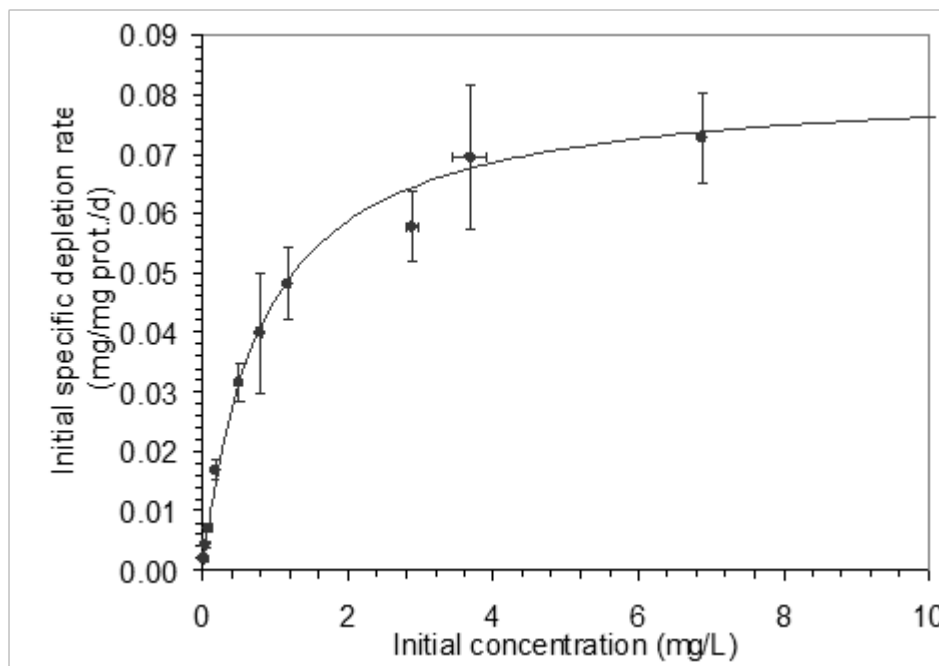


Figure 6.2 Initial specific depletion rate of TCE versus initial concentration of

butane in the suspended cell batch reactor at 30 °C

The experimental data agrees with the Michaelis-Menten kinetic model. The value of the initial specific depletion rate of TCE positively correlates with initial concentration of this compound in the aqueous phase and reaches a maximum depletion rate ($q_{max, TCE, susp}$) of up to $0.08 \text{ mg}_{TCE}\text{mg}_{prot}^{-1}\text{d}^{-1}$. The affinity constant of the enzyme ($k_{s, TCE, susp}$), representing the concentration of substrate necessary to ensure the reaction takes a specific rate of biodegradation equal to half of the maximum speed, has been estimated at 0.8 mgL^{-1} .

6.1.3 Kinetic study of butane uptake in the presence of TCE in the suspended cell batch test

The kinetic study of butane was carried out in the presence of a constant concentration of TCE in the aqueous phase (around 0.5 mg L^{-1}). The effect of TCE on the biodegradation of butane was evaluated and the initial specific depletion rate of butane in presence of TCE was calculated against different initial concentrations of butane. To determine the type of inhibition (i.e. competitive, a-competitive and non-competitive), the $q_{max, but, susp}$ and $k_{s, but, susp}$ determined in the butane kinetic test were used as input parameters to estimate the inhibition constants ($K_{iTCE, but, susp}$) for three different inhibition models. Competitive inhibition best represented the experimental data, selected on the basis of the coefficient R^2 (equation 6.9).

$$q_{but, susp} = \frac{q_{max, but, susp} \cdot C_{but}}{K_{s, but, susp} \cdot \left(1 + \frac{C_{TCE}}{K_{iTCE, but, susp}}\right) + C_{but}} \quad (6.9)$$

Figure 6.3 presents the effect of TCE on butane uptake by comparing the initial specific depletion rate of butane versus the initial concentration of this compound with and without the presence of a constant amount of TCE in the aqueous phase.

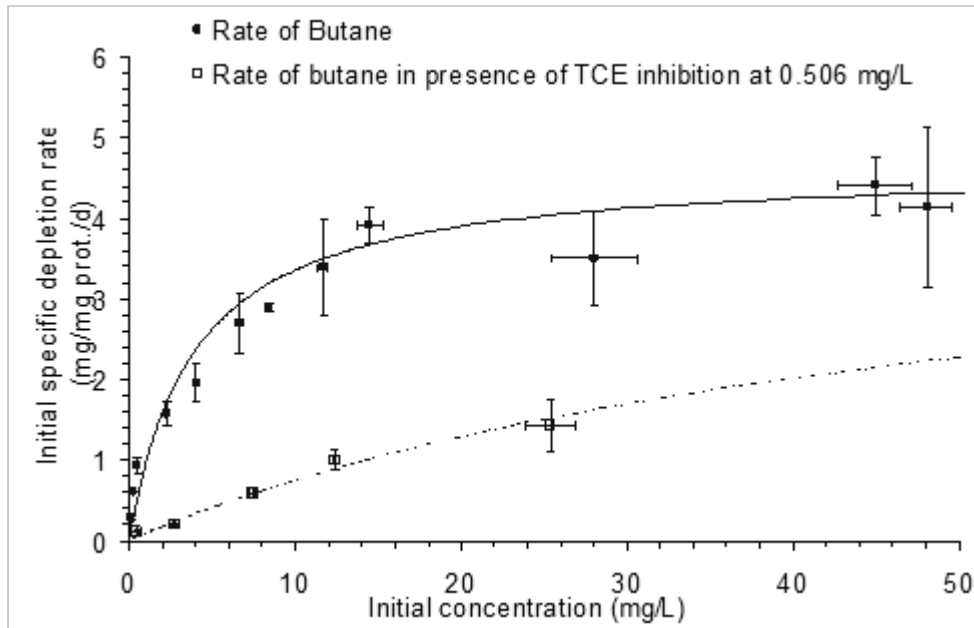


Figure 6.3 Effect of TCE inhibition on butane uptake

Initial specific depletion rate of butane ($\text{mg}_{\text{but}}\text{mg}_{\text{prot}}^{-1}\text{d}^{-1}$) vs. the initial concentration of butane in the liquid phase (mg/L), in the absence and in the presence of TCE (0.5 mg/L).

These results confirm the effect of competitive inhibition of TCE on the butane initial specific depletion rate. The value of $K_{i\text{TCE},\text{but},\text{susp}}$ was obtained by the least squares method (competitive model) and estimated at 0.045 mg L^{-1} .

6.1.4 Kinetic study of TCE biodegradation in the presence of butane in the suspended cell batch test

The test was conducted by exposing the microcosms to different concentrations of TCE, in the presence of a constant concentration of butane in the liquid phase equal to 1.2 mg L^{-1} . When the butane concentration decreased to 20-30 percent of the initial concentration, the vials were injected with pulses of butane.

The values of $q_{\text{max}, \text{TCE}}$ and $k_{\text{s}, \text{TCE}}$, which were estimated in the kinetic study of TCE, were used to estimate the inhibition constant $K_{i\text{but}, \text{TCE}}$ for each type of inhibition

(competitive, a-competitive and non-competitive). On the basis of the coefficient R^2 , competitive inhibition (equation 6.10) best represents the experimental data.

$$q_{TCE} = \frac{q_{\max, TCE} C_{TCE}}{K_{s, TCE} \left(1 + \frac{C_{but}}{K_{ibut, TCE}}\right) + C_{TCE}} \quad (6.10)$$

The initial specific depletion rate of TCE with and without the presence of a constant concentration of butane is shown in Figure 6.4.

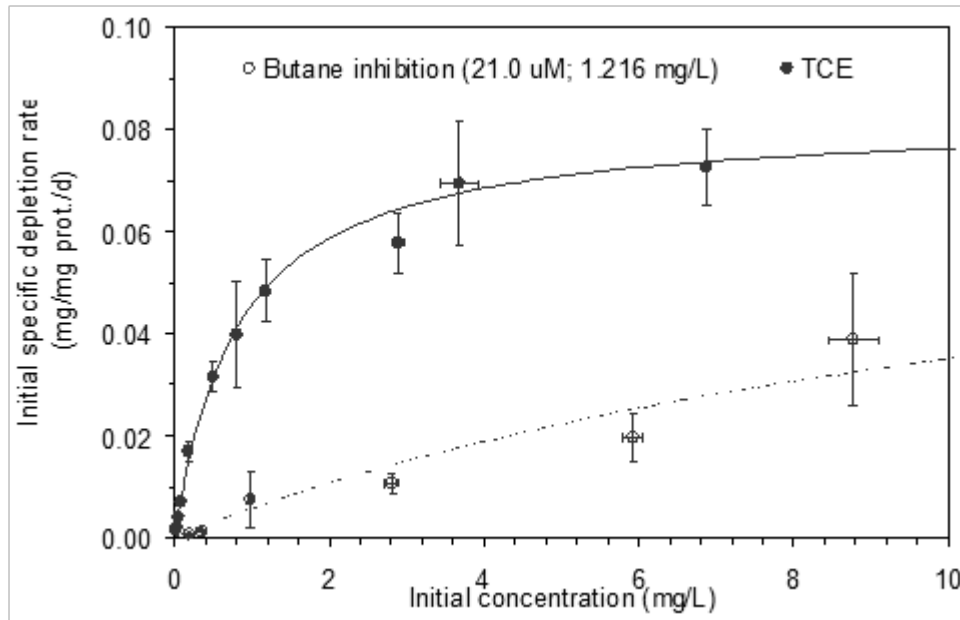


Figure 6.4 Effect of butane inhibition on TCE uptake in suspended cell batch test.

Initial specific depletion rate of TCE ($\text{mgbut mgprot}^{-1} \text{d}^{-1}$) vs. the initial concentration of TCE in the liquid phase (mg/L), in the absence and in the presence of butane (1.2 mg/L).

In the presence of a constant concentration of butane in the aqueous phase (1.2 mgL^{-1}), the biodegradation rate of TCE decreased considerably, due to the phenomenon of competitive inhibition intervening between the primary substrate and the co-metabolic substrate.

6.2 Kinetic study of substrates uptake in the attached cell batch tests at 30°C

Sterile glass vials with a volume of 119 mL were filled up to 60 mL with the Biomax carriers and 50 mL of selected consortium culture. The glass vials were subjected to pulses of oxygen and butane (4 mg L⁻¹) and injection of TCE (1 mg L⁻¹) for three months, in order to create sufficient attached biomass on the carriers. On a regular basis sterile water replaced the liquid phase in the vials.

Kinetic studies of TCE and butane uptake were carried out in separate tests. In the last step, TCE inhibition on butane uptake and butane inhibition on TCE biodegradation were evaluated in the attached cell batch test at 30°C.

6.2.1 Kinetic study of butane uptake in the attached cell batch test

Vials containing sterile fresh water and biofilm formed on the Biomax carrier were flushed with pure oxygen and subjected to this kinetic study. Butane was injected into the sealed vials in such a way as to have different concentrations of butane in the aqueous phase in each bottle (with different conditions reproduced in triplicate) and vials were kept at 30°C and stirred at 125 rpm to maintain equilibrium between the gas and liquid phases. Gas chromatography analysis was performed to monitor the butane concentration over time. The Michaelis-Menten kinetic model was used to interpret the experimental data obtained from the gas chromatograph analysis and the following mass balance was used, assuming liquid/gas equilibrium:

$$-\frac{dC_{but}}{dt} \left(\frac{Vl + H_{but,30}V_g}{V_{react}} \right) = R_{but, attached} \quad (6.11)$$

$$q_{but, attached} = \frac{R_{but, attached}}{X_{0, attached}} = \frac{q_{max, but, attached} C_{but}}{K_{s, but, attached} + C_{but}} \quad (6.12)$$

where:

C_{but} is the initial concentration of butane in the liquid phase ($\text{mg}_{but}\text{L}^{-1}$).

$H_{but, 30}$ is the dimensionless equilibrium liquid/gas constant of butane at 30°C.

V_g is the head space volume of the batch bioreactor (L).

V_l is the liquid phase volume of the batch bioreactor (L).

V_{react} is the working volume, in which the reaction takes place by removal of the substrate.

$R_{but, attached}$ is the butane initial net degradation rate of butane ($\text{mg}_{but}\text{L}^{-1}\text{d}^{-1}$) in the biofilm batch test.

$X_{0, attached}$ is the concentration of the biofilm on the supports ($\text{mg}_{prot}\text{L}^{-1}$).

$q_{but, attached}$ is the specific degradation rate of butane in the biofilm batch test ($\text{mg}_{but}\text{mg}_{prot}^{-1}\text{d}^{-1}$).

$q_{max, but, attached}$ is the maximum specific degradation rate of butane in the biofilm batch test ($\text{mg}_{but}\text{mg}_{prot}^{-1}\text{d}^{-1}$).

$K_{s, but, attached}$ is the affinity constant of the enzyme for butane in the biofilm batch test ($\text{mg}_{but}\text{L}^{-1}$).

Therefore, the initial specific depletion rate of butane $q_{but, attached}$ was obtained as the ratio between the net degradation rate of butane and the concentration of attached biomass on the carriers. The best estimation of $K_{s, but, attached}$ and $q_{max, but, attached}$ was obtained by the

method of least squares, by simulating the performance of specific rate versus the initial concentration of butane.

Figure 6.5 presents the initial specific depletion rate of butane versus the initial concentration of butane in the aqueous phase.

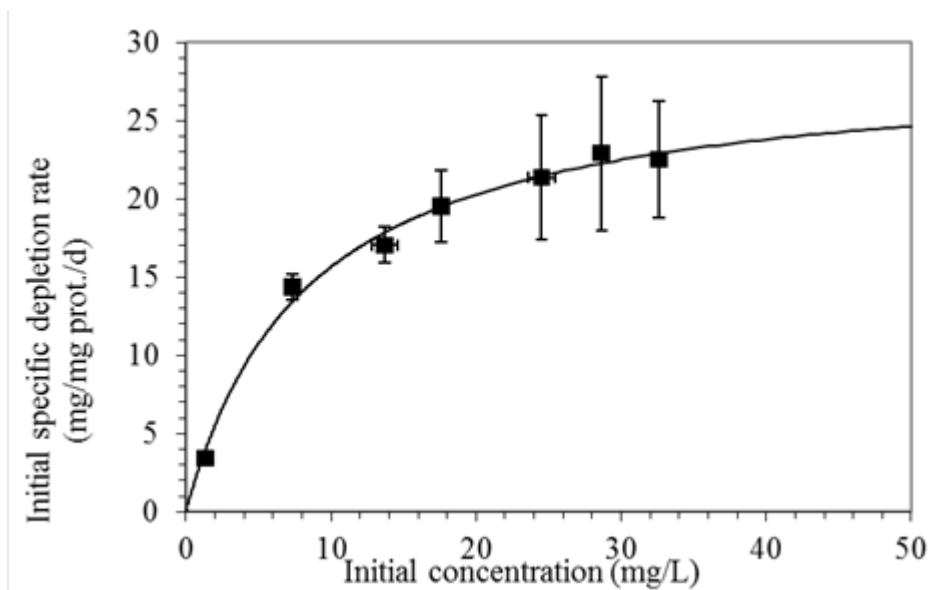


Figure 6.5 Initial specific depletion of butane ($\text{mg}_{\text{butane}}\text{mg}_{\text{prot}}^{-1}\text{d}^{-1}$) vs. initial concentration of butane present in the liquid phase (mg/L) in the attached cell batch test

In the biofilm batch test, the depletion rate of butane follows the Michaelis-Menten kinetic model. Exposing the microcosms to higher concentrations of butane leads to a higher specific degradation rate. The maximum degradation rate ($q_{\text{max, but, attached}}$) $28.6 \text{ mg}_{\text{butane}} \text{ m g}_{\text{prot}}^{-1}\text{d}^{-1}$, is six times higher than the same parameter in suspended cell test ($q_{\text{max, but, susp}}$). In addition, $K_{\text{s, but, attached}}$ in the attached cell kinetic test was estimated to be 8 mgL^{-1} which is about two times higher than the same parameter obtained from the kinetic

test performed with suspended cells. We conclude attached cells in the biofilm presented a faster degradation rate of butane than cells in a suspended form.

6.2.2 Kinetic study of TCE biodegradation in the attached cell batch test

Vials containing sterile fresh water and biofilm formed on the Biomax carrier were flushed with pure oxygen and subjected to this kinetic study. Different volumes of TCE were added to the vials to achieve different concentrations of TCE in the aqueous phase. Negative controls were prepared identically, except without biomass, in order to evaluate the possible abiotic reaction of TCE. The microcosm was kept at 30°C and stirred at 125 rpm. The gas chromatograph analysis was performed to monitor the concentration of TCE in aqueous phase over time. The Michaelis-Menten model was used to interpret experimental data, and the following mass balance was used under the assumption of a liquid/gas equilibrium:

$$-\frac{dC_{TCE}}{dt} \left(\frac{V_l + H_{TCE,30}V_g}{V_{react}} \right) = R_{TCE, attached} \quad (6.13)$$

$$q_{TCE, attached} = \frac{R_{TCE, attached}}{X_{0, attached}} = \frac{q_{max, TCE, attached} C_{TCE}}{K_{s, TCE, attached} + C_{TCE}} \quad (6.14)$$

where:

C_{TCE} is the initial concentration of TCE in the liquid phase ($\text{mg}_{TCE}\text{L}^{-1}$).

$H_{TCE, 30}$ is the dimensionless equilibrium liquid/gas constant of TCE at 30°C.

V_g is the head space volume of the batch bioreactor (L).

V_l is the liquid phase volume of the batch bioreactor (L).

V_{react} is the reaction volume in which the reaction takes place by removal of TCE (L).

$R_{TCE, attached}$ is the net initial degradation rate of TCE in the batch biofilm test ($\text{mg}_{TCE} \text{L}^{-1} \text{d}^{-1}$).

$X_{0, attached}$ is the concentration of the biofilm on the supports ($\text{mg}_{prot} \text{L}^{-1}$).

$q_{TCE, attached}$ is the specific degradation rate of TCE in the biofilm batch test ($\text{mg}_{TCE} \text{mg}_{prot}^{-1} \text{d}^{-1}$).

$q_{TCE, but, attached}$ is the maximum specific degradation rate of TCE in the biofilm batch test ($\text{mg}_{TCE} \text{mg}_{prot}^{-1} \text{d}^{-1}$).

$K_{s, TCE, attached}$ is the affinity constant for TCE in the biofilm batch test ($\text{mg}_{TCE} \text{L}^{-1}$).

Therefore, the initial specific degradation rate of TCE ($q_{TCE, attached}$) was calculated as the ratio of the net degradation rate of TCE to the concentration of attached biomass on carriers. Simulation of the data using Michaelis-Menten model provided the values of $q_{max, TCE, attached}$ and $k_{s, TCE, attached}$.

Figure 6.6 shows the initial specific degradation of TCE versus the initial concentration of TCE in the aqueous phase.

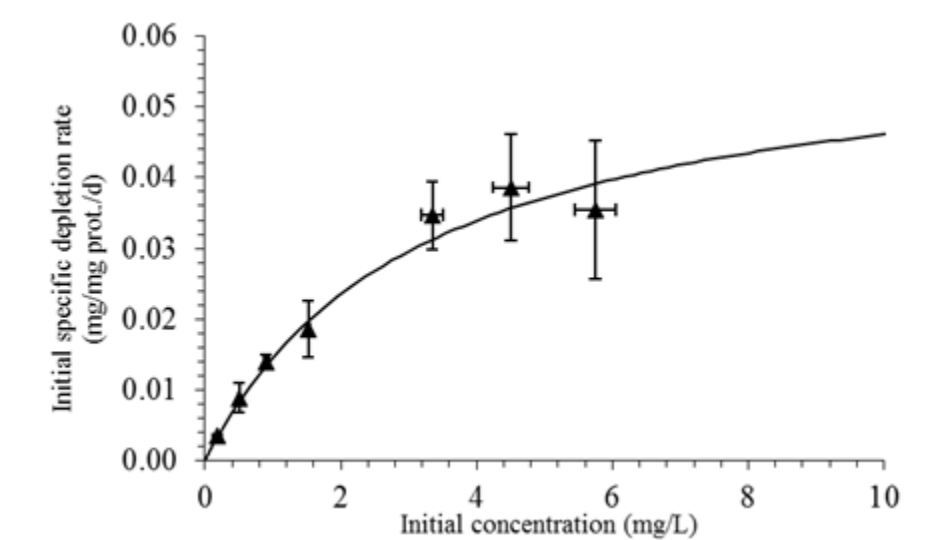


Figure 6.6 Initial specific degradation rate vs. the initial concentration of TCE in attached cell test

The initial specific degradation of TCE increases with the increase of initial concentrations of TCE in the aqueous phase to reach the maximum value ($q_{max, TEC, attached}$) equal to $0.06 \text{ mg}_{TCE}\text{mg}_{prot}^{-1}\text{d}^{-1}$. The $q_{max, TEC, attached}$ in the attached cell test is lower than in the suspended cell test. Additionally, $K_s, TCE, attached$ at 2.7 mg/L is three times less than the same value in the suspended cell test. We conclude the biodegradation rate of TCE in the attached cell test is slower than the biodegradation rate of TCE in suspended cell test.

6.2.3 Kinetic study of butane degradation in the presence of TCE in the attached cell batch test

The objective of this test was to evaluate the effect of the presence of TCE on specific degradation rates of butane. The microcosms were exposed to different concentrations of butane and to a constant concentration of TCE (0.38 mgL^{-1}). To determine the type of inhibition (competitive, a-competitive and non-competitive), this test was conducted similarly to the suspended cell test. In addition, the $q_{max, but, attached}$ and $k_s, but, attached$

determined in previous kinetic tests were used as input parameters to estimate the inhibition constants $K_{iTCE, but, attached}$ for each type of inhibition. Based on the coefficient R^2 , competitive inhibition (equation 6.15) was selected as the model best representing the experimental data.

$$q_{but, attached} = \frac{q_{max, but, attached} C_{but}}{K_{s, but, attached} \left(1 + \frac{C_{TCE}}{K_{iTCE, but, attached}}\right) + C_{but}} \quad (6.15)$$

The value of the constant $K_{i, TCE, but, attached}$ estimated on the basis of experimental data and the model of competitive inhibition, was obtained by the least squares method (competitive model).

The curves in Figure 6.7 show the initial specific degradation versus concentrations of butane, both in the absence and in the presence of TCE in the attached cell test at 30°C.

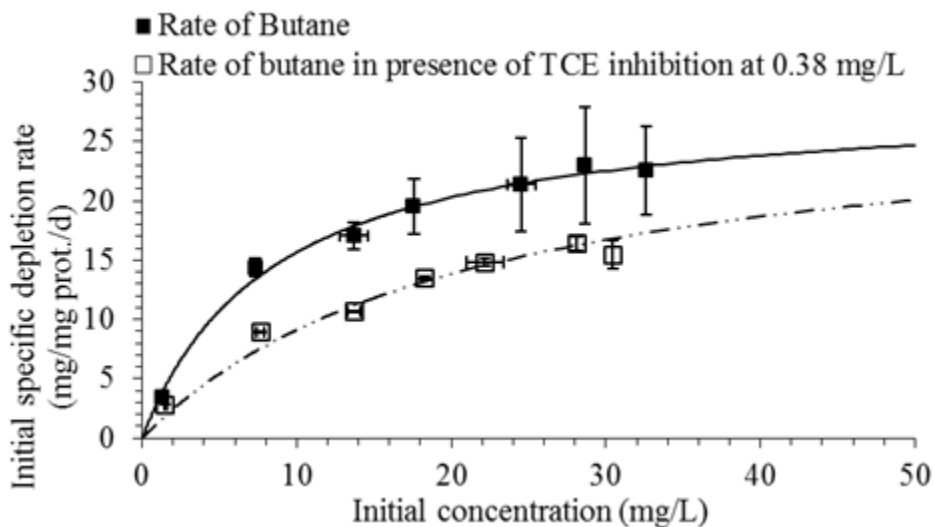


Figure 6.7 Effect of TCE inhibition on butane uptake in attached cell test.

Initial specific depletion rate of butane ($\text{mg}_{\text{but}}\text{mg}_{\text{prot}}^{-1}\text{d}^{-1}$) vs. the initial concentration of butane in the liquid phase (mg/L), in the absence and in the presence of TCE (0.38 mg/L).

In the presence of TCE 0.38 mgL^{-1} in the aqueous phase, the initial specific depletion rate of butane in the attached cell test decreases due to the competitive inhibition phenomena that arise when both substrates are present. However, the attached cells on the supports were significantly less sensitive to inhibition of TCE during consumption of butane.

6.2.4 Kinetic study of TCE biodegradation in the presence of butane in the attached cell batch test

This test was performed in the same way as explained in section 6.2.2, for kinetic study of TCE biodegradation in attached cell test at $30 \text{ }^{\circ}\text{C}$ —except a constant concentration of butane in the aqueous phase equal to 1.5 mgL^{-1} was added to the microcosms and the microcosms were subjected to gas chromatograph analysis. Here, $q_{\text{max, TCE, attached}}$ and $k_{\text{s, TCE, attached}}$ were calculated and the inhibition constants $K_{i\text{TCE, but, attached}}$ for three different

inhibition models were estimated. In this test, competitive inhibition (equation 6.16) represented the experimental data better than the other two inhibition models.

$$(6.16) \quad q_{TCE, attached} = \frac{q_{max, TCE, attached} C_{TCE}}{K_{s, TCE, attached} \left(1 + \frac{C_{TCE}}{K_{i, but, TCE, attached}}\right) + C_{TCE}}$$

Figure 6.8 shows the initial specific degradation rate of TCE with or without butane inhibition versus the initial concentration of TCE in the aqueous phase.

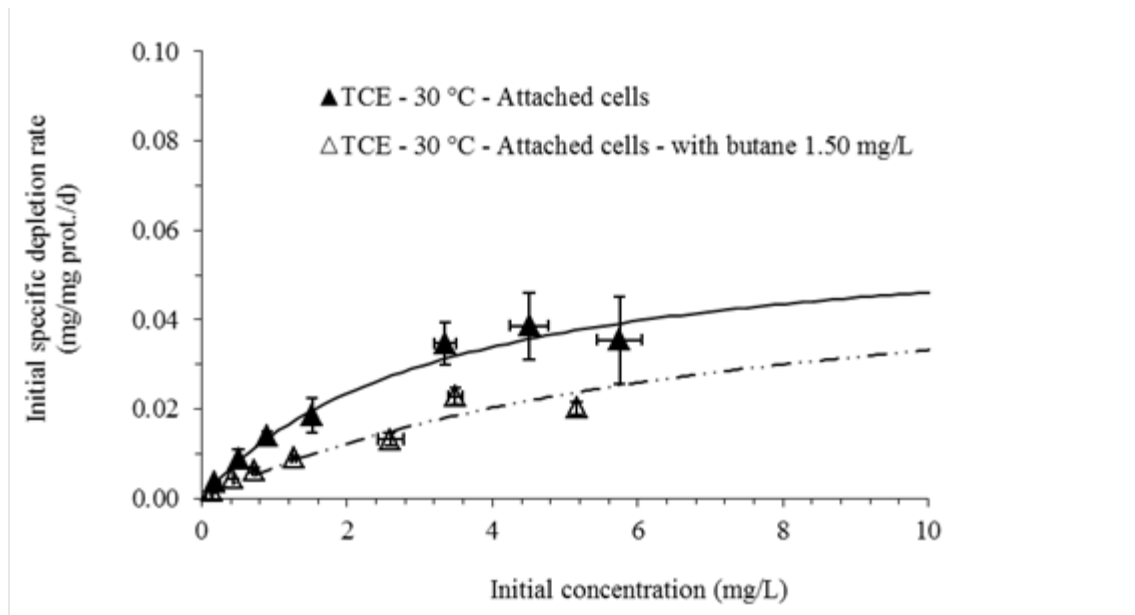


Figure 6.8 Effect of butane inhibition on TCE biodegradation in attached cell test.

Initial specific depletion rate of TCE ($\text{mg}_{\text{TCE}}\text{mg}_{\text{prot}}^{-1}\text{d}^{-1}$) vs. the initial concentration of TCE in the liquid phase (mg/L), in the absence and in the presence of butane (1.5 mg/L).

The initial specific degradation rate of TCE decreases in the presence of butane because of competitive inhibition. Comparison of the inhibition constant of butane upon TCE uptake in the suspended cell test and attached cell test reveals that the attached cells on

Biomax, compared to cells grown in the free form, were less sensitive to the inhibition of butane upon the biodegradation of TCE.

Table 6.1 compares the estimated kinetic parameters of butane uptake and TCE biodegradation in attached or suspended cell tests at 30°C. It can be observed that attached cell has a remarkable influence on kinetic parameters.

Table 6.1 Best estimate kinetic parameters relative to butane uptake and TCE biodegradation in suspended or attached cell tests with 95% confidence intervals

Cell condition	Temp.	Butane			TCE		
		$q_{max, but}^2$	$K_{s, but}^3$	$K_{i, TCE, but}^2$	$q_{max, TCE}^1$	$K_{s, TCE}^2$	$K_{i, but, TCE}^2$
Suspended	30	4.5±0.5	4±2	0.045±0.01	0.082±0.02	0.8±0.07	0.07±0.02
Attached	30	29±2	8±2	0.24±0.03	0.06±0.02	2.7±2	1.4±0.7

Overall, the attached cell test is significantly the more effective method for aerobic co-metabolic biodegradation of TCE. Butane uptake increases when moving from a suspended cell test to an attached cell test, along with a slight decrease in the TCE biodegradation rate. This latter observation might be related to the difference between bacterial consortia of the suspended cell and attached cell tests. Additionally, the mutual inhibition of Butane and TCE, as described by the competitive inhibition model, is lower in the attached cell test.

² Mg mg_{prot}⁻¹ d⁻¹
³ mgL⁻¹

7 Design procedure for biofilm reactor scale-up

This chapter presents the progress made in the framework of the MINOTAURUS project regarding the development of a PBR process specifically designed for aerobic co-metabolism biodegradation of chlorinated solvents, with specific focus on the following points:

- development of a procedure for the design of a PBR specifically aimed at treating chlorinated solvents via aerobic co-metabolism, including criteria for the scale-up from lab-scale pilot reactors to full-scale reactors
- development of a procedure for optimizing the schedule of substrate and oxygen pulsed feed to the bioreactor

7.1 Pulsed feed of oxygen and growth substrate

The pulsed supply of growth substrate and oxygen is a crucial element of the application of aerobic co-metabolism in both *in-situ* processes and on-site packed bed reactors. This technique consists of supplying the growth substrate and oxygen to the bioreactor inlet as alternated pulses. As a result mainly of hydrodynamic dispersion, a partial overlapping of the two pulses occurs while they travel along the bioreactor. This overlapping occurs at low concentrations of substrate and oxygen and discontinuously at each point.

In this way, substrate consumption and biomass growth occur homogeneously throughout the column, yielding a long and well-developed bioreactive zone. This fulfills three objectives:

- to avoid an excessive biomass growth at the beginning of the column, thus minimizing the risk of porosity clogging
- to avoid too low a biomass concentration in the terminal portion of the column
- to minimize the substrate competitive inhibition on CAH co-metabolism

The pulsed supply of growth substrate and oxygen was initially proposed by Roberts *et al.* [47] in the first published work on *in-situ* implementation of aerobic co-metabolism. The optimization of *in-situ* application of this technique was then described by Goltz *et al.* [48] and applications to on-site bioreactors proposed by Ciavarelli *et al.* [11] and Frascari *et al.* [49]. Though the pulsed feed in principle is relatively simple, the optimization of the pulsing procedure is complex and requires a complete understanding of time-dependent behaviour in the whole length of the bioreactive zone. In particular, the key points are:

- Quantification of the amount of growth substrate to be fed per pulsation cycle, to sustain a pseudo-stationary level of biomass concentration in the column.
- Pulsation cycle duration (or frequency): on the one hand it is crucial to maximize the number of substrate pulses per day to increase the substrate consumption rate and thus reduce the column length necessary to reach an acceptable growth substrate conversion; on the other hand, the pulse frequency should not be too high, so as to avoid excessively reducing the space distance between two subsequent substrate pulses. Indeed, if the substrate pulses are too close, they can mix with each other in the last part of the column and the positive effects of the pulsing procedure lost due to the consequent homogenization of substrate concentration.

- The cycle length should not be too long, to avoid the risk of exhausting of the reducing power in the cells (NADH) during the time between two subsequent substrate pulses.

A simplified flow-sheet of an on-site PBR process for the aerobic co-metabolic treatment of CAHs is shown in Figure 7.1. The pulsed supply of growth substrate is obtained by supplying a concentrated solution of the selected substrate to the groundwater entering the bioreactor, while the oxygen pulses are obtained by forcing groundwater through a packed bed containing an Oxygen Releasing Compound (ORC). ORCs are a formulation of phosphate-intercalated magnesium peroxide (MgO_2) that, when hydrated, produce a controlled release of oxygen, with $Mg(OH)_2$ as the only by-product. They are widely used in aerobic bioremediation processes, and typically have the form of a white powder less than 10 microns in diameter.

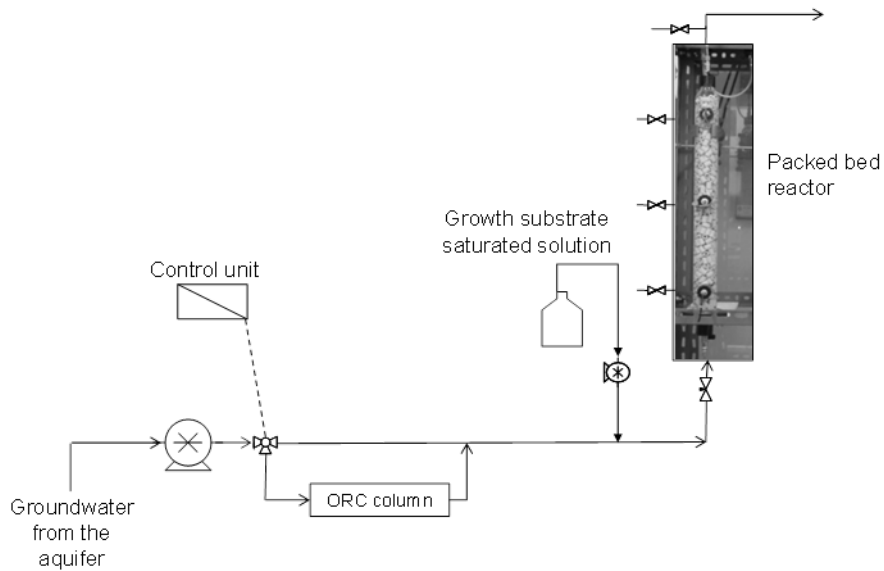


Figure 7.1 Flow-sheet of an on-site PBR process for the aerobic co-metabolic treatment of CAHs with pulsed supply of oxygen and growth substrate

7.2 Fluid-dynamic characterization of a packing of the selected biofilm carrier

The procedure for design of the PBR (interstitial velocity, hydraulic retention time and length) and of the schedule of pulsed oxygen/substrate supply requires the availability of a fluid-dynamic model of the packed bed filled with the selected biofilm carrier. A one-dimensional fluid-dynamic model is generally considered acceptable for this purpose. In the absence of chemical/biochemical reaction, sorption and interfacial transport, the mass balance equation relative to a generic compound i is therefore:

$$\frac{\partial c_i}{\partial t} = -v \cdot \frac{\partial c_i}{\partial z} + D_{L,i} \cdot \frac{\partial^2 c_i}{\partial z^2} \quad (7.1)$$

where:

v indicates the interstitial velocity.

$D_{L,i}$ is the diffusion/dispersion coefficient relative to compound i .

$D_{L,i}$ can be expressed as:

$$D_{L,i} = D_{mol} + \alpha_L \cdot v_{int} \quad (7.2)$$

where:

$D_{mol,i}$ indicates the diffusion coefficient of compound i .

α_L is the longitudinal dispersivity of the selected biofilm carrier.

Thus, the one dimensional fluid-dynamic model contains two parameters to be estimated: the carrier's effective porosity ε necessary to calculate the interstitial velocity from the

measured flow rate, and the carrier's longitudinal dispersivity. These two parameters can be estimated through a best fit of the 1-D fluid-dynamic model to the experimental outlet concentrations obtained in tests consisting in a step supply of a non-adsorbed tracer such as KCl. These tests are typically conducted in a prototype of the final full-scale PBR, filled with the selected biofilm carrier. To estimate ε and α_L , it is necessary to perform a numerical integration of equation 7.1 for different values of the (ε, α_L) vector, until the attainment of the minimum value of an objective function defined so as to quantify the overall deviation between measured and calculated outlet concentrations.

7.2.1.1 Fluid-dynamic characterization of the selected biofilm carrier

The fluid-dynamic study of the selected biofilm carrier, Biomax, was based on the operation of tracer tests in a 60-cm long glass column filled with the carrier. The tests consisted of pulse and step supplies of oxygen, TCE and NaCl, and were operated at different interstitial velocities. The overall elaboration of the experimental data resulted in an effective porosity of 64 percent and in a longitudinal dispersivity of 0.054 m.

7.3 Sizing of the PBR and preliminary design of the schedule of pulsed oxygen/substrate supply

The rational design of both the bioreactor and the tentative schedule of substrate and oxygen pulsed feed can be summarized in the following steps:

- In the first place, in the case of a multiple contamination it is necessary to identify the key pollutant, whose desired conversion will determine the bioreactor sizing.
- The key pollutant mass to be converted per time unit ($\dot{m}_{C,g}$) is assessed on the basis of the inlet concentration ($c_{C,inlet}$) and of the desired conversion (η_c):

$$\dot{m}_{C,g} = Q \cdot c_{C,inlet} \cdot \eta_C \quad (7.3)$$

where:

Q indicates the volumetric flow rate of groundwater fed to the PBR.

- The amount of biomass necessary to accomplish the desired conversion of the key pollutant (m_X) is calculated using the pollutant mass balance and the kinetic model, assuming average concentrations along the PBR:

$$m_X = \frac{\dot{m}_{C,g}}{\bar{q}_C \cdot \varepsilon_{biofilm}} = \frac{Q \cdot c_{C,inlet} \cdot \eta_C}{\bar{q}_C \cdot \varepsilon_{biofilm}} \quad (7.4)$$

$\varepsilon_{biofilm}$ indicates the biofilm efficiency, defined for each section of the PBR as the ratio of the average key CAH concentration in the biofilm to the concentration measured in the bulk of the liquid phase, and \bar{q}_C indicates the key CAH specific biodegradation rate evaluated at the average key CAH concentration along the bioreactor.

- A rigorous approach includes the estimation of the biomass concentration in the effluent, $c_{X,suspended,outlet}$. This estimate requires a complete fluid dynamic and kinetic modelling of the process, including a term accounting for the biofilm detachment rate. However, given the very low superficial velocities typical of the PBRs, the biomass concentration in the effluent is very low and as a first approximation can be neglected.
- The mass of growth substrate to be degraded in order to sustain the calculated amount of biomass in a pseudo-steady state is calculated using the biomass mass balance:

$$\dot{m}_{S,g} = \frac{1}{Y_S} \cdot \left[Q \cdot c_{X,suspended,outlet} + b \cdot m_X + \frac{\dot{m}_{C,g}}{T_{c,C}} \right] \quad (7.5)$$

where:

Y_S indicates the biomass/substrate yield.

b is the endogenous decay constant.

$T_{c,C}$ is the TCE transformation capacity.

- The feed substrate concentration ($c_{S,inlet}$) is normally chosen as high as possible (close to the solubility in water, in the case of a gaseous substrate), to reduce the fraction of the cycle time dedicated to substrate feeding t_S^* .
- The desired substrate conversion, η_S , is set to a high value (for example, 95 percent), so as to minimize the amount of substrate released in the PBR outlet; the expected outlet and average substrate concentrations can thus be easily calculated.
- The fraction of the cycle time to dedicate to substrate feed (t_S^*) is determined using the substrate mass balance:

$$t_S^* = \frac{\dot{m}_{S,g}}{Q \cdot c_{S,inlet} \cdot \eta_S} \quad (7.6)$$

Three elements are missing to complete the design procedure: the PBR section (S_t), length (L), and cycle duration. Once the biofilm carrier (with its porosity and dispersivity) has been chosen, given the PBR section and length one can calculate the interstitial velocity ($v = Q/(\varepsilon S_t)$), the hydraulic retention time ($HRT = L/v$) and the Péclet number ($Pe = \text{convection/dispersion} = L/\alpha_L$). Finding the values for S_t , L and cycle duration, which will allow the desired conversion of substrate and key pollutant with the

previously calculated or assigned values of t^*_S and $c_{S,inlet}$, however, requires a complete fluid-dynamic simulation of the process. This simulation is required to solve the system of PDE equations corresponding to the mass balances of oxygen, substrate, key pollutant and biomass, and to evaluate the resulting values of η_S and η_C as a function of the input parameters S_t , L and cycle duration. Some conceptual guidelines can be provided in order to help the PBR designer in this process, to reduce the number of simulations to be performed. In the first place, the cycle duration is chosen as a compromise between two opposed necessities: i) to increase the cycle duration, broadening the time without substrate and thus decreasing substrate inhibition on CAH co-metabolism; versus ii) to reduce the time without substrate, avoiding complete NADH depletion. The evaluation of the optimal cycle duration therefore requires the kinetic model integrate terms taking into account the production and depletion of NADH, an aspect that has not yet been fully investigated by the research on aerobic co-metabolic processes. In addition, the Péclet number (Pe) must be sufficiently high to provide fluid-dynamic behavior acceptably close to plug flow, so as to avoid a significant widening of the substrate pulses travelling along the bioreactor. This aspect is crucial in order to decrease mutual substrate-CAH inhibition, in cases where this inhibition is a relevant phenomenon. On the basis of the results obtained in the MINOTAURUS project, Pe should be at least greater than 100. Given the numerous uncertainties associated with the simulation-based design procedure described above, it is advisable to dedicate the first period of operation of the PBR to the experimental optimization of the schedule of substrate and oxygen pulsed feed.

7.3.1.1 Application of the PBR sizing procedure and operation of a 31-L pilot-scale PBR

The sizing procedure illustrated in section 7.3 was applied to the attached-cell TCE-degrading consortium previously kinetically characterized in chapter 6. The last step of

the procedure was implemented with the use of a coupled kinetic/fluid dynamic model inclusive of the mutual butane-TCE inhibition. Numerous long-term simulations were conducted, to evaluate the effect of the variations of the following parameters on TCE and butane conversions: cycle duration, substrate feed duration/cycle duration (t_S^*), bioreactor length and hydraulic retention time.

Simulations dedicated to the optimization of the schedule of substrate/oxygen pulsed supply and performed with an oversized PBR, indicated that a cycle duration of 2 days and a t_S^* of 12 percent provided optimal results. On the basis of further simulations, a relatively high Péclet number (i.e. $Pe = 320$) was necessary to avoid an excessive widening of the butane pulses along the bioreactor, and therefore to reduce mutual butane-TCE inhibition. With the longitudinal dispersivity as estimated for the Biomax-filled PBR (0.054 m), a Pe of 320 corresponds to a reactor length of 17.5 m, which was attained by connecting 14 columns of 1.25 m length in series. The hydraulic retention time required to attain a 90 percent butane conversion was 4.5 days. The interstitial velocity was therefore set to $17.5 \text{ m}/4.5 \text{ days} = 3.9 \text{ m/day}$. On the basis of the groundwater flow rate to be treated (set to 0.2 L/h) and of the porosity of the selected biofilm carrier (68 percent), the resulting PBR diameter was 4.76 cm. To perform a temperature control, the 14 columns were immersed in a temperature-controlled bath, as shown in Figure 7.2 and Figure 7.3.

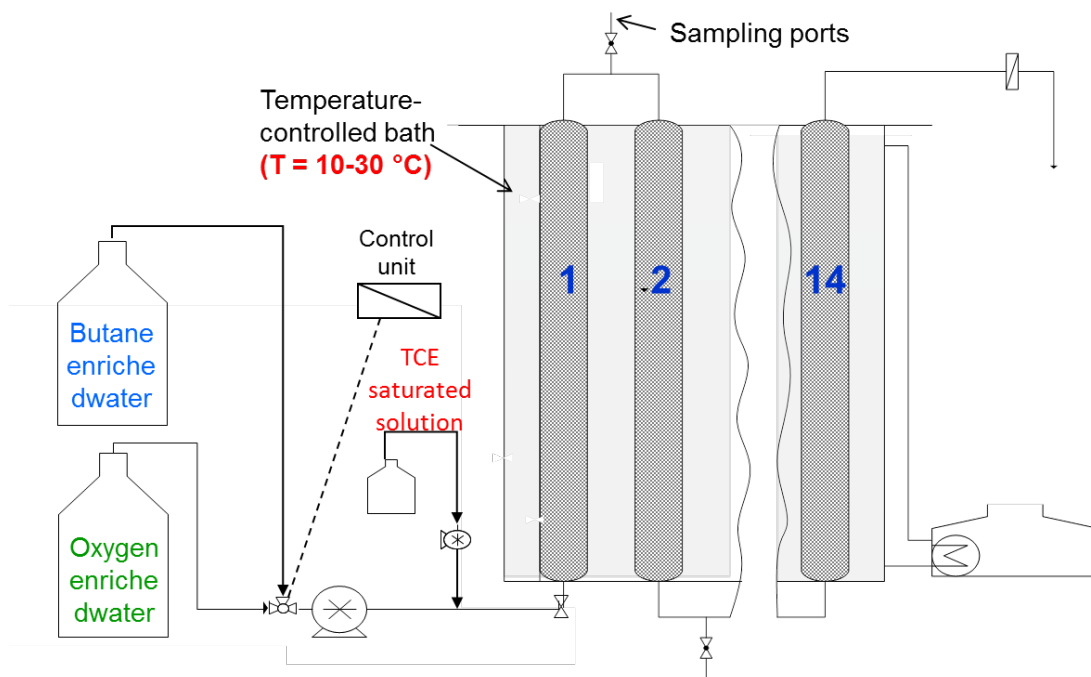


Figure 7.2 Schematic picture of designed up-scaled packed bed bioreactor for aerobic co-metabolism biodegradation of chlorinated solvents



Figure 7.3 View of the 31-L lab-scale PBR

8 Conclusions, part 1

The conclusions from the first part of this work can be summarized as follows:

- Among four different substrates, butane was selected as the optimal growth substrate and a suspended-cell consortium capable of performing a rapid aerobic co-metabolic biodegradation of TCE was developed from the site's indigenous biomass.
- Given the slow degradation rate expressed by the selected consortium for TeCA, a chemical pre-treatment converting TeCA into TCE was selected.
- Attachment of the selected consortium to four porous biofilm carriers led to the selection of the ceramic porous carrier Biomax and to the development of an attached-cell consortium characterized by a lower level of mutual butane-TCE inhibition.
- Preliminary development of the continuous-flow PBR process in a 1-L column packed with Biomax demonstrated that the initial schedule of substrate and oxygen pulsed feed led to homogenous growth and activity of the selected consortium.
- A kinetic study of butane and TCE biodegradation by the two consortia indicated that the attached-cell consortium is characterized by a lower TCE specific degradation rate and by a lower level of mutual butane-TCE inhibition. Butane-TCE inhibition can be effectively described for both consortia with the competitive inhibition model.
- A 31-L packed-bed modular bioreactor consisting of 14 columns connected in series was designed and implemented.

Overall, aerobic co-metabolism in on-site PBRs appears to be a promising approach for the bioremediation of CAH-contaminated aquifers.

Part 2:

Aerobic biodegradation of polymers with and without chemical pre-treatment

9 Polymer biodegradation

9.1 The diffusion of plastics and the possible chemical/biodegradation treatment approaches

The first synthesized polymer was made almost a century ago and since then the production and consumption of this material has increased dramatically. The production cost of polymers is relatively low and because of their stability the demand for utilization of polymers is increasing [50]. It is estimated that the global production of polymers is 140 million tons per year. Now a day, polymers are used for different application and in different sections such as industry, packaging, agriculture, medical devices, automation and many other sectors. The types of polymers which are used the most are polyethylene (PE), polypropylene (PP), polyvinyl chloride (PVC), polystyrene (PS) and polyethylene terephthalate (PET). Table 9.1 shows the data for the global market share of different types of synthetic polymers.

Table 9.1 Global market share of plastics by volume produced [51].

Plastic type	Market share by volume produced
Polyethylene (PE)	29%
Polyvinyl chloride (PVC)	17%
Polypropylene (PP)	12%
Polystyrene (PS)	9%
Polyurethane (PUR)	5%
Others	28%
Total	100%

Consequently, the increase in production and consumption of polymers has caused serious environmental concerns in form of solid wastes. Since the synthesized polymers present in environment not more than 100 years ago, there is no new enzymes produced by microorganism capable of degrading this material. Therefore, polymers have been known to be resistant against microbial attack [51].

Now, the main amount of plastic wastes is either burned in incinerator for disposal or buried in landfills which the former produces toxic gas and the latter causes environmental concerns and ground water pollution. Also, some of the polymer wastes are recycled but the costs for recycling are very high. In general, all of these solution cause significant resource loss [51].

Therefore the biodegradation of polymers can be an alternative solution. Despite of several attempts, the knowledge about biodegradation pathways and microorganisms capable of degrading of synthesized polymers is very limited yet. The main reason for non-biodegradability of polymer is due to their high molecular weight and their hydrophobic nature, which prevent polymers to be directly transported into the cell [52]. Only partial degradation of polyethylene (PE) was observed after 32 years of burying in soil [53]. New pretreatment steps may be needed to improve biodegradability of polymers by decreasing the molecular weight and creating functional group to improve the wettability of polymers. Albertsson et al. [54, 55] proposed that UV light as an oxidation agent is needed prior to biodegradation of inert polymer materials and without the pretreatment step the biodegradation polymer takes more than 10 years. Gilan et al. [56] showed that the U.V. Irradiated PE initiated the biodegradation of PE by *Rhodococcus ruber*. Hadad et al. [57] showed that the biodegradation of U.V. pretreated polyethylene increases with prolongation of treatment time. The U.V. irradiation causes photo-

oxidation of polymer leads to breaking the polymeric chain and decrease the molecular weight [58, 59].

There are other oxidation methods such as ozonation [60, 61] and thermal treatment [62, 63, 64, 65] which can improve the biodegradability of polymers by breaking the polymeric chain, reducing its molecular weight and creating functional groups such as carboxyl and carbonyl groups on the polymer surface and improve the wettability of polymers. Among different oxidation methods, ozonation has advantages such as uniformly oxidized the polymer surface even with complicated shapes and being relatively low cost processes [66].

The aim of second part of my PhD thesis was to evaluate the effect of the chemical oxidation method on the degradation of Linear Low Density Polyethylene (LLDPE), polypropylene (PP), polyvinyl chloride (PVC), polystyrene (PS), as well as to investigate the enhancement in biodegradability of the mentioned polymers due to pretreatment. To obtain these aims, a) ozonation and b) U.V. /ozone treatment as two physical- chemical oxidation methods have been chosen. The exposure of four different polymers to these oxidation methods was optimized in terms of exposure time and generation of functional groups on the polymer's surfaces. Moreover, the effect of these oxidation methods as a pretreatment process for improving polymer biodegradability has been investigated by incubating pretreated polymers with a) a pure bacterial culture; b) a mixed bacterial culture; and c) a pure fungal culture.

This part of my Ph.D. program was carried out in the framework of the Eu-funded research program Bioclean (BIOTEchnologiCaL approaches for biodegrading and promoting the environmEntal biotrAnsformation of syNthetic polymeric materials) [67], and was carried out in the laboratories of the University of Applied Sciences and Arts

Northwestern Switzerland, School of Life Sciences, Institute for Ecopreneurship, in
Basel, Switzerland.

10 Materials and methods for the evaluation of plastic (bio)degradation

10.1 Experimental setup for chemical treatment of plastics

There are two main reasons for pretreatment of polymers, to reduce the molecular weight and to improve hydrophilic property of polymers [58, 66]. Thermal irradiation, photo and chemical oxidation of polymers reduce the polymeric chain size and form oxidatized groups such as carboxyl, carbonyl and hydroxyl groups. These effects can promote the degradation of polymers. Three typical oxidation methods are involved in carbonyl groups generation:

- Ozonation,
- U.V. irradiation,
- Thermal treatment
- Plasma treatment.

Among these methods, ozonation of plastics is an easy process, cost and time effective process to be performed. The reactions of ozone onto polymers lead to numerous chemical modification. Ozone leads rapidly to formation of oxidized functions and a chemical reaction occurred at the surface of the polymer as well as in the depth of a material. When polymers exposed to ozone, peroxide, carbonyl and carboxyl groups are formed. The carbonyl and carboxyl groups themselves are hydrophilic so by ozonation the hydrophilicity of polymers can be improved [61]. Combination of UV and ozone treatment can be another method for surface modification of polymers [67].

Ozonation and UV-ozonation of polymers, in distilled water and in gaseous phase are described in the following sections.

10.1.1 Materials

Linear low density Polyethylene (LLDPE), Polypropylene (PP), Polystyrene (PS) and Polyvinylchloride (PVC) in the form of film and powder were selected for this study. Table 10.1 shows the film's thickness and powder's diameter for each type of polymer. These materials kindly provided by different companies for BioClean project. PVC films and PVC powder provided by FABBRI COMPANY and SOLVIN SA, Italy respectively. PP films and powder provided by LYONDELL BASE, Italy. LLDPE and PS in both type of film and powder provided by VERSALIS, Italy. All the materials were sent to Bologna University by mentioned companies and distributed to project partners.

Table 10.1 Characterization of studied polymers

Polymer	Mw film/	Film thickness	Powder particle's
	Mw powder (Da)	(mm)	diameter (mm)
LLDPE	150000/ 196000	0.448	0.48
PP	350000/ 443891	0.200	0.7
PVC	87500/ 63100	0.01	0.15
PS	259000/ 187000	0.281	-

10.1.1.1 Ozone properties

The comparison of ozone and oxygen properties is shown in Table 10.2.

Table 10.2 Ozone and oxygen properties [68]

Property	Ozone	Oxygen
Molecular formula	O ₃	O ₂
Molecular weight	48	32
Colour	Light blue	Colorless

Smell	Smell after lightning storm	Odorless
Solubility in water at 0°C (mg/L)	0.64	0.049
Density (g/L)	2.144	1.429
Electrochemical potential	2.07	1.23

10.1.2 Ozonation procedure

Oxygen gas was fed to the ozone generator (model TOGC2 ozone generator ,Triogen Ltd.). Flow was controlled by flow meter and pressure gauge. Ozone was generated at a controlled rate to ensure that it was a certain percentage of the oxygen gas mixture (rate was controlled by adjusting the output power knob) in the generator and was released into the ozone gas analyzer (PCI-WEDECO, model HC 400, Environmental Technologies OZONE MONITOR) and then into the reactor.

The reactor was a Plexiglas cylindrical column equipped with glass gas diffuser. The reactor was operated by feeding the mixture of oxygen/ozone –containing gas continuously. The exhausted gas left the reactor into ozone destruct unit and destroyed at 259°C.

Plastic films and powder were (in case of films, samples were cut into pieces of 1x1 cm) put in the reactor prior to starting of the gaseous phase ozonation. When the ozonation time finished, ozone generator was turned off, and the oxygen purge to the reaction system for 15 minutes. Samples were taken out of the reactor and the effect of ozonation was monitored by using FTIR analysis.

10.1.2.1 Ozonation in aqueous phase

Polymer films were cut, installed and fixed at the wall of the reactor. In order to avoid overlapping during aqueous phase ozonation, distilled water was placed in the reactor and films reacted with ozone according to the ozonation procedure for 10 hours. During the ozonation, every hour the ozone generator was stopped and oxygen gas sparged for 15 minutes and then some of samples were taken out, the water was removed with clear tissue paper and samples were dried at room temperature (22-23°C) for 2 hours. FTIR analysis was used to monitor the surface modification of dried samples.

10.1.2.2 Ozonation in gaseous phase

The ozonation procedure was the same as explained in aqueous phase ozonation except that there was no water in the reactor. The treatment time was prolonged to 20 hours and the test was performed for plastics in type of film and powder.

10.1.3 UV/ozonation procedure

Mercury-xenon UV lamp, model L8886 (HAMAMATSU), with the high intensity of 100 mW/cm² and wavenumber 230-470 nm was installed inside the ozonation reactor. For the plastic treatment the intensity of UV source was set at 50% of the maximum intensity. The film polymer samples were installed and fixed on the reactor's wall, with the 3-4 cm distance from the UV source. The ozonation procedure was the same as explained in the previous sections. The UV irradiation was started at the same time when the ozone generator was started.

10.1.3.1 UV/ozonation in aqueous phase

water. The UV source and ozone generator were started at the same time and exposure of plastic film samples (LLDPE, PP and PS) to the UV/ozone was prolonged to 10 hours. The ozone generator and UV source was stopped every one hour and after sparging

oxygen for 15 minutes the film samples were taken out, dried and the FTIR analysis was carried out for the samples.

10.1.3.2 UV/ozonation in gaseous phase

same as explained in the section 10.1.3.1, except there was no water inside the reactor.

Aim of this study was to examine the effect of ozone on generation of functional groups on the polymers' surface and optimize the treatment time. Table 10.3 Description of the treatment conditions relative to ozonation and UV/ozonation of plastics in gaseous and aqueous phases.shows the treatment conditions.

Table 10.3 Description of the treatment conditions relative to ozonation and UV/ozonation of plastics in gaseous and aqueous phases.

Treatment condition	Ozone dose (wt%)	Ozone concentration (mg/L)	UV intensity (mW/cm ²)	UV wavenumbers (cm ⁻¹)	Reaction time (hours)
O ₃ - gaseous phase	1.3	20	-	-	20
O ₃ - aqueous phase	1.3	20	-	-	10
UV/O ₃ gaseous phase	1.3	20	50	230-470	10
UV/O ₃ aqueous phase	1.3	20	50	230-470	10

10.2 Experimental setup for biological treatment test of plastics

Over the last 30 years, several studies have shown different isolated microorganism capable of using polymers as the only carbon source for growth [52, 55, 54, and 50]. All of these studies confirm the biodegradation process under normal condition and without any pretreatment step for plastics is very slow and despite all of these efforts, the complete metabolic pathway for biodegradation of polymers is not still very clear. However, once the molecular weight of polymer reduced to the acceptable range for enzyme action (typically from 10 to 50 carbons), the metabolic pathway of polymer biodegradation is similar to hydrocarbons [69].

In the present work, pretreated and untreated polymers were applied as the only carbon source of pure or mixed bacterial cultures. The abiotic and biotic degradation of polymers were studied, using different analytical methods.

10.2.1 Experimental setup of biodegradation test of plastics by bacterial cultures

Polymer films (LLDPE, PP and PS) of size 1×1 cm and powder (PVC) with average diameter of 0.15 mm were selected for this study. The gaseous phase ozonation for 20 hours was the pretreatment method for this study. All the samples including treated and untreated, were gone through disinfected procedure. Pre-weighted disinfected polymers (ozone-treated and untreated) were added to the mineral medium in sterilized glass vials. The final concentration of plastic in media adjusted at 20 g/L. Pure or mixed active bacterial culture were inoculated to these aliquots and they were kept under shaking at 120 rpm at 28°C. Polymers were the only carbon source for bacterial growth. Abiotic controls set up with a mineral medium containing plastics without the bacterial culture.

All samples were prepared and run simultaneously in triplicate (biotic and abiotic conditions).

10.2.1.1 Bacterial cultures

Pure active bacterial culture of *Rhodococcus ruber* was used as the pure bacterial strain. Moreover, five bacterial strains were selected, mixed and utilized as the mixed bacterial culture. This mixed culture consisted of five strains isolated from marine and landfill environment:

- *Salinibacterium amurskyense*
- *Rhodococcus ruber*
- *Shewanella baltica*,
- *Pseudomonas xanthomarina*,
- *Lysinibacillus macrolides*

The isolation of used bacterial strain was carried out in the frame work of BioClean project at University of Applied Sciences and Arts Northwestern Switzerland, School of Life Sciences, Institute for Ecopreneurship.

10.2.2 Experimental setup for co-metabolic biodegradation test of PS by fungal culture

UV/zonated and non-UV/ozonated PS films were place in sterile glass vials containing 15 ml sugar-free Czapek Dox medium to have the final concentration of 6 g/L of PS in glass vials. Saccharose was added to the vials as a co-substrate with the final concentration of 0.6 g/L. All the glass tubes were kept under shaking at 120 rpm and 24°C. The dry weight of Fungal culture at the beginning of incubation was measured 0.27 g/L as the initial

concentration of fungal culture in each glass vials. Abiotic controls were prepared in the same way without fungal culture inoculation and incubated at the same time.

10.2.2.1 Fungal culture

In the frame work of BioClean project, several microorganisms have been isolated from landfill, sludge and marine environment by research groups which are participating in this project. Among different microorganism, *Penicillium variable* was isolated and recognized to be capable of degrading PS in a co-metabolic process by professor Čeněk Novotný's research group in Department of Biology and Ecology, Faculty of Science, University of Ostrava, Czech Republic.

The *Penicillium variable* as a pure fungal culture was chosen and I tested and evaluated the effect of this fungal culture on biodegradation of UV/ozonated PS in a co-metabolic process.

10.2.3 Disinfection procedure

The disinfection procedure adopted consisted of washing pre-weighted polymers (ozone-treated and untreated) into ethanol 70% for 30 minutes following by rinsing with sterile water and drying at 45°C in a sterilized condition. The goal of sterilization was to avoid any contamination during incubation of plastics with pure or mixed bacterial culture.

10.2.4 Mineral salt medium

The synthetic mineral salt medium composition which was used as media for bacterial culture is described in the Table 10.4.

Table 10.4 4 Mineral salt medium composition

salts	Amount (g L⁻¹)
Na ₂ HPO ₄	1.41
KH ₂ PO ₄	1.36
(NH ₄) ₂ SO ₄	0.39
MgSO ₄	0.09
CaCl ₂	0.02
Na EDTA	0.003
FeSO ₄ * 7 H ₂ O	0.002
ZnSO ₄ * 7 H ₂ O	0.001
MnSO ₄ * H ₂ O	0.001
CuSO ₄ * 5 H ₂ O	0.0003
Co(NO ₃) ₂ * 6 H ₂ O	0.0002
(NH ₄) ₆ Mo ₇ O ₂₄ * 4 H ₂ O	0.0001

The sugar free Czapek Dox medium composition which was used as fungal culture media is described in Table 10.5.

Table 10.5 Composition of sugar free Czapek Dox medium

salts	Amount
	(g L⁻¹)
NaNO ₃	3
K ₂ HPO ₄	1
MgSO ₄ ·7H ₂ O	0.5
KCl	0.5
FeSO ₄ ·7H ₂ O	0.01

10.2.5 Removing the biofilm from taken plastic samples for analysis

During the incubation, glass tubes containing each type of samples were periodically withdrawn for analysis in triplicate. The samples were left in sodium dodecyl sulfate (SDS) 2% for 4 hours, and then washed with ethanol 70% and water in order to wash off the biofilm.

10.3 Analytical methods for the evaluation of plastic (bio)degradation

There are many ways to monitor the degree of polymer's degradation. The basic idea is to understand it from microcosmic and macroscopic points of view. So melting rheology test, Fourier transform infrared analysis (FTIR), Differential scanning calorimetry (DSC), Thermogravimetric Analysis (TGA), weight loss measurement and microscopic method such as Atomic Force Microscopy (AFM) and Scanning Electron Microscope (SEM) were applied to investigate the molecular, chemical, thermal and mechanical properties of

tested plastics during degradation processes. The bacterial growth monitoring was applied as an indication of biodegradation by Colony forming unit (CFU).

10.3.1 Melt rheology analysis

Rheology is the study of deformation and flow of a material. Specially, this test is interesting to be performed for a material which does not follow the Newton's Law of viscosity. Newtonian materials flow in the usual way whereas non-Newtonian materials flow in an unusual way, exhibiting various and particular phenomenon. In short, rheology is a set of observations related to how the stress on a material or force applied to a material is related to deformation or change of the shape of the material. This analysis can be applied for polymers to study the flow behaviour and structure of polymer. Polymers consist of long chain macromolecules, which largely determine their non-Newtonian flow behaviour. They are further determined as viscoelastic materials which means that their behaviour is somewhere between that of elastic solids and viscous fluids. Low shear rate measurements in the melt's linear viscoelastic region of polymers can provide data that can be linked directly to the polymer's molecular structure such as molecular weight and molecular weight distribution-factors [70].

In this study, polymer films were subjected to melt rheology test to follow the structural changes of polymer due to chemical and biological degradation processes. Film samples have been studied in molten viscoelasticity. They are placed in between parallel plates (diameter 8 mm, gap 1.5 mm) and an oscillatory frequency sweep is performed at a constant temperature. In any cases, the maximum amplitude of the sinusoidal strain wave has been checked to be sure to remain within the viscoelastic domain. The in phase and the out of phase components of the complex viscosity (η^*) are determined at frequencies

ranging from 0.1 rad/s to 100 rad/s at temperatures of 160 °C and 190 °C respectively for LLDPE and PS films.

For each materials, the complex viscosity modulus (η^*) and the tangent of the loss angle factor ($\tan\delta$) were measured over range of frequencies. The level of the complex viscosity is in direct correlation with the average weight molecular weight (Mw) of the materials and the loss angle factor with the mobility of the macromolecular chains. For melt rheology test, the samples were sent to Institut de Chimie de Clermont-Ferrand, Université Blaise Pascal (CNRS), France and this test was performed by dr. Vincent Verney.

10.3.2 Fourier transform infrared analysis (FTIR)

FT-IR is short for Fourier Transform Infrared. In this study, FTIR analysis was used to detect the chemical changes on plastic surface due to chemical and biological treatments.

Fourier Transform Infrared spectroscopy is an experiment that probes the interaction of infrared light with chemical bonds in molecules. When the infrared radiation hits some matter, it can be absorbed, causing some chemical bonds to vibrate. Light is formed by two kinds of waves, one is an electric wave and the other is a magnetic wave. These two waves travel in two separate planes which are perpendicular to each other. The third plane, which is perpendicular to the two planes mentioned above, is the light traveling plane. The electric part of light can interact with molecules. This electric vector of light has a sine wave manner and the amplitude is changing over time. The wavelength is the distance between two adjacent wave peaks, valleys or same points in phase.

$$W = \frac{1}{\lambda} \tag{10.1}$$

Where,

λ is being used to represent wavelength (cm)

W is representing wavenumber (cm⁻¹)

Wavenumber is the most common way of denoting the different kinds of light. The wavenumber of a particular light wave is proportional to the energy contained in the light wave. Equation 10.1 presents the relation of wavelength and wavenumber.

In this study, the infrared lights are defined between 500 cm⁻¹ to 4000 cm⁻¹. All matter in the universe gives off infrared radiation above absolute zero. When infrared radiation meets the molecules in matter, it can be absorbed and cause the chemical bonds to vibrate. Light with a certain wavenumber can be absorbed by the only correlated chemical bond or bonds, no matter what the rest of the molecule structures are. In this way, measuring the absorption or the transmittance of the light with different wavenumbers can determine the types of chemical bonds or the function groups included in molecules and the rough amount of them. If there is more of one kind of bond, the percentage of the absorption or the transmittance of this correlated wavenumber would be more [71].

FTIR detects the vibration characteristics of chemical functional groups on the surface of treated and non-treated samples. By FTIR spectra, the functional groups induced on the films were characterized:

- The peaks of C=O between 1710 to 1750 cm⁻¹ for R(C=O)-H, R(C=O)-R
- The peaks of -CH₂- around 1465 cm⁻¹
- The peaks of O-H occur around 3300 cm⁻¹
- The peaks of C-O-C are at 1080 to 1110 cm⁻¹ [71].

10.3.2.1 Quantification of carbonyl groups generation

For comparison of ozonation effect on different polymers (LLDPE, PS and PP), the carbonyl index was calculated as it is shown in equation 10.2. It reflects the abundance of carbonyl groups. The use of this carbonyl index compensates the differences in thickness of polymer (54)

$$\text{Carbonyl Index} = \frac{I_{C=O}}{I_{CH_2}} \quad (10.2)$$

Where, $I_{C=O}$ and I_{CH_2} correspond to relative absorbance intensities of carbonyl group and methylene band respectively.

In this research the carbonyl groups generated by different oxidation processes as well as changes in the chemical composition of the polymers are detected by FTIR analysis. The polymer surfaces were characterized for their functional groups by the Fourier transform infrared spectrometer, MKII Golden Gate single reflection ATR system (Specac, USA). The samples (film or powder) were placed on to the surface of the diamond. 32 scans for each sample were collected in transmission mode (wavenumber range of 4000 cm^{-1} to 500 cm^{-1} ; spectral resolution of 8 cm^{-1}). Data analysis was carried out by Agilent Technology software version 5.2.

10.3.3 Differential scanning calorimetry (DSC)

Differential Scanning Calorimetry (DSC) is a well-known technology which is applied in many thermal research areas. Characteristic caloric values, such as heat capacity, heat of transition, kinetic data, purity and glass transition, can be obtained with this measurement. The heat flow of the samples as a function of temperature is scanned in a

constant heating rate [72]. In this study, DSC analysis was used as a method to detect the changes in thermal stability of studied plastics relative to chemical and biological treatment.

A Perkin Elmer DSC 8500 was used in this research and the data were analysed with Pyris software. There were two measuring spots inside the heating chamber, which is adiabatic from the outside environment. One was used to locate the testing sample and the other one was for a reference sample. The sample was kept in a small sealed aluminum pan and the reference sample was just a sealed aluminum pan without any object inside. The two samples were seated on the two spots symmetrically in order to achieve equally high heat flow flowing through the pans. If the two samples were ideally symmetrical (same pans and same testing materials inside the pans), the heat flow rates traveling into and out from the two pans would be the same and the differential temperature signal ΔT (originally a difference of electric potentials measured and captured by system) could be zero. So the balance could be disturbed by adding testing material into one of the pans and in this way, a differential signal of temperature or electric potential would be generated. The onset melting temperature of the samples were measured and compared in this study. The heat flow of the samples as a function of temperature is scanned in a constant heating rate. Figure 10.1 shows a typical DSC curve.

DSC was used to heat up polymer samples from 30 °C to 200 °C at a constant heating rate of 20 °C/min. The runs were conducted under nitrogen atmosphere. Mass of the samples was kept between 2 to 4 mg.

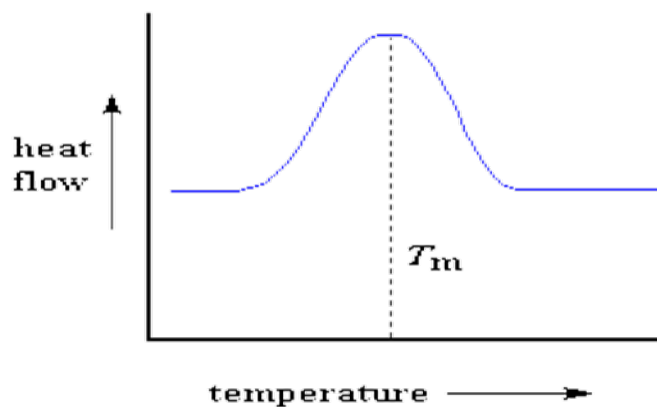


Figure 10.1 Typical DSC curve

10.3.4 Thermogravimetric Analysis (TGA)

Thermogravimetric Analysis (TGA) is a technology which can be used to measure a material's thermo stability. The changes in mass of a substance can be detected and graphically recorded when cooling or heating, as a function of temperature or time. And the curve or trace provided in TGA is known as a thermogram or thermo-weighing curve.

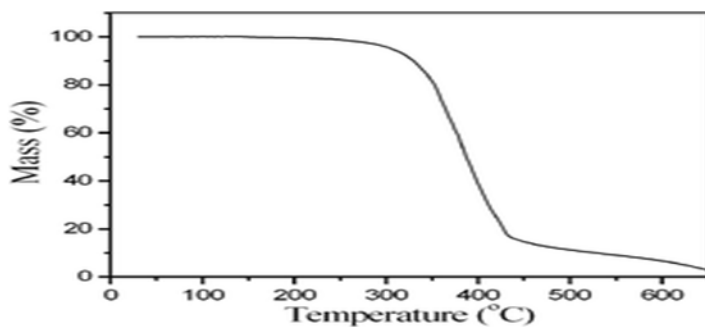


Figure 10.2 Typical thermogram curve

Thermal degradation begins with the breaking of the bonds which form the weakest links in polymer molecule chains. As there are irregularities that can act as the weak links,

most polymers decompose at a substantially lower temperature than the comparable smaller molecules [73].

The thermogravimetric analysis of the polymers was carried out on a Perkin Elmer TG analyser 4000 under nitrogen atmosphere. Sample weights varied from 2 to 7 mg. The thermograms were recorded for the range from room temperature to 800 °C at a heating rate of 5 °C/min. The nitrogen gas flow was 20 mL/min. The maximum degradation temperature (TDTG) of the samples was compared. The Pyris software was utilized for data analysis.

10.3.5 Microscopic pictures of polymer's surfaces

The Atomic Force Microscopy (AFM), is an important tool for imaging surfaces. In AFM, a sharp tip at the end of a cantilever is scanned over a surface. While scanning, surface features deflect the tip and thus the cantilever. By measuring the deflection of the cantilever, a topographic image of the surface can be obtained. With sufficient sensitivity in the spring deflection sensor, the tip can reveal surface profiles with sub-nanometer resolution. In this study, AFM were used to evaluate the surface topography by measuring the roughness of the surfaces. Characterization of surface roughness was conducted by silicon cantilever [74].

Also, a Scanning Electron Microscope (SEM) was used to monitor the polymer's surfaces. SEM scans a focused electron beam over a surface to create an image. The electrons in the beam interact with the sample, producing various signals that can be used to obtain information about the surface topography and composition.

10.3.6 Colony forming unit (CFU) of bacterial growth

The growth of bacterial that use polymers as the only carbon source can be considered as biodegradation indication. In this research colony forming unit (CFU) was applied to evaluate the growth of bacteria in presence of polymers as the only carbon substrate. The bacterial growth of the cultures, incubated with polymers, was monitored by plating method. In this method, 10 μ L of the aliquot of incubated polymers in the medium was diluted serially and incubated on standard agar solid media in sterile petridish for 24 hours.

10.4 Advantages/disadvantages of analytical methods

In this study, the mentioned analytical methods were important and useful methods to evaluated different aspect of plastic properties after and before chemical and biological treatments.

- FTIR analysis was used to detect the chemical modification of plastic surface relative to chemical and biological treatment.
- DSC and TGA analysis measured melting temperature and decomposition temperature of studied plastics respectively.
- Melt rheology test was used to evaluate the changes relative to structure and molecular weight of plastics.
- Microscopic images taken by AFM and SEM could monitor the topography of plastic surface.

As it will be shown in results of next chapter, most of these analytical methods such as FTIR, DSC, TGA and melt rheology can detect precisely the changes related to chemical treatment which has a strong influence in chemical, thermal and structural properties of studied plastics. The main disadvantage of these methods is that they cannot detect the

small changes due to biological treatments (which mainly affect just the surface of plastic).

On the other hand, microscopic methods such as AFM and SEM and weight loss measurement are more powerful to monitor the signs related to biological treatment. However, it should be considered that the error measurement these methods are significantly high.

11 Chemical treatment of polymers

11.1 Results of analytical methods

In this study, the generation of carbonyl groups (as a functional group for improving hydrophilic property of different polymers) by ozonation and also UV/ozonation in gaseous phase and aqueous phase, was investigated. For all of the experiments, applied ozone dose in gaseous phase was 1.3 wt% with ozone concentration of 20 mg/L and flow rate of 5 L/min.

11.1.1 FTIR analysis of LLDPE film and powder in gaseous phase ozonation

Figure 11.1 presents the infrared spectra of virgin LLDPE film and 6, 12, 18 and 20 hours ozonated LLDPE films in gaseous phase. A peak of hydrophilic group C=O occurs at 1709 cm^{-1} after ozonation and enhances with ozonation time.

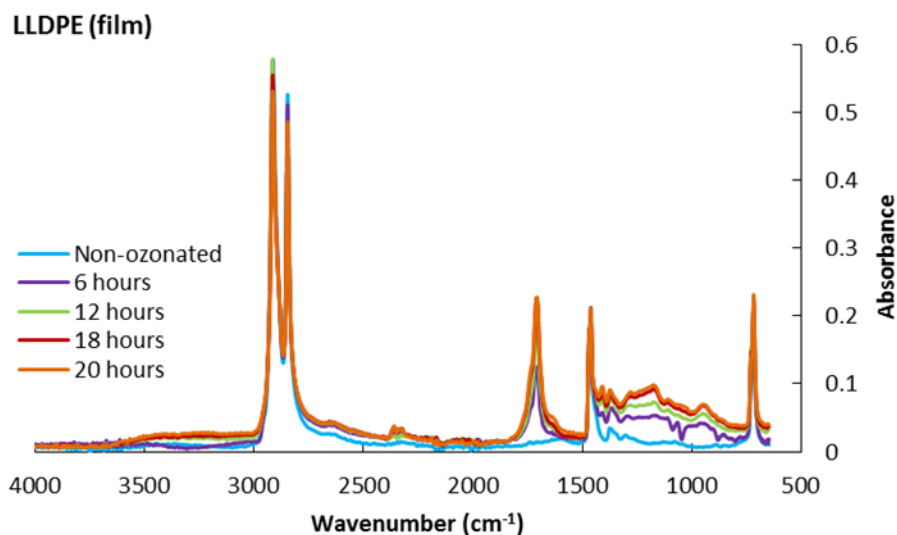


Figure 11.1 FTIR spectra of LLDPE film

virgin LLDPE film (blue), 6 hours ozonated LLDP film (purple), 12 hours ozonated LLDPE film (green), 18 hours ozonated LLDPE film (red) and 20 hours ozonated LLDPE film (orange)

Figure 11.2 presents the infrared spectra of virgin LLDPE powder and 6, 12, 18 and 20 hours ozonated LLDPE powder in gaseous phase. A peak of hydrophilic group C=O occurs also at 1709 cm^{-1} after ozonation of LLDPE powder and enhances with ozonation time.

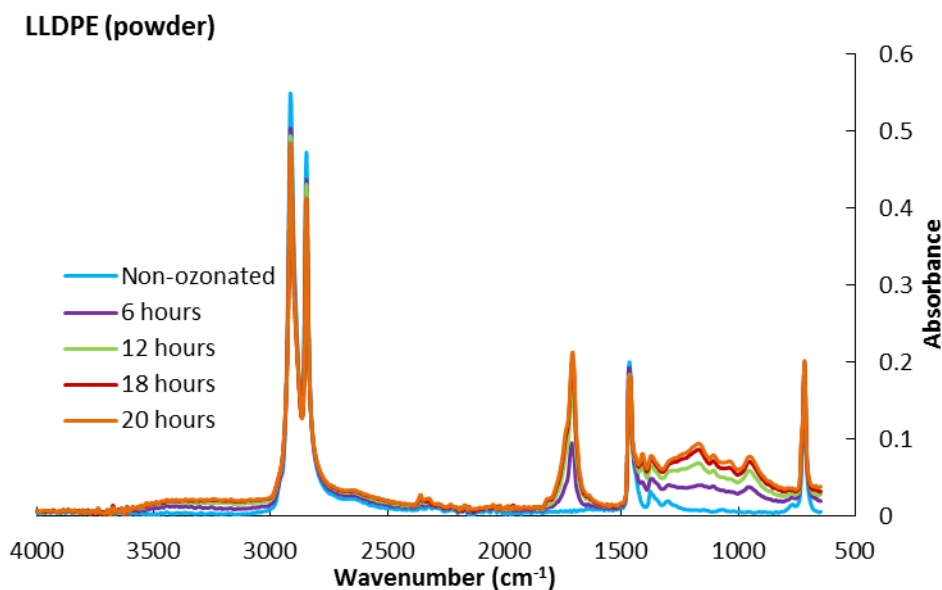


Figure 11.2 FTIR spectra of LLDPE powder

virgin LLDPE powder (blue), 6 hours ozonated LLDP powder (purple), 12 hours ozonated LLDPE powder (green), 18 hours ozonated LLDPE powder (red) and 20 hours ozonated LLDPE powder (orange)

11.1.2 Carbonyl index of gaseous phase ozonated LLDPE

Figure 11.3 shows the formation of carbonyl groups on the surface of LLDPE films and powder exposed to ozone in different exposure time.

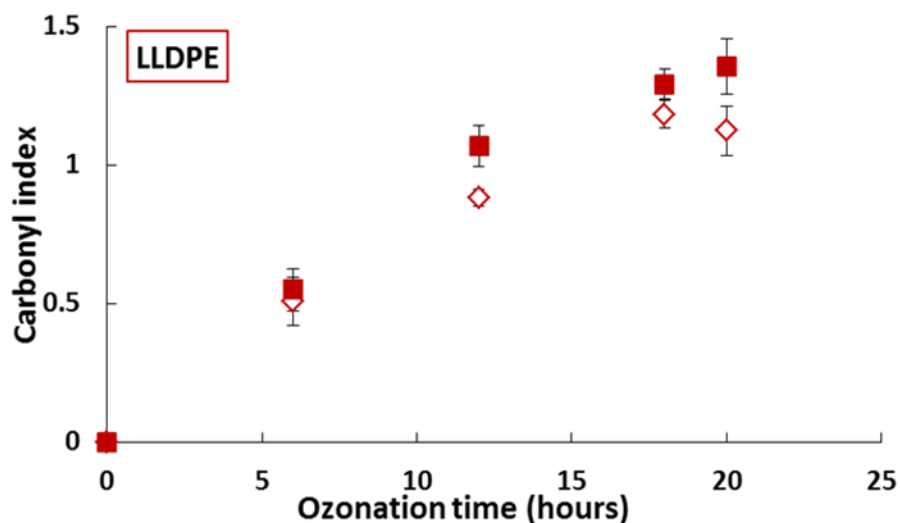


Figure 11.3 carbonyl index versus different ozonation time
 LLDPE film (empty diamonds), LLDPE (filled square)

The Carbonyl index value increases with prolongation in ozonation. Comparison of carbonyl index of film and powder ozonated LLDPE reveals that this value is slightly higher on the powder surface.

11.1.3 FTIR analysis of PP film and powder in gaseous phase ozonation

Figure 11.4 presents the infrared spectra of virgin PP film and 6, 12, 18 and 20 hours ozonated PP films in gaseous phase. The formation of hydrophilic group C=O was observed to be the same results as of ozonated LLDPE films. Carbonyl peak occurs at 1709 cm^{-1} after ozonation and enhances with ozonation time.

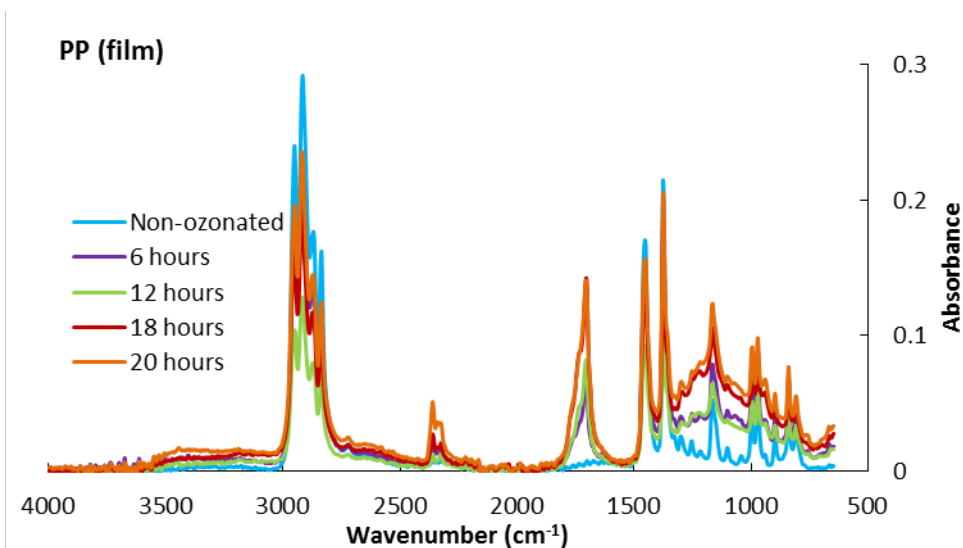


Figure 11.4 FTIR spectra of PP film

virgin PP film (blue), 6 hours ozonated PP film (purple), 12 hours ozonated PP film (green), 18 hours ozonated PP film (red) and 20 hours ozonated PP film (orange).

Figure 11.5 presents the infrared spectra of virgin PP powder and 6, 12, 18 and 20 hours ozonated PP powder in gaseous phase. A peak of hydrophilic group C=O occurs also at 1709 cm^{-1} after ozonation of PP powder and enhances with ozonation time.

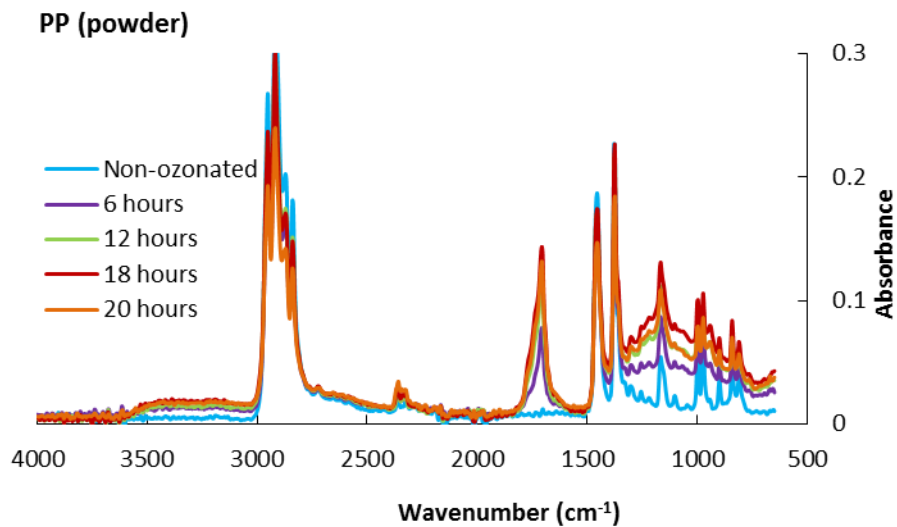


Figure 11.5 FTIR spectra of PP powder

virgin PP powder (blue), 6 hours ozonated PP powder (purple), 12 hours ozonated PP powder (green), 18 hours ozonated PP powder (red) and 20 hours ozonated PP powder (orange).

11.1.4 Carbonyl index of gaseous phase ozone ozonated PP

Figure 11.6 shows the formation of carbonyl groups on the surface of PP films and powder exposed to ozone in different exposure time. The carbonyl index of ozonated PP film and powder increase with ozonation time. This value reaches 1.2 and 1.09 after 20 hours ozonation for PP film and powder respectively.

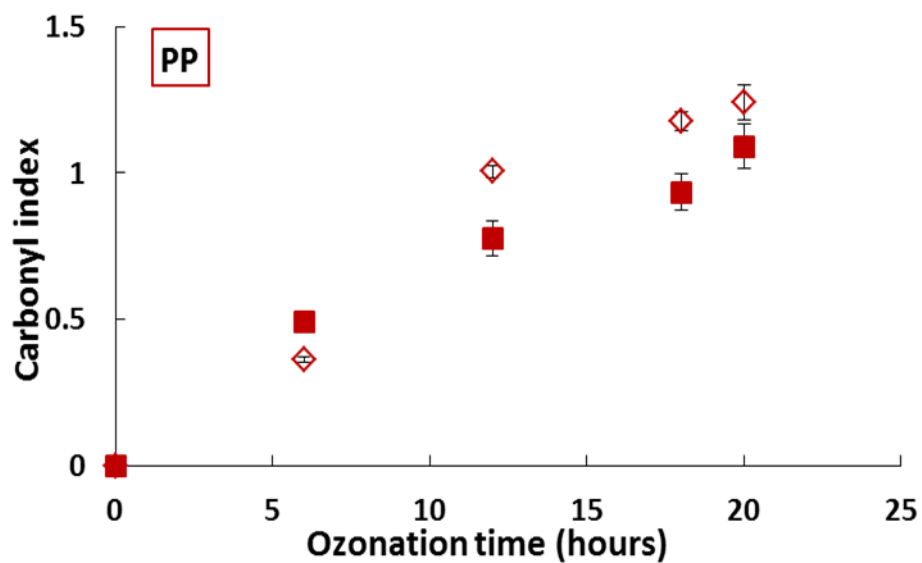


Figure 11.6 carbonyl index versus different ozonation time

PP film (empty diamonds), PP (filled square)

11.1.5 FTIR analysis of PS film and powder in gaseous phase ozonation

Figure 11.7 presents the infrared spectra of virgin PS film and 6, 12, 18 and 20 hours ozonated PS films in gaseous phase. The formation of hydrophilic group C=O was observed to be the same as results of ozonated LLDPE and PP films. Carbonyl peak occurs at 1735 cm^{-1} after ozonation and enhances with ozonation time.

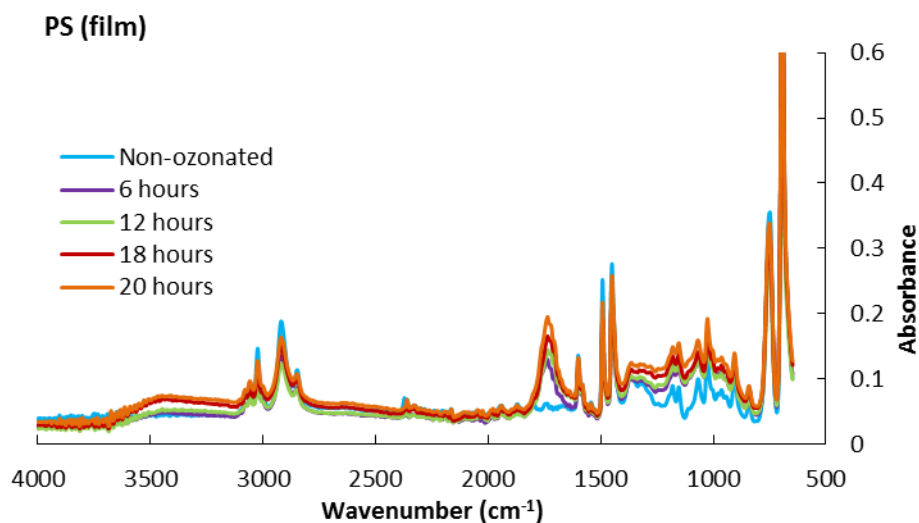


Figure 11.7 FTIR spectra of PS film

virgin PS film (blue), 6 hours ozonated PS film (purple), 12 hours ozonated PS film (green), 18 hours ozonated PS film (red) and 20 hours ozonated PS film (orange).

Figure 11.8 presents the infrared spectra of virgin PS powder and 6, 12, 18 and 20 hours ozonated PS powder in gaseous phase. A peak of hydrophilic group C=O occurs also at 1735 cm^{-1} after ozonation of PS powder and enhances with ozonation time.

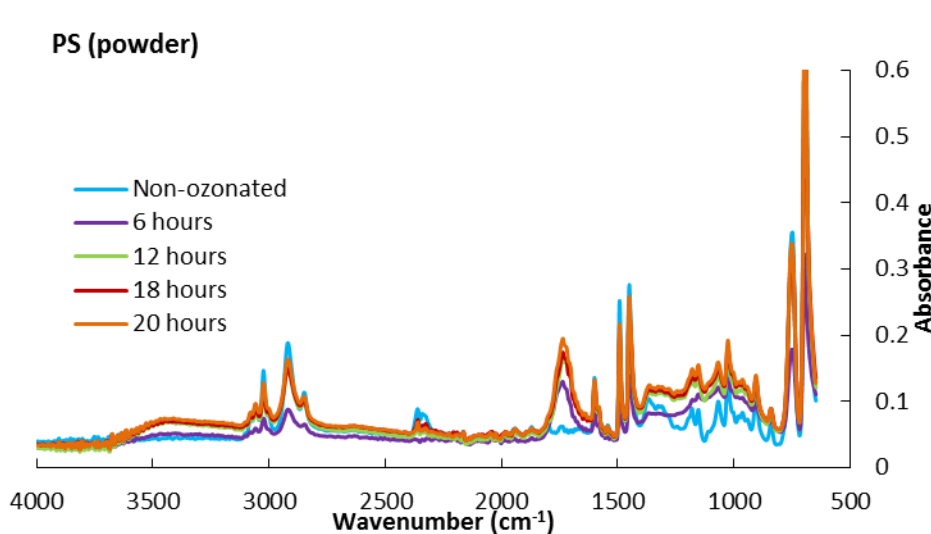


Figure 11.8 FTIR spectra of PS powder

virgin PS powder (blue), 6 hours ozonated PS powder (purple), 12

hours ozonated PS powder (green), 18 hours ozonated PS powder (red) and 20 hours ozonated PS powder (orange).

11.1.6 Carbonyl index of gaseous phase ozonated PS

Figure 11.9 shows the formation of carbonyl groups on the surface of PS films and powder exposed to ozone in different exposure time. The carbonyl index of ozonated PS film and powder increase with ozonation time. This value reaches 0.83 and 1.02 after 20 hours ozonation for PS film and powder respectively.

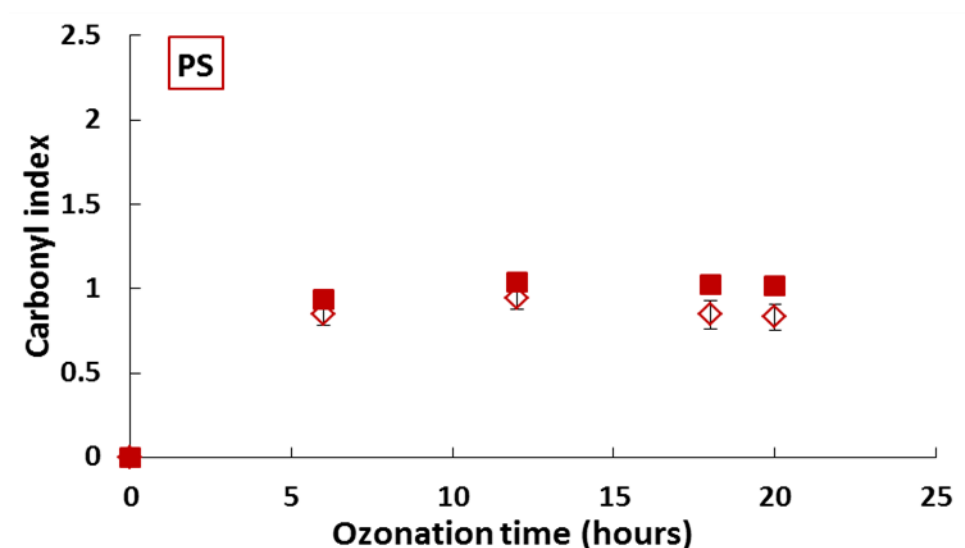


Figure 11.9 carbonyl index of PS versus different ozonation time

PS film (empty diamonds), PS (filled square)

11.1.7 FTIR analysis of PVC film and powder in gaseous phase ozonation

Figure 11.10 presents the infrared spectra of virgin PVC film and 10, 15 and 20 hours ozonated PVC film in gaseous phase. The presence of a peak of carbonyl groups at 1732 cm^{-1} , confirms that PVC samples contain additives. FTIR spectra do not reveal any significant effect of ozonation of the surface of PVC films.

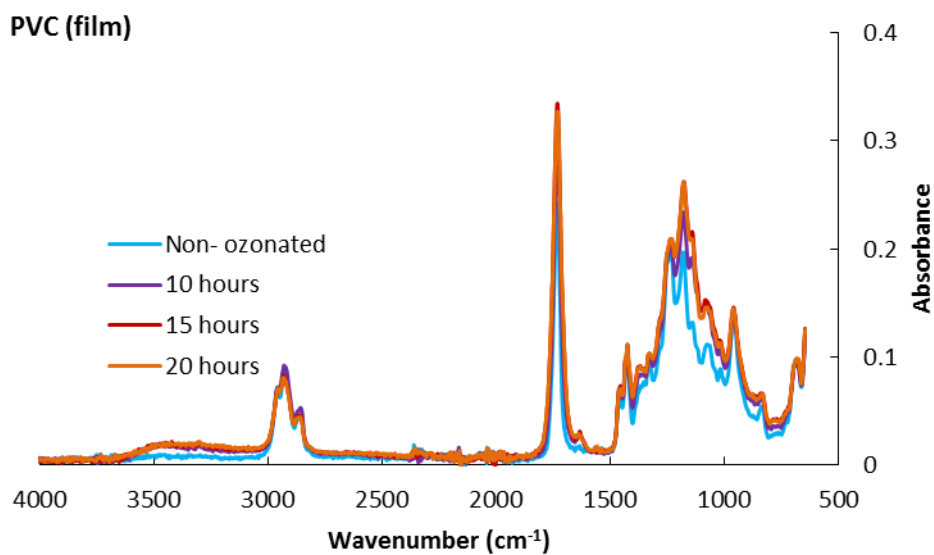


Figure 11.10 FTIR spectra of PVC film

PVC film (blue), 10 hours ozonated PVC film (purple), 15 hours ozonated PVC film (red), and 20 hours ozonated PVC film (orange).

Figure 11.11 presents the infrared spectra of virgin PVC powder and 6, 12, 18 and 20 hours ozonated PVC powder in gaseous phase. It can be concluded from this graph that ozonation does not have any significant effect of formation of functional groups on the PVC surface without any additives.

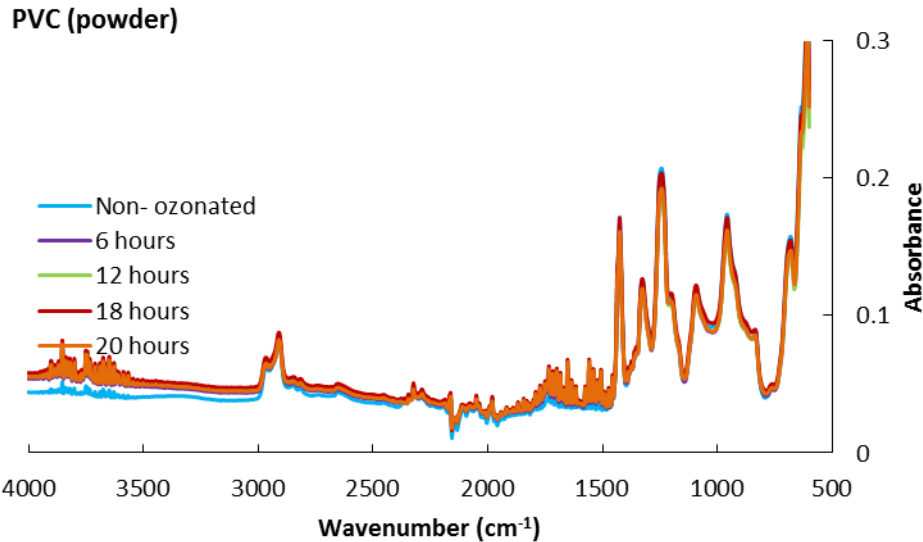


Figure 11.11 FTIR spectra of PVC powder

virgin PVC powder (blue), 6 hours ozonated PVC powder (purple), 12 hours ozonated PVC powder (green), 18 hours ozonated PVC powder (red) and 20 hours ozonated PVC powder (orange).

11.1.8 Carbonyl index of gaseous phase ozonated PVC

Figure 11.12 shows the formation of carbonyl groups on the surface of PVC films exposed to ozone in different exposure time. The carbonyl index of virgin PVC film measured 1.12 and after ozonation of films for 15 and 20 hours this value reached 2.2 and 1.8 respectively.

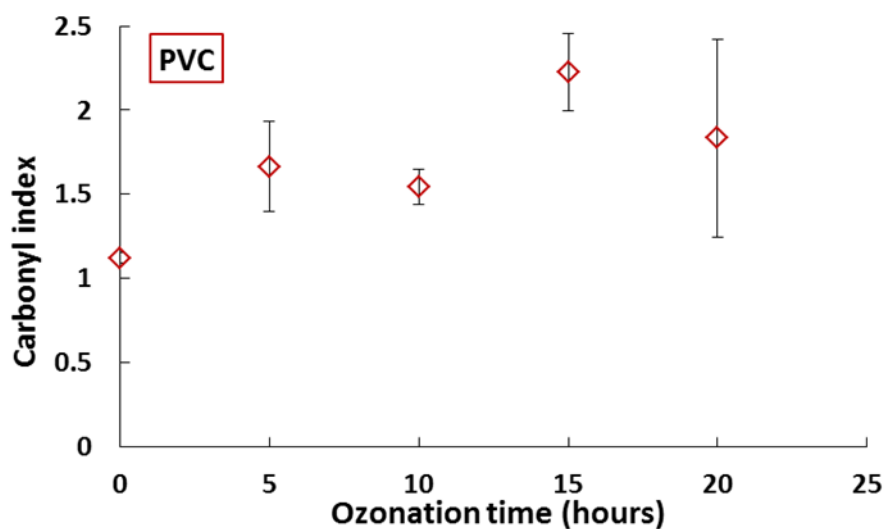


Figure 11.12 Carbonyl index versus different ozonation time of PVC film

11.1.9 Effect of different treatment on carbonyl groups generation

FTIR analysis of gaseous phase ozonated polymers revealed the positive effect of ozonation on formation of functional groups on the surface of LLDPE, PP and PS film and powder. In the next set of treatment tests these polymers were chosen in the form of film and exposed to ozone and UV/ozone for 10 hours in gaseous and aqueous phases. The effects of different kind of treatments on formation of carbonyl groups have been compared.

11.1.10 Ozone and UV/ozone treatment of LLDPE in gaseous and aqueous phases

LLDPE films were exposed to ozone and UV/ozone in separated batches of gaseous and aqueous phases for 10 hours. Some samples were taken during the treatments and analyzed with FTIR analysis. For all of the treatment processes, the formation and enhancing of carbonyl peak were observed. In order to compare the efficiency of

different type of treatment carbonyl index of treated LLDPE films was calculated and compared.

Figure 11.13 shows the value of carbonyl index versus time for treated LLDPE film. The carbonyl index increases after exposing LLDPE film to ozone and UV/ozone. However, the gaseous phase treatment is more effective in terms of carbonyl groups generation. Furthermore, the UV/ozone treatment is the most effective method to create hydrophilic groups on the surface of LLDPE films.

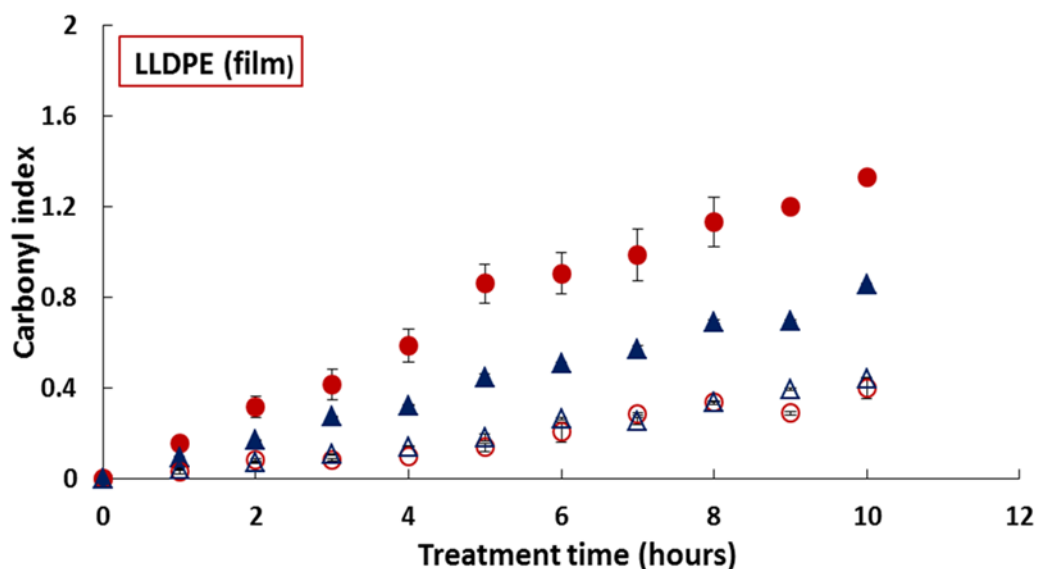


Figure 11.13 Carbonyl index versus treatment time of LLDPE film

UV/O3 gaseous phase (filled circle), UV/O3 aqueous phase (empty circle), O3 gaseous phase (filled triangle), O3 aqueous phase (empty triangle)

11.1.11 Ozone and UV/ozone treatment of PP in gaseous and aqueous phases

PP film samples were subjected to ozone and UV/ozone treatment in separated batches of gaseous and aqueous phases for 10 hours. The carbonyl index of treated PP film was

calculated and compared for different type of treatment. Figure 11.14 presents the carbonyl index of PP films versus time of treatment. The effect of ozonation and UV/ozonation of PP film in aqueous phase is almost the same in terms of carbonyl groups generation while comparing to the same treatments in gaseous phase is significantly less. The results of gaseous phase UV/ozone treatment of PP films reveals that this treatment is the most effective oxidation method for generation of carbonyl groups.

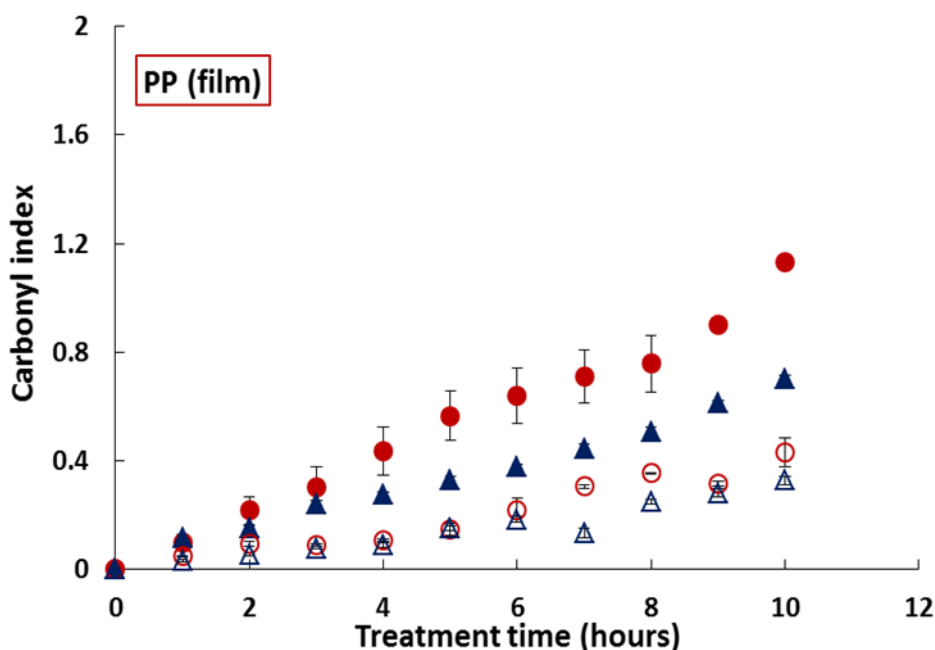


Figure 11.14 Carbonyl index versus treatment time of PP film

UV/O3 gaseous phase (filled circle), UV/O3 aqueous phase (empty circle), O3 gaseous phase (filled triangle), O3 aqueous phase (empty triangle)

11.1.12 Ozone and UV/ozone treatment of PS in gaseous and aqueous phases

PS films were subjected to ozone and UV/ozone treatment in separated batches of gaseous and aqueous phases for 10 hours. Figure 11.15 Presents the carbonyl index versus treatment time of PS film samples. Carbonyl index of ozonated and UV/ozonated PS in aqueous phase with treatment time for 4 to 5 hours and after 5 hours the value stays

constant. The same results have been obtained from FTIR analysis of PS ozone and UV/ozone treated in gaseous phase. This observation might be related to chain recombination and cross linking in PS due to oxidation processes.

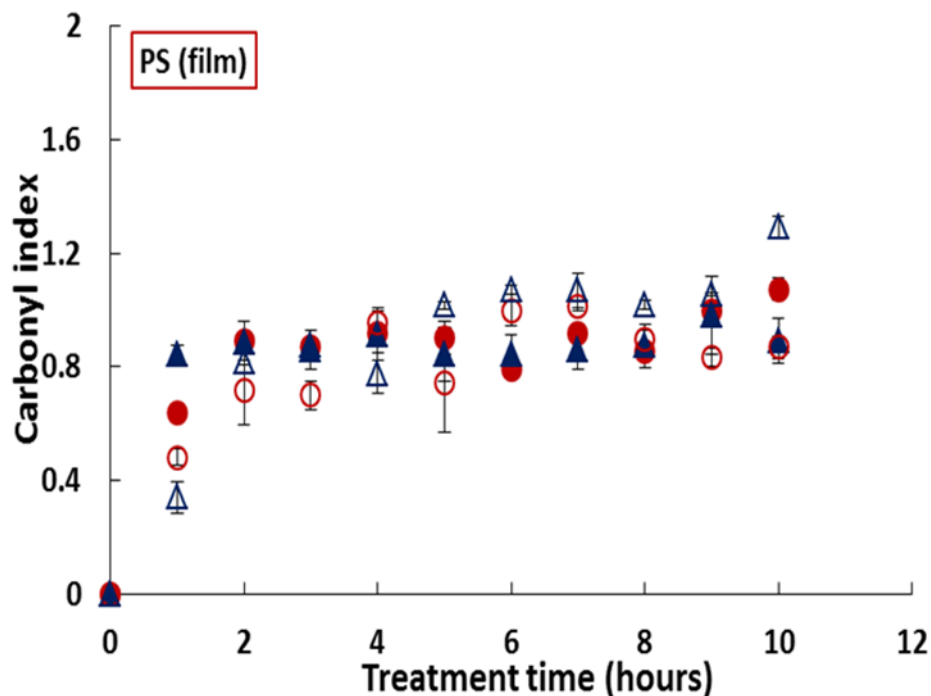


Figure 11.15 Carbonyl index versus treatment time of PS film

UV/O3 gaseous phase (filled circle), UV/O3 aqueous phase (empty circle),
O3 gaseous phase (filled triangle), O3 aqueous phase (empty triangle)

11.1.13 Effect of longer exposure time to UV/ozone

As the results of last section shows, the gaseous phase UV/ozone treatment is the most effective treatment method to produces the higher amount of carbonyl groups on the surface of LLDPE and PP. Furthermore, carbonyl index of PS exposed to different kind of oxidation treatments reaches a stable value after 4 or 5 hours of treatment. The effect of longer exposure time to gaseous phase UV/ozone was studied for LLDPE and PP film

samples. For this, LLDPE and PP films were treated in gaseous phase UV/ozone reactor for 44 hours. The samples were taken for FTIR analysis every 4 hours and the carbonyl index of treated LLDPE and PP films was calculated.

Figure 11.16 presents the carbonyl index versus UV/ozone treatment time of LLDPE in gaseous for 44 hours. The carbonyl index increases with longer exposure to UV/ozone. However the rate of carbonyl index increase was slowed down.

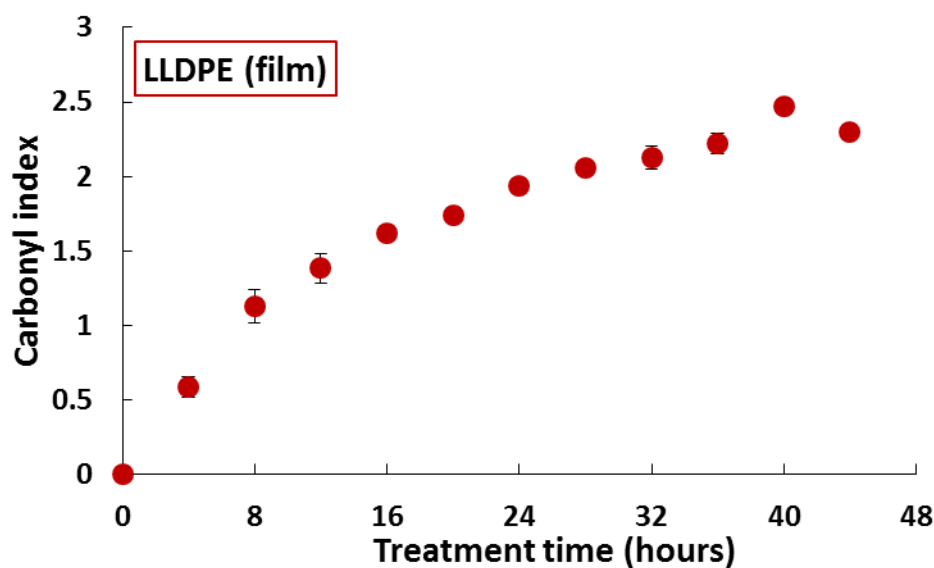


Figure 11.16 Carbonyl index versus gaseous UV/ozonation time of LLDPE film

Figure 11.17 shows the carbonyl index versus UV/ozonation time of PP films in gaseous phase reactor. After 25 hours of treatment the carbonyl index reaches a constant value. Furthermore, after 18 hours of UV/ozonation the film samples got very fragile.

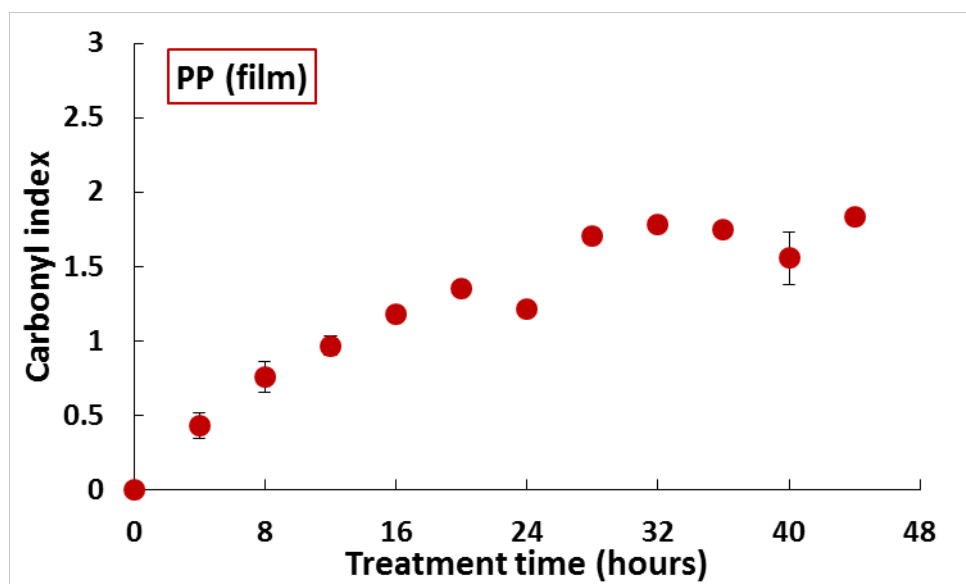


Figure 11.17 Carbonyl index versus gaseous UV/ozonation time of PP film

11.2 Aging test on the treated polymer films

Stability of generated carbonyl groups, generated by UV/ozone treatment, was examined. LLDPE, PP and PS films were treated in gaseous and aqueous UV/ozone reactor for 10 hours. The carbonyl index of treated films was analyzed immediately after treatment processes. The treated polymer films were introduced to two different aging conditions : i) in water and ii) in ethanol 70%, for 12 days and during this aging time some of film samples were taken for FTIR analysis and carbonyl index measurements.

11.2.1 Carbonyl groups stability of UV/ozonated LLDPE films

The stability of carbonyl groups generated on LLDPE films after UV/ozonation in gaseous phase and aqueous phase was compared. Figure 11.18 presents the carbonyl index of gaseous phase UV/ozonated LLDPE stored in water and in ethanol 70%. The reduction of carbonyl index value aged in water and in ethanol 70% after 12 days is 6% and 24% respectively.

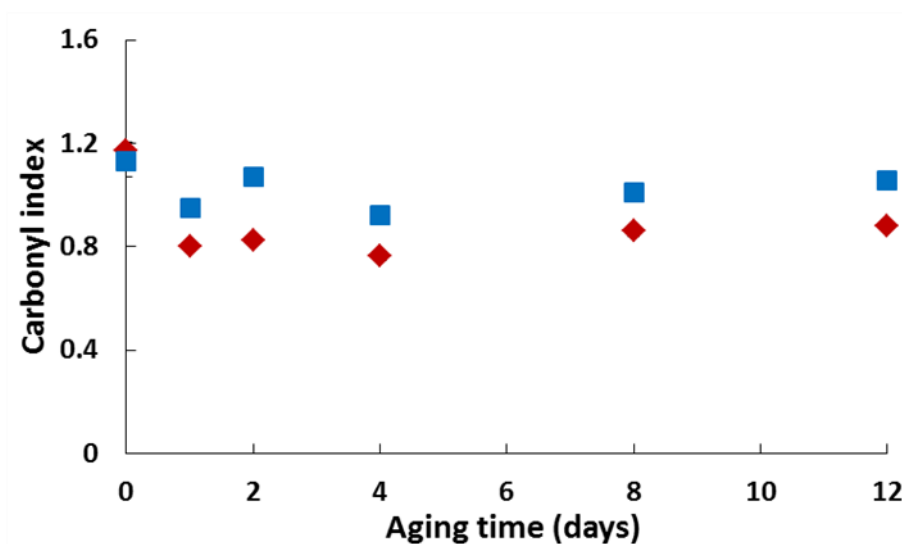


Figure 11.18 carbonyl index versus aging time of gaseous phase UV/O₃ LLDPE
In water (blue Square) and in ethanol 70% (red diamond)

Figure 11.19 presents the effect of aging in water and in ethanol 70% on reduction of carbonyl index of aqueous phase UV/ozonated LLDPE films. The reduction of carbonyl index value aged in water and in ethanol 70% after 12 days is 1.8% and 1% respectively. It can be concluded, stability of carbonyl groups generated by aqueous phase UV/ozonated LLDPE is higher.

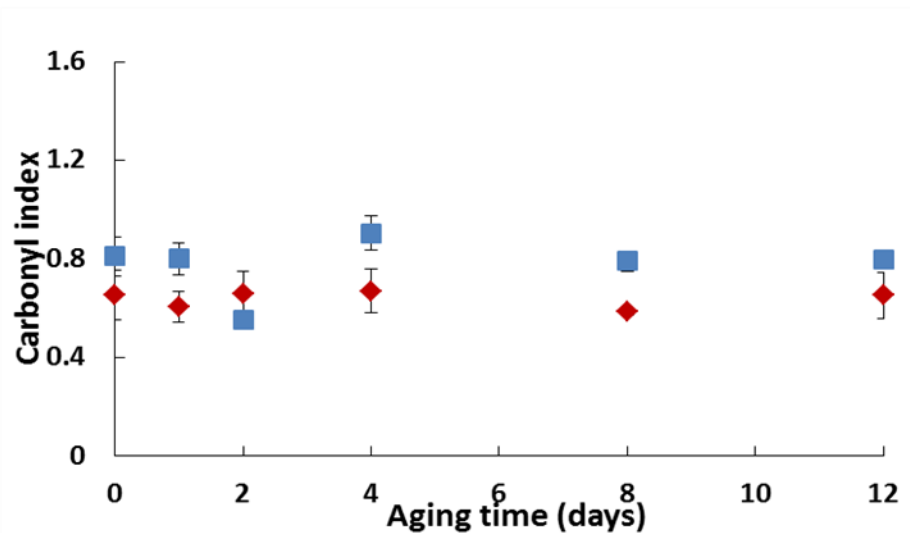


Figure 11.19 carbonyl index versus aging time of aqueous phase UV/O₃ LLDPE
 In water (blue Square) and in ethanol 70% (red diamond)

11.2.2 Carbonyl groups stability of UV/ozonated PP films

Gaseous phase UV/ozonated PP films were analysed immediately after treatment and after 12 days being stored in water and ethanol 70%. Figure 11.20 shows the carbonyl index of aged gaseous phase UV/ozonated PP. The reduction of carbonyl index value aged in water and in ethanol 70% after 12 days is 26% and 35% respectively.

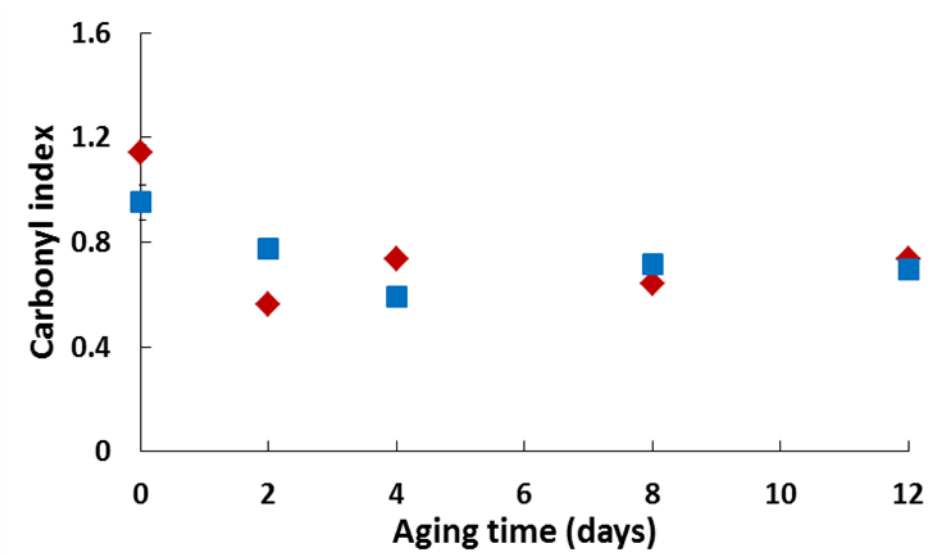


Figure 11.20 carbonyl index versus aging time of gaseous phase UV/O₃ PP
 In water (blue Square) and in ethanol 70% (red diamond)

Figure 11.21 presents the carbonyl index of aqueous phase UV/ozonated PP film versus aging time in water and in ethanol 70%. The reduction of carbonyl index value aged in water and in ethanol 70% after 12 days is around 12% for both aging conditions.

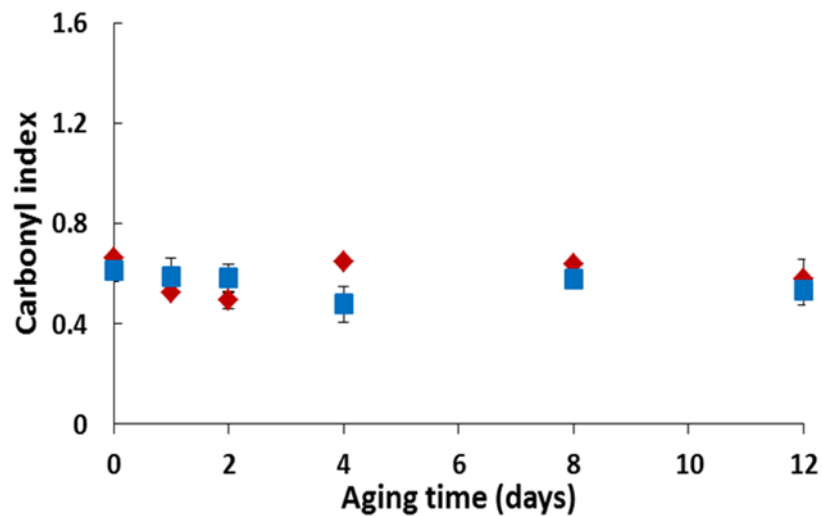


Figure 11.21 carbonyl index versus aging time of aqueous phase UV/ozonated PP
 In water (blue Square) and in ethanol 70% (red diamond)

11.2.3 Carbonyl groups stability of UV/ozonated PS films

Gaseous phase UV/ozonated PS films aged in water and ethanol for 12 days. Figure 11.22 shows that the carbonyl index reduced up to 40% and 76% for samples aged in water and in ethanol 70% respectively.

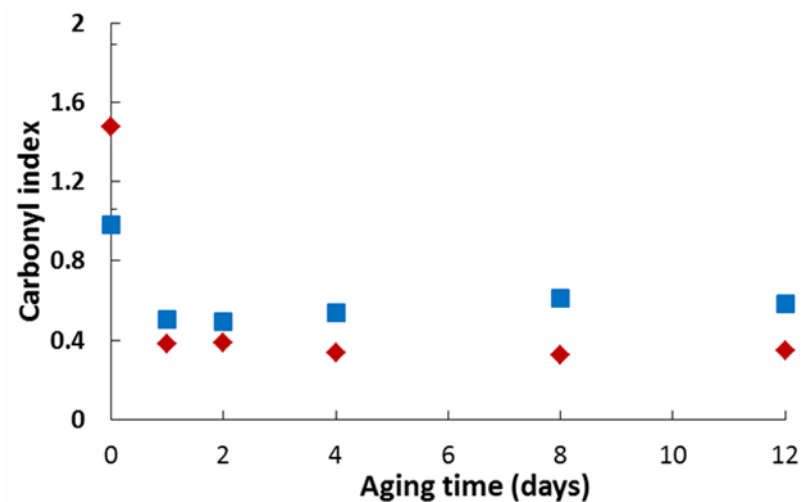


Figure 11.22 carbonyl index versus aging time of gaseous phase UV/ozonated PS

In water (blue Square) and in ethanol 70% (red diamond)

Figure 11.23 presents the carbonyl index of aqueous phase UV/ozonated PS film versus aging time in water and in ethanol 70%. The reduction of carbonyl index value aged in water and in ethanol 70% after 12 days is 35% and 47% respectively.

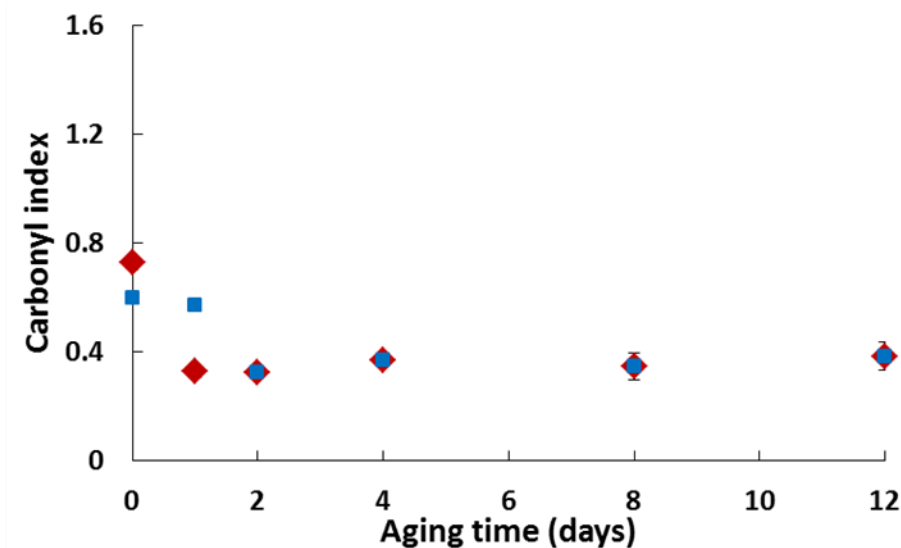


Figure 11.23 Carbonyl index versus aging time of aqueous phase UV/O₃ PS

In water (blue Square) and in ethanol 70% (red diamond)

Although, the generation of carbonyl groups on the surface of polymers is less effective in aqueous phase UV/ozonation but these results confirm that the carbonyl groups of aqueous phase treated polymers are more stable.

Overall, the results of the ozonation and UV/ozonation plastic pre-treatment show that carbonyl groups (C=O) occurs after these oxidation methods and enhances with ozonation time. Gaseous phase UV/ozonation is the most effective in method in terms of carbonyl groups generation.

12 Plastic biodegradation with pure or mixed bacterial cultures

12.1 Results of biological treatment of PS films with *Rhodococcus ruber*

In this set of experiments, gaseous phase ozonated (for 20 hours) and non-ozonated PS films were incubated with pure culture of *Rhodococcus ruber*, as the only carbon source of bacterial growth, for 88 days. The samples were prepared and incubated in biotic and abiotic conditions at the same time. The samples were taken after 12, 40 and 88 days of incubation. FTIR and melt rheology test were performed for taken samples and the effect of biotic and abiotic condition on chemical composition and structure of PS were investigated. The bacterial growth was monitored by colony forming unit (CFU) on the standard agar plates.

12.1.1 FTIR analysis of incubated PS with *Rhodococcus ruber*

FTIR analysis of ozonated and non-ozonated PS were performed for incubated samples under biotic and abiotic conditions. Washing procedure was carried out for all of the taken samples. The results were compared with the PS films at time zero of incubation. The FTIR spectra of non-ozonated PS film incubated with and without pure bacterial culture of *Rhodococcus ruber* did not show any significant differences (including appearance or disappearance of peaks) with samples before starting the incubation. The FTIR spectra of ozonated PS films incubated under biotic and abiotic conditions were performed and the carbonyl index of the samples was calculated based on the FTIR spectra. Figure 12.1 presents the carbonyl index of ozonated PS versus incubation time with pure bacterial culture. As it is shown, there are no changes on the chemical structure of PS surface related to biotic activity of bacteria culture.

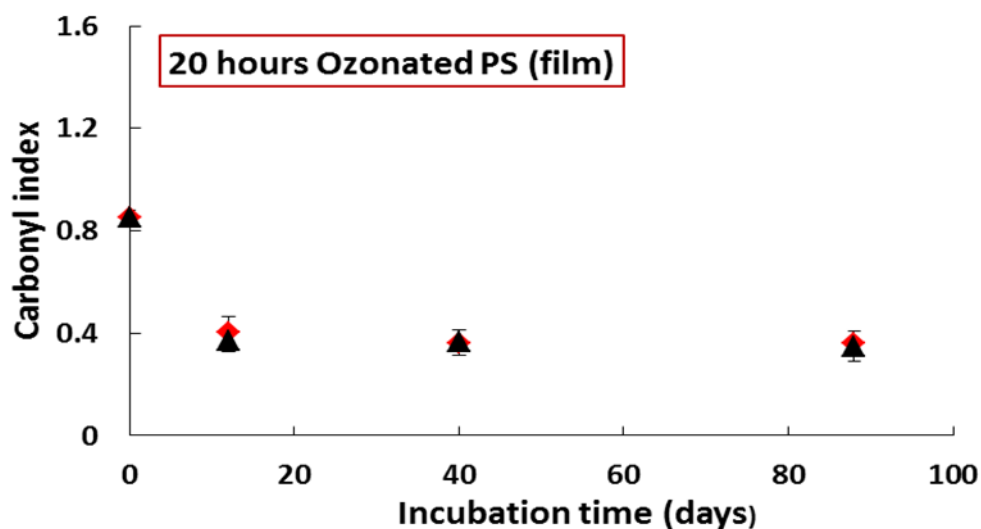


Figure 12.1 Carbonyl index versus incubation time of PS with *R. ruber*
 Ozonated PS incubated under biotic conditions (red diamond) and under abiotic conditions (black triangle)

12.1.2 Bacterial growth of *Rhodococcus ruber* on ozonated and non-ozonated PS

The bacterial growth was monitored by CFU method. In this test, ozonated and non-ozonated PS were the only carbon source for bacterial growth. Figure 12.2 presents the bacterial growth (CFU/mL) versus incubation time of PS with *Rhodococcus ruber*. As it is shown the growth of bacteria in the culture containing ozonated PS is slightly higher than the ones incubated with virgin PS. It can be an indication of positive effect of ozonation on enhancing the bioavailability of PS.

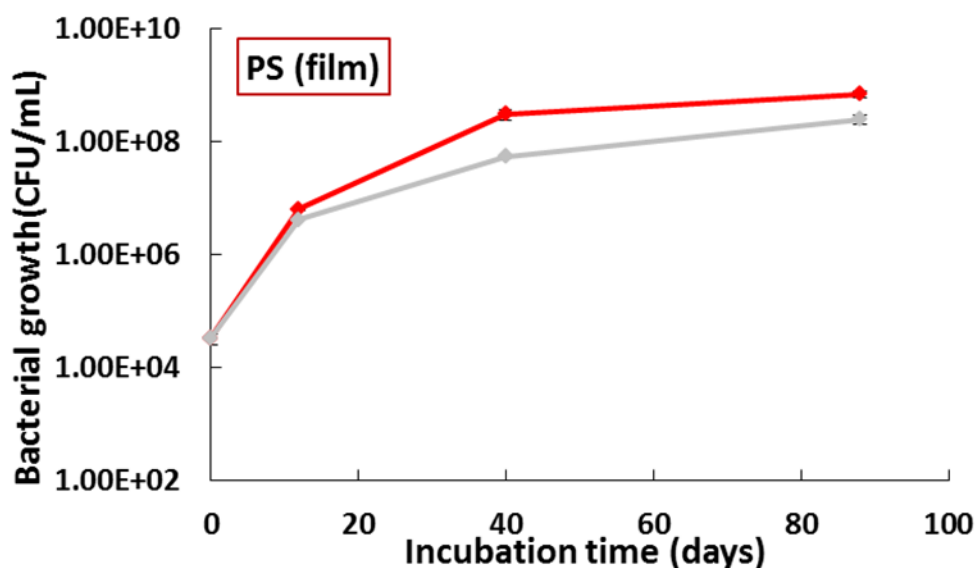


Figure 12.2 growth of pure bacterial culture versus incubation time with PS
Ozonated PS (red), non-ozonated PS (grey)

12.1.3 Effect of chemical and biotic treatment on melt rheology analysis of PS

Melt rheology test of ozonated and non-ozonated PS films were carried out before and after incubation with pure bacterial culture. Figure 12.3 and Figure 12.4 show the complex viscosity modulus (η^*) and the tangent of the loss angle factor ($\tan\delta$) respectively. As it was described before, the level of the complex viscosity is in direct correlation with the average weight molecular weight (M_w) of the materials and the loss angle factor with the mobility of the macromolecular chains. It can be concluded from Figure 12.3 and Figure 12.4 that:

- There is no difference between the structure of PS samples incubated in abiotic conditions and the ones exposed to biotic condition.

- Increase of the complex viscosity indicates that macromolecular chains recombine till to the cross-linked material. This is probably due to formation oxidative products formed onto the aromatic ring.
- Loss angle value decrease with ozonation due to chain recombination.

All of these results conclude that the chemical exposition to ozone leads to a higher molecular weight of PS film with a lower mobility of macromolecular chains. Then the mechanism is a chain recombination one.

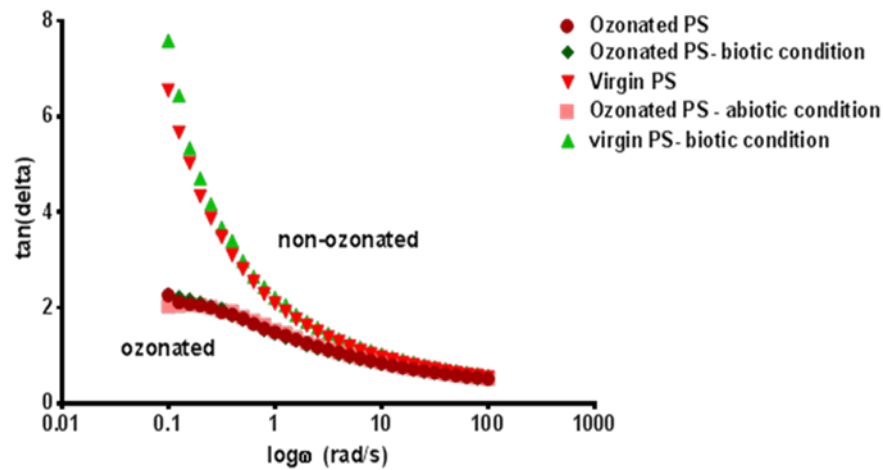


Figure 12.3 Tangent of the loss angle of PS versus oscillatory frequency

Ozonated PS (dark red circle), ozonated PS exposed to *R.ruber* (green diamond), non-ozonated PS (red triangle), ozonated PS in abiotic condition (pink square) and non-ozonated PS exposed to *R.ruber* (green triangle)

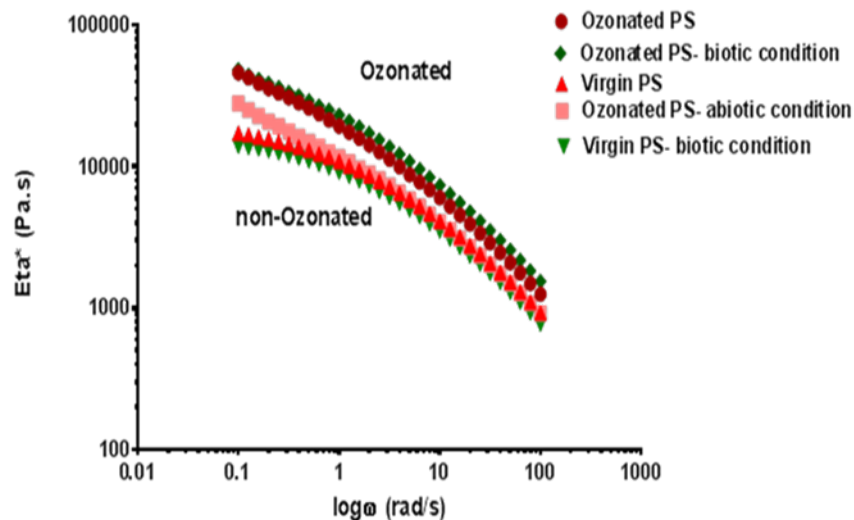


Figure 12.4 Complex viscosity of PS versus oscillatory frequency

Ozonated PS (dark red circle), ozonated PS exposed to *R.ruber* (green diamond), non-ozonated PS (red triangle), ozonated PS in

12.2 Biological treatment of PVC powder with *Rhodococcus ruber*

PVC powder samples (20 hours gaseous phase ozonated and non-ozonated) were subjected to the biodegradation test. The samples were incubated with pure bacterial culture of *Rhodococcus ruber* over 77 days. During the incubation period, some samples were taken out after 20, 40 and 77 days of incubation. In order to wash out the possible formed biofilm from the surface of PVC powder, the washing procedure was performed. The FTIR analysis of the PVC powder incubated under biotic and abiotic condition was carried out. The bacterial growth was monitored by CFU method.

12.2.1 FTIR analysis of incubated PVC with *Rhodococcus ruber*

The chemical composition of ozonated and non-ozonated PVC powder's surface were monitored with FTIR analysis. Figure 12.5 presents the spectra of pretreated PVC powder

after exposure to the biotic and abiotic conditions. There are no changes in the chemical composition of PVC powder as an indication of biological treatment. The same spectra obtained from non-ozonated PVC powder incubated under biotic and abiotic conditions

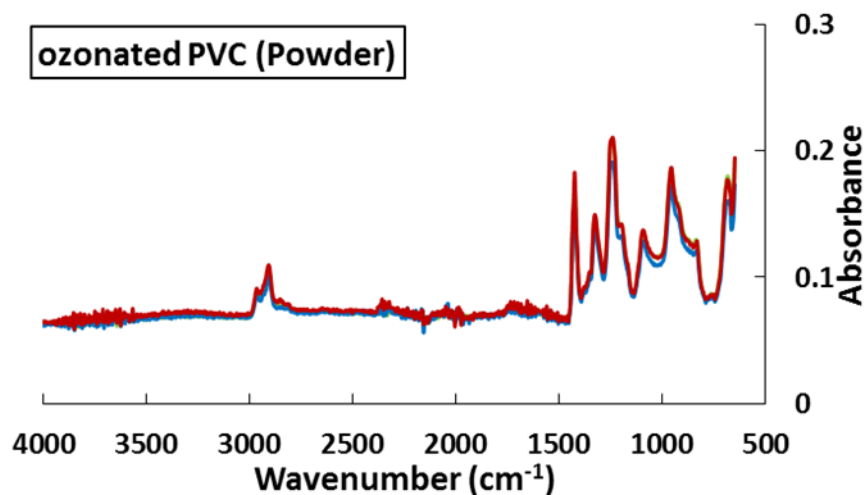


Figure 12.5 FTIR spectra of ozonated PVC powder after incubation

Biotic condition (red), abiotic condition (blue), virgin polymer (green)

12.2.2 Bacterial growth of *Rhodococcus ruber* on ozonated and non-ozonated PVC

The bacterial growth was monitored by CFU method. In this test, ozonated and non-ozonated PVC were the only carbon source for bacterial growth. Figure 12.6 presents the bacterial growth (CFU/mL) versus incubation time of PVC with *Rhodococcus ruber*. As it is shown the growth of bacterial in the culture containing ozonated and non-ozonated PVC are similar. The Growth of bacteria reaches the stationary phase after 40 day of incubation time.

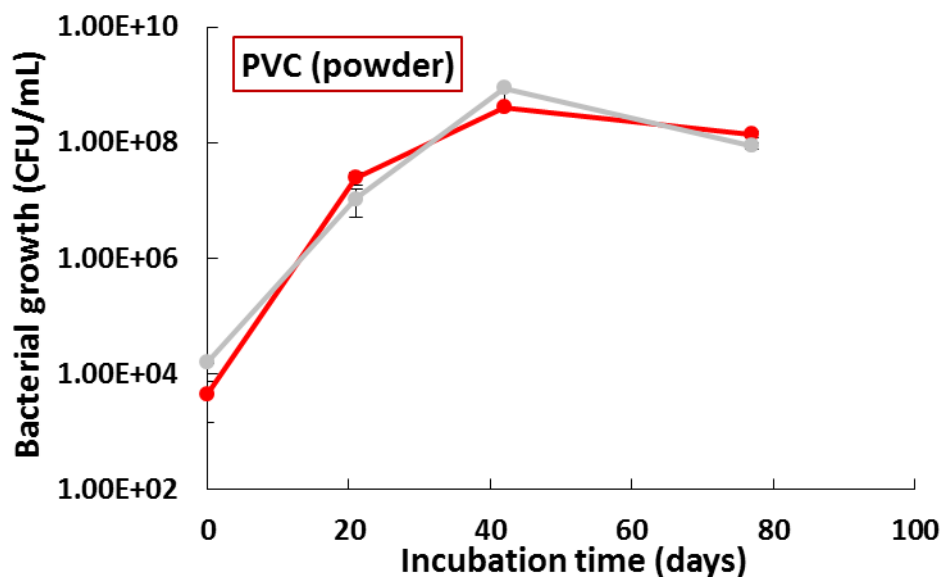


Figure 12.6 growth of pure bacterial culture versus incubation time with PVC
 Ozonated PVC (red), non-ozonated PVC (grey)

12.3 Biological treatment of LLDPE films with *Rhodococcus ruber*

In this set of experiments, gaseous phase ozonated (for 20 hours) and non-ozonated LLDPE films were incubated with pure culture of *Rhodococcus ruber*, as the only carbon source of bacterial growth, for 88 days. The samples were prepared and incubated in biotic and abiotic conditions at the same time. The samples were taken after 12, 40 and 88 days of incubation. FTIR and melt rheology test were performed for taken samples and the effect of biotic and abiotic condition on chemical composition and structure of LLDPE were investigated. The bacterial growth was monitored by colony forming unit (CFU) on the standard agar plates.

12.3.1 FTIR analysis of incubated LLDPE with *Rhodococcus ruber*

The ozonated and non-ozonated LLDPE films were taken out after 12, 40 and 88 days of incubation with and without pure bacterial culture. The biofilm was washed off from the all taken samples and FTIR analysis was performed. The FTIR spectra of non-ozonated LLDPE did not show any changes in the peaks of LLDPE film incubated under biotic and abiotic conditions. The carbonyl index of the ozonated samples was calculated based on the FTIR spectra. Figure 12.7 presents the carbonyl index of ozonated LLDPE versus incubation time with pure bacterial culture. As it is shown, there are no changes on the chemical structure of PS surface related to biotic activity of bacteria culture.

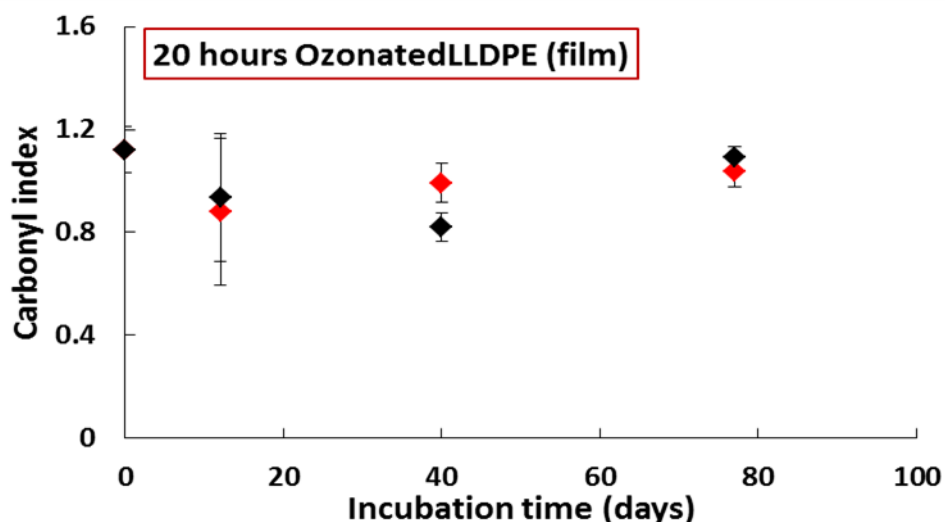


Figure 12.7 Carbonyl index versus incubation time of LLDPE with *R.ruber*

Ozonated LLDPE incubated under biotic conditions (red diamond) and under abiotic conditions (black triangle)

12.3.2 Bacterial growth of *Rhodococcus ruber* on ozonated and non-ozonated LLDPE

The growth of pure bacterial culture in presence of ozonated and non-ozonated LLDPE as the sole carbon substrate plotted in Figure 12.8. The significant rapid bacterial growth in

the presence of ozonated LLDPE is seen in this graph which indicates the positive effect of ozonation. However, the growth of bacteria can be seen with a slower rate in case of non-ozonated LLDPE as sole bacterial substrate.

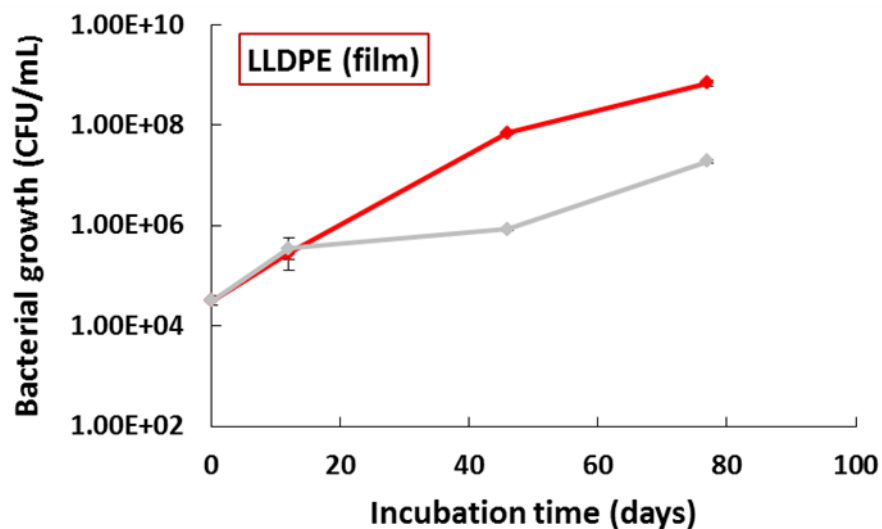


Figure 12.8 Growth of pure bacterial culture versus incubation time with LLDPE
Ozonated LLDPE (red), non-ozonated LLDPE (grey)

12.3.3 Effect of chemical and biotic treatment on melt rheology analysis of LLDPE

Melt rheology test of ozonated and non-ozonated LLDPE films were carried out before and after incubation with pure bacterial culture. Figure 12.9 and Figure 12.10 show the complex viscosity modulus (η^*) and the tangent of the loss angle factor ($\tan \delta$) respectively. As it was described before, the level of the complex viscosity is in direct correlation with the average weight molecular weight (M_w) of the materials and the loss angle factor with the mobility of the macromolecular chains. It can be concluded from Figure 12.9 and Figure 12.10 that:

- Any difference between abiotic control and biotic exposed samples was not observed.
- A decrease of the complex viscosity during ozonation can be observed. Then ozonation leads to chain scission and to a decrease of the molecular weight.
- Loss angle values decreases as the ozonation proceeds, meaning that there is also chain recombination due to ozonation.
- The chemical exposure to ozone leads to a lower molecular weight.

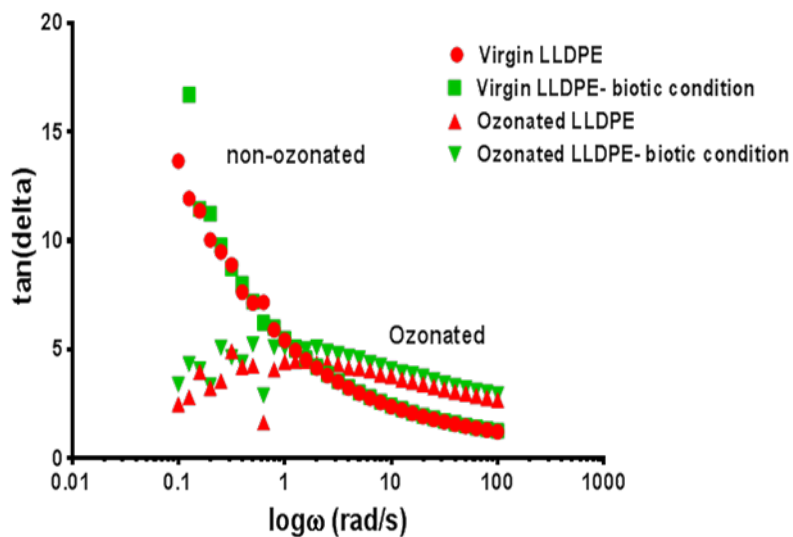


Figure 12.9 Tangent of the loss angle of LLDPE versus oscillatory frequency

Ozonated LLDPE (red triangle), ozonated LLDPE exposed to *R.ruber* (green triangle), non-ozonated LLDPE (red circle),and non-ozonated LLDPE exposed to *R.ruber* (green square)

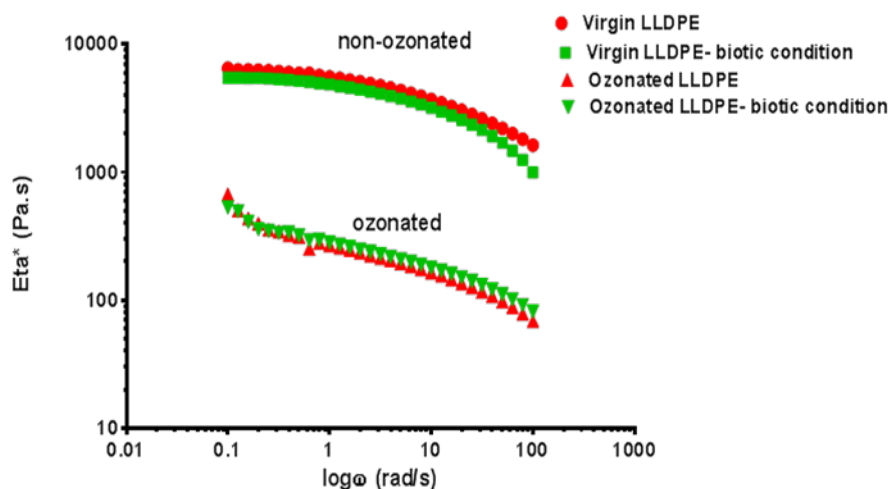


Figure 12.10 Complex viscosity of LLDPE versus oscillatory frequency

Non ozonated LLDPE (red circle), Non-ozonated LLDPE exposed to *R.ruber* (green square), ozonated LLDPE (red triangle) and ozonated LLDPE exposed to *R.ruber* (green triangle)

12.3.4 Microscopic analysis of chemically and biologically treated LLDPE

The surface of LLDPE was monitored with AFM and SEM microscopic techniques to evaluate topography and effect of biodegradation and ozonation on the surface of LLDPE. Before taking the microscopic images, all the film samples washed as it was described in the section 10.2.5. Figure 12.11 compares the AFM pictures of ozonated and biologically treated samples with the virgin LLDPE. The ozonated samples display a considerable increase in the surface roughness when compared to the non-ozonated LLDPE samples.

Figure 12.12 presents the SEM images of LLDPE films before and after chemical treatment and biodegradation tests. The morphological changes after exposure of LLDPE films to ozone and bacterial culture can be confirmed by the microscopic images.

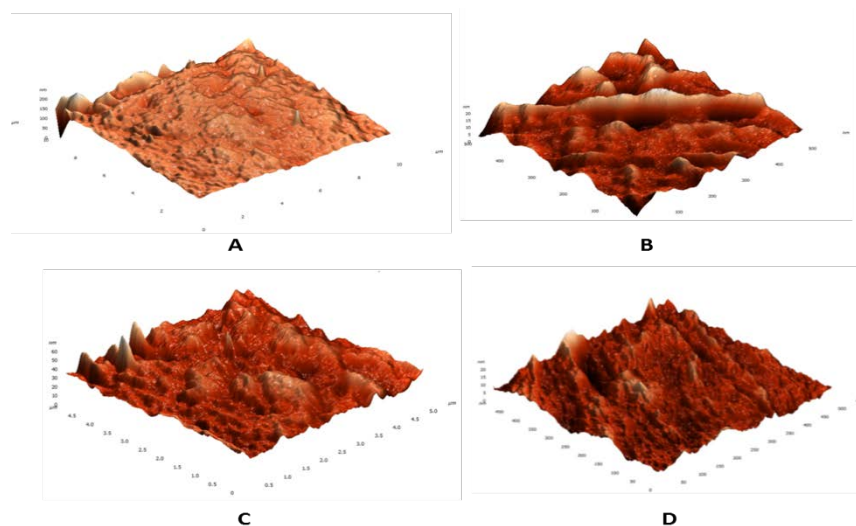


Figure 12.11 AFM images of LLDPE films

Virgin LLDPE (A), ozonated LLDPE (B), virgin LLDPE exposed to *R.ruber* (C) and ozonated LLDPE exposed to *R.ruber* (D)

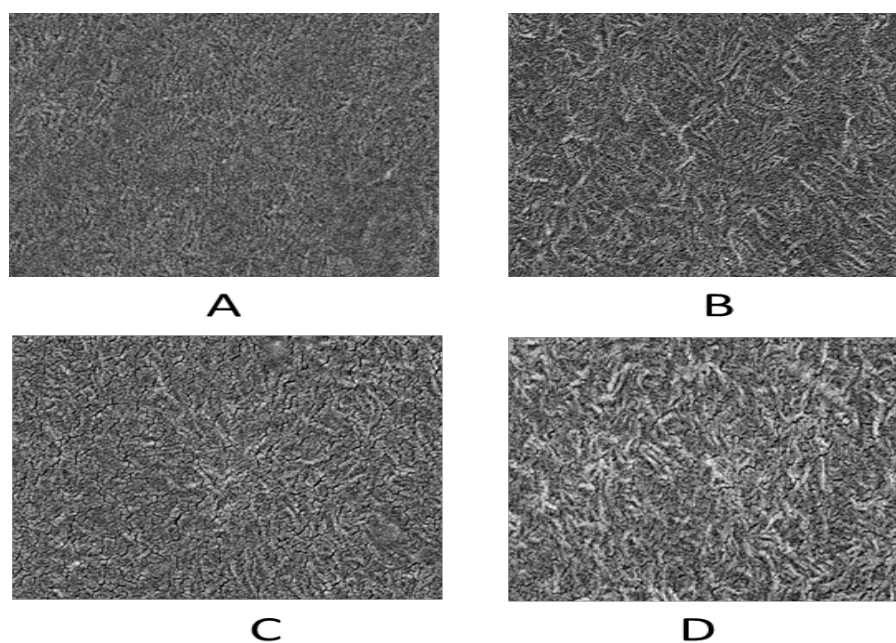


Figure 12.12 SEM images of LLDPE film

Virgin LLDPE (A), ozonated LLDPE (B), virgin LLDPE exposed to *R.ruber* (C) and ozonated LLDPE exposed to *R.ruber* (D)

12.4 Biological treatment of PP films with *Rhodococcus ruber*

The procedure for treatment and incubation of PP films with pure bacterial culture were the same as explained in previous sections. Gaseous phase ozonated (for 20 hours) and non-ozonated PP films were incubated with pure culture of *Rhodococcus ruber*, as the only carbon source of bacterial growth, for 88 days. The samples were prepared and incubated in biotic and abiotic conditions at the same time. The samples were taken after 20, 42, 62 and 88 days of incubation. FTIR and TGA test were performed for taken samples and the effect of biotic and abiotic condition on chemical composition and structure of PP were investigated. The microscopic images of the PP film surface were taken and compared for the samples before and after biological treatment. The bacterial growth was monitored by colony forming unit (CFU) on the standard agar plates.

12.4.1 FTIR analysis of incubated PP with *Rhodococcus ruber*

The ozonated and non-ozonated PP films were taken out after 20, 42, 62 and 88 days of incubation with and without pure bacterial culture. The biofilm was washed off from the all taken samples and FTIR analysis was performed. The FTIR spectra of non-ozonated PP did not show any changes in the peaks of PP film incubated under biotic and abiotic conditions. The carbonyl index of the ozonated samples was calculated based on the FTIR spectra. Figure 12.13 presents the carbonyl index of ozonated PP versus incubation time with pure bacterial culture. As it is shown, there are no changes on the chemical structure of PP surface related to biotic activity of bacteria culture.

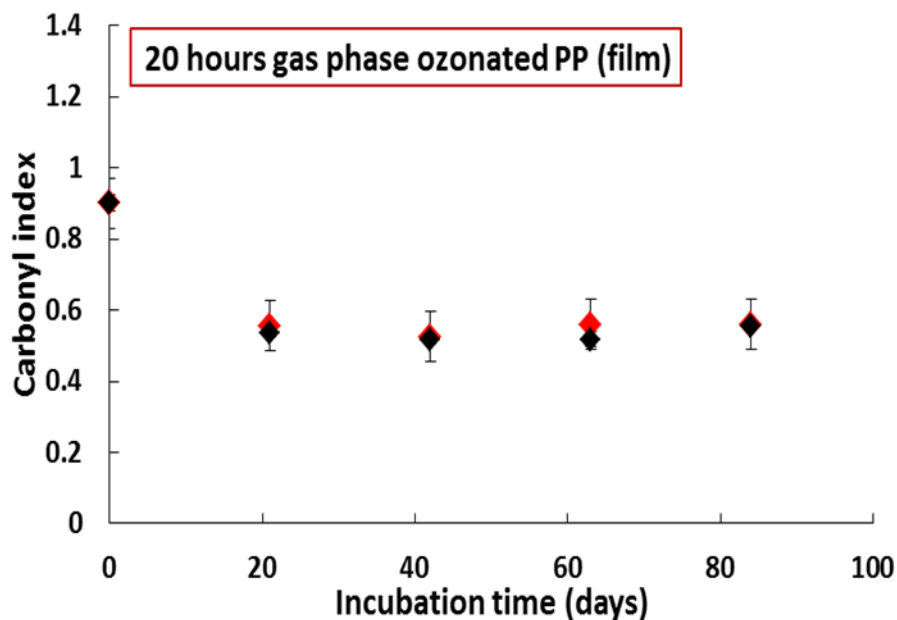


Figure 12.13 Carbonyl index versus incubation time of PP with *R.ruber*

Ozonated PP incubated under biotic conditions (red diamond) and under abiotic conditions (black diamond)

12.4.2 Bacterial growth of *Rhodococcus ruber* on ozonated and non-ozonated PP

The growth of pure bacterial culture in presence of ozonated and non-ozonated PP as the sole carbon substrate plotted in Figure 12.14. The significant rapid bacterial growth in the presence PP film (ozonated and non-ozonated) is seen in for the first 20 days of incubation. After 20 days of incubation the bacterial growth reaches the stationary phase.

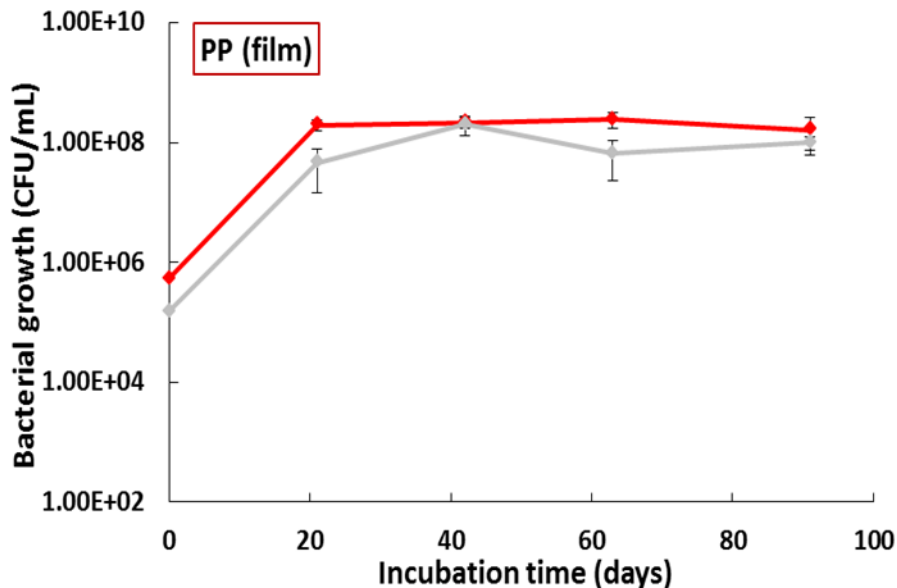


Figure 12.14 Growth of pure bacterial culture versus incubation time with PP
Ozonated PP (red), non-ozonated PP (grey)

12.4.3 Microscopic analysis of chemically and biologically treated PP

The surface of PP was monitored with AFM and SEM microscopic techniques to evaluate topography and effect of biodegradation and ozonation on the surface of PP. Before taking the microscopic images, all the film samples washed as it was described in the section **Error! Reference source not found.** Figure 11.15 compares the AFM pictures of ozonated and biologically treated samples with the virgin PP. The ozonated samples display a considerable increase in the surface roughness when compared to the non-ozonated PP samples.

Figure 12.16 presents the SEM images of PP films before and after chemical treatment and biodegradation tests. The morphological changes after exposure of PP films to ozone and bacterial culture can be confirmed by the microscopic images.

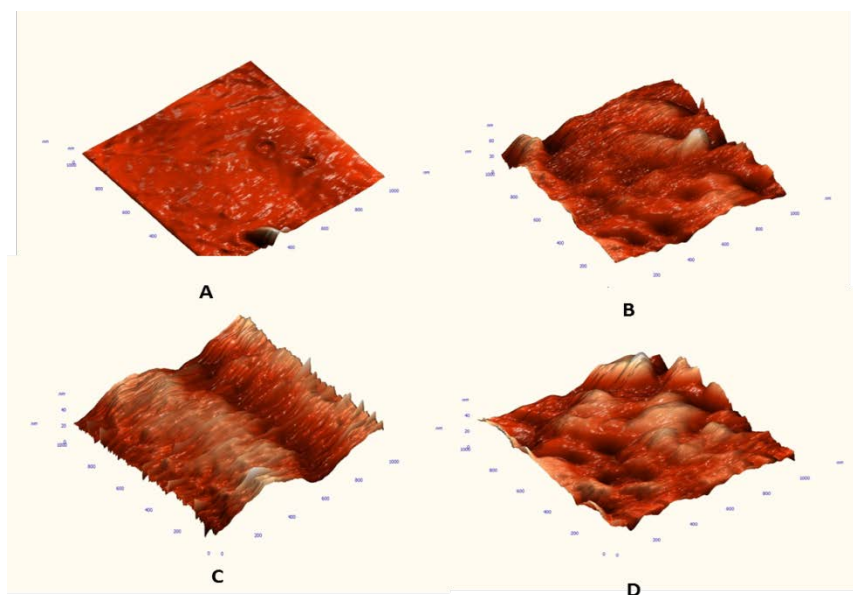


Figure 12.15 AFM images of PP films

Virgin PP (A), ozonated PP (B), virgin PP exposed to *R.ruber* (C) and ozonated PP exposed to *R.ruber* (D)

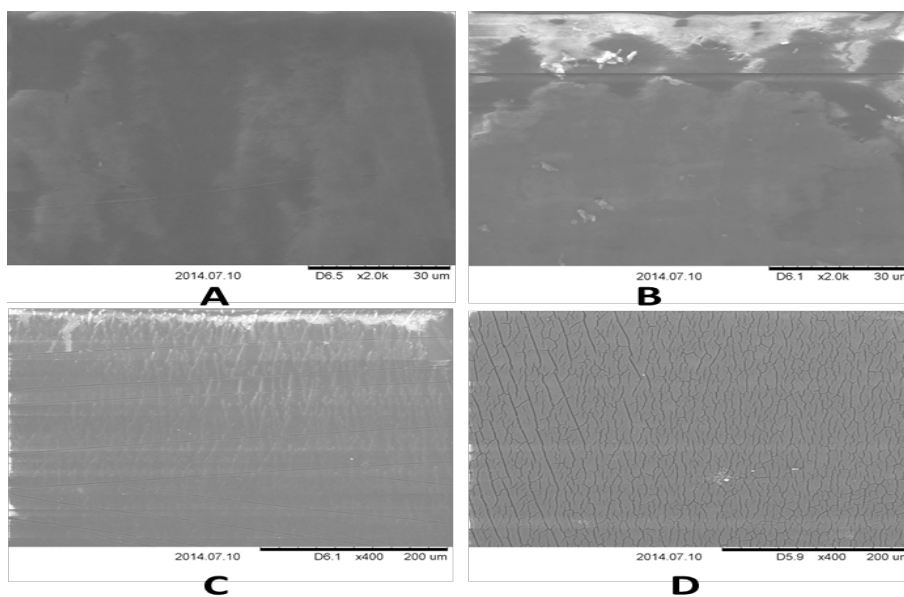


Figure 12.16 SEM images of PP film

Virgin PP (A), ozonated PP (B), virgin PP exposed to *R.ruber* (C) and ozonated PP exposed to *R.ruber* (D)

12.4.4 Biofilm formation on PP films incubated with *Rhodococcus ruber*

The formation of biofilm on the ozonated and non-ozonated PP was evaluated by fluorescent microscope images. Pieces of ozonated and non-ozonated PP films were transferred from the medium and to Eppendorf containing 4,6-diamidino-2-phenylindole (DAPI) 300 nM in order to dye the bacterial cells and the samples were kept in dark place for 15 minutes. The films were washed with buffer solution and put on a microscope slide (Menzel, Germany) and viewed under the fluorescence microscope (Olympus BX41, Switzerland) with a 40x-objective, a DAPI filter and a mercury lamp (Olympus U-RFL-T, Switzerland). Figure 12.17 confirms the formation of biofilm on the non-ozonated PP film samples with higher density than non-ozonated PP films.

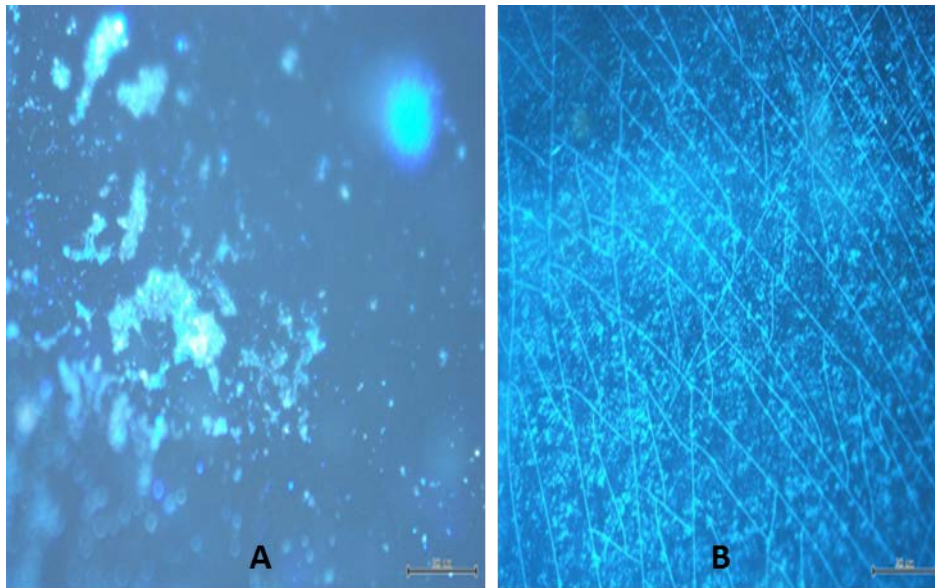


Figure 12.17 Fluorescence microscope images of biofilm formation on PP film samples

Non ozonated PP film (A) and ozonated PP film (B)

12.4.5 TGA analysis of incubated PP with *Rhodococcus ruber*

Ozonated and non-ozonated PP films after being incubated with pure bacterial culture were subjected to TGA analysis as explained in section 10.3.4. The decomposition temperature of samples were calculated and compared. Figure 12.18 compared the decomposition temperature of PP films after chemical and biological treatments. The effect of ozonation on structural change of PP can be observed from reduction in decomposition temperature up to 15 °C after ozonation. Reduction in decomposition temperature of ozonated and non-ozonated PP up to 10 °C after 70 days incubation with *R. ruber* represents a clear indication of bacterial attack. Abiotic controls did not show any sign regarding to structural changes after incubation.

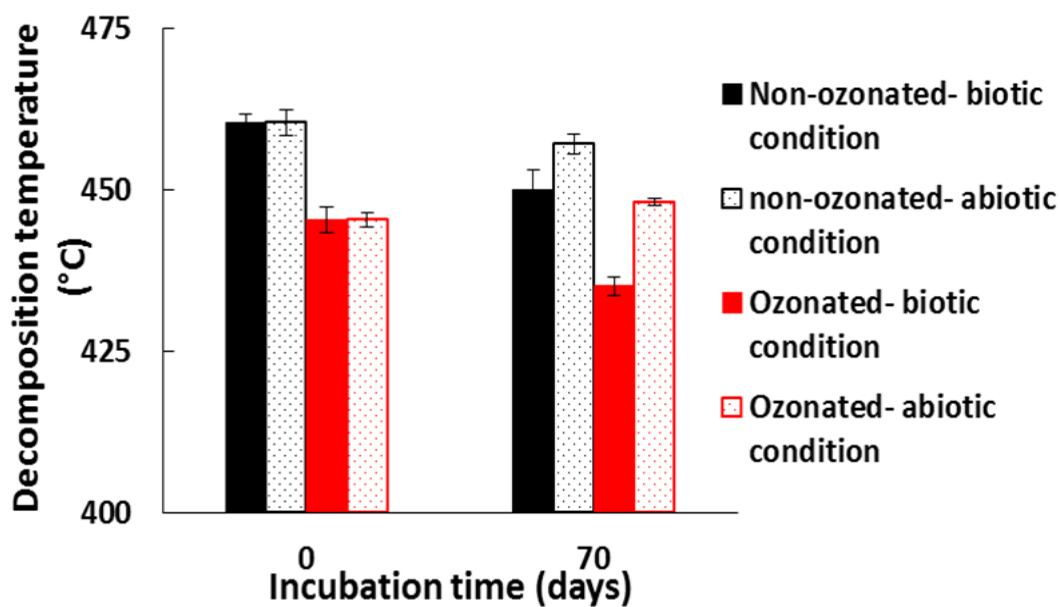


Figure 12.18 Decomposition temperature of PP film versus incubation time with *R. ruber*

12.5 Biological treatment of PP films with mixed bacterial culture

As it was explained in section **Error! Reference source not found.** ozonated (20 hours in gaseous phase) PP and non-ozonated PP were incubated with a mixed bacterial culture containing following strains:

- *Salinibacterium amurskyense*
- *Rhodococcus ruber*
- *Shewanella baltica*,
- *Pseudomonas xanthomarina*,
- *Lysinibacillus macrolides*

The samples were incubated with the mixed culture for 157 days. The results of analysis on PP samples are explained in the following sections.

12.5.1 FTIR analysis of incubated PP with the mixed bacterial culture

During the incubation period, PP film samples were subjected to FTIR analysis. The analysis of non-ozonated PP incubated with and without mixed bacterial culture did not show any changes on FTIR spectra of these polymers. The carbonyl index of ozonated PP which were incubated under biotic and abiotic condition are plotted versus incubation time and presented in Figure 12.19. There are no changes on the chemical structure of PP surface related to biotic activity of mixed bacteria culture.

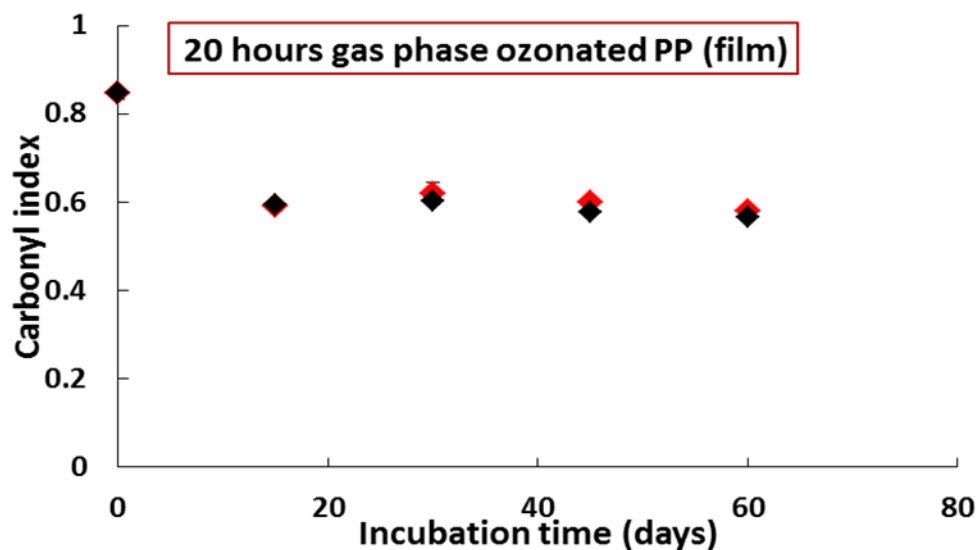


Figure 12.19 Carbonyl index versus incubation time of PP with mixed bacterial culture

Ozonated PP incubated under biotic conditions (red diamond) and under abiotic conditions (black diamond)

12.5.2 Bacterial growth of mixed culture on ozonated and non-ozonated PP

The growth of mixed bacterial culture in presence of ozonated and non-ozonated PP as the sole carbon substrate plotted in Figure 12.20. The significant rapid bacterial growth in the presence ozonated PP film is seen in for the first 30 days of incubation. However, after 30 days of incubation the bacterial growth reaches the stationary phase for and there is a negative growth after 60 days of incubation.

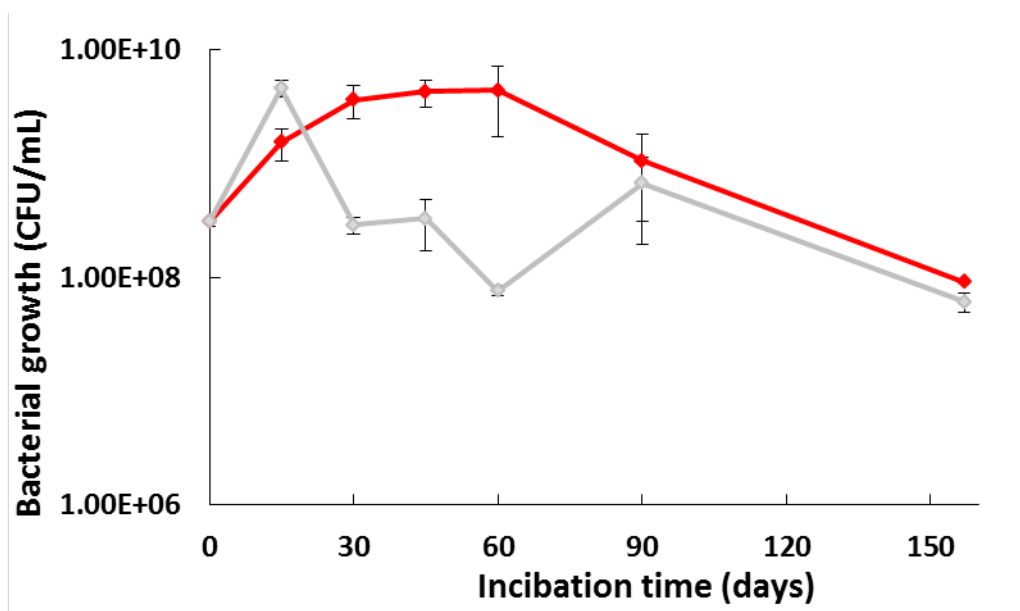


Figure 12.20 Growth of mixed bacterial culture versus incubation time with PP
Ozonated PP (red), non-ozonated PP (grey)

12.5.3 DSC analysis of incubated PP with mixed bacterial culture

The onsets melting temperature of incubated PP samples with mixed bacterial culture were calculated by DSC analysis. Figure 12.21 presents the onset melting temperature of PP films versus incubation time with mixed bacterial culture. The effect of ozonation on decrease of melting temperature (13°C) of PP film samples can be clearly seen. There is a decrease on melting temperature of ozonated PP after biological treatment. However, there are no significant differences between melting temperature of non-ozonated PP incubated under biotic and abiotic condition.

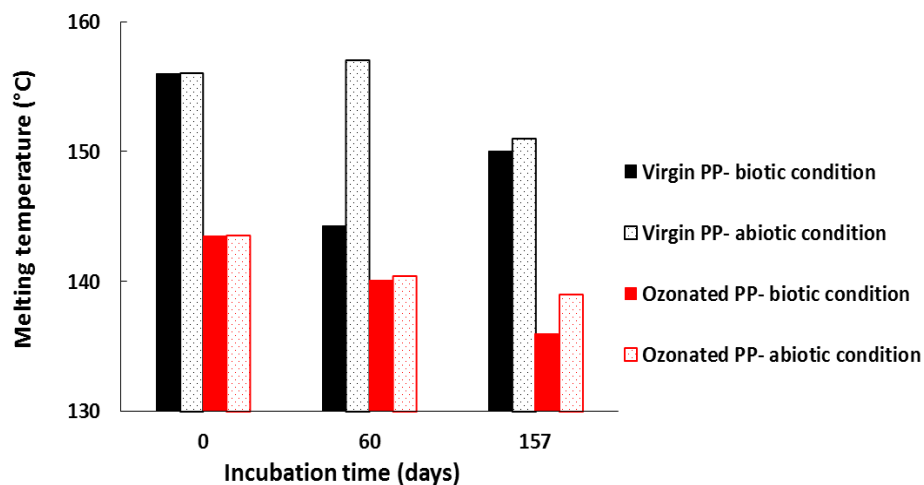


Figure 12.21 Melting temperature of PP film versus incubation time with mixed bacterial culture

12.5.4 Weight loss measurement of PP film incubate with mixed bacterial culture

The weight loss of the samples during incubation was monitored and it is presented in Figure 12.22. The weight loss of ozonated PP films incubated under biotic condition is varied between 4-6% during 157 days of incubation. This value was measured 3.6% for the ozonated PP incubated under abiotic condition.

The maximum weight loss of non-ozonated PP during 157 days of incubation was 1.5% while this value was 0.8% for non-ozonated PP incubated as abiotic control.

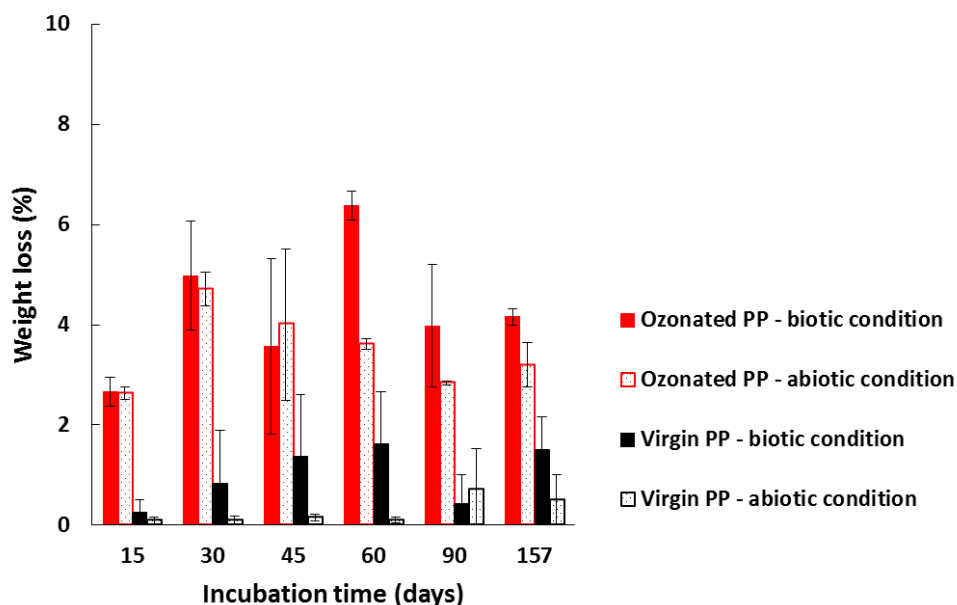


Figure 12.22 Weight loss measurements of PP films incubated with mixed bacterial culture

12.5.5 TGA analysis of incubated PP with mixed bacterial culture

Ozonated and non-ozonated PP films after being incubated with mixed bacterial culture were subjected to TGA analysis as explained in section 10.3.4. The decomposition temperature of samples were calculated and compared. Figure 12.23 compared the decomposition temperature of PP films after chemical and biological treatments. The effect of ozonation on structural change of PP can be observed from reduction in decomposition temperature up to 15 °C after ozonation. However, the effect of biological treatment of ozonated and non-ozonated PP was not very significant during 157 day of incubation.

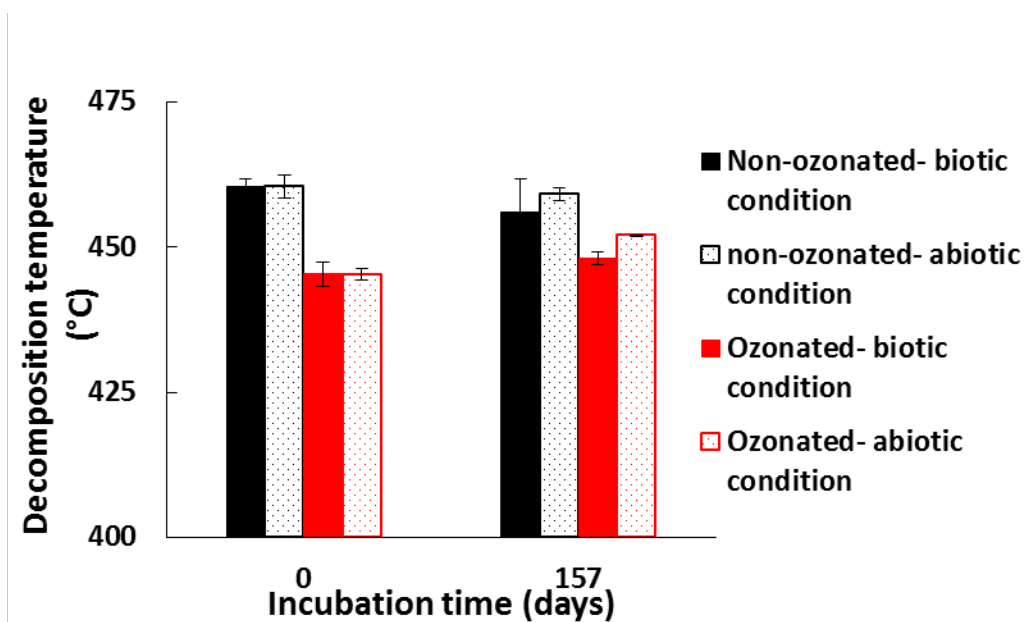


Figure 12.23 Decomposition temperature of PP film versus incubation time with Mixed bacterial culture.

Overall, the results of the biodegradation tests performed with bacteria show that pretreatment of plastic accelerate the biodegradation. However, the sign of bacterial attack also was observed on non-pretreated plastics. Abiotic reactions of ozonated and non-ozonated plastics need more investigation.

13 Plastic biodegradation with a pure fungal culture

13.1 Evaluation of the biodegradation of PS incubated with pure fungal culture

As it was explained, the optimum UV/ozone treatment time for PS film in gaseous phase is 4 hours. So the PS films were subjected to gaseous phase UV/ozonation for 4 hours as a pre-treatment step.

In order to evaluate the effect of biodegradation on PS film samples, the FTIR analysis and weight loss measurement were carried out for taken samples during the incubation time. Furthermore, the fungal growth was monitored by dry weight measurement of suspended biomass and attached biofilm of fungal culture in each of the glass tubes..

13.1.1 FTIR analysis of incubated PS with *Penicillium variable*

The vials containing UV/ozonated and non-ozonated PS films as well as abiotic controls were taken out every 2 weeks (in triplicates). The biofilm washing procedure was carried out with SDS 2% as explained in section **Error! Reference source not found.** The FTIR analysis was performed for UV/ozonated and non-ozonated PS incubated with and without pure fungal culture. There are no changes on chemical structure of non-ozonated PS after abiotic and biotic treatment. The absorbance of the peak relating presence of carbonyl groups on the surface of UV/ozonated PS decreased for samples incubated under biotic and abiotic conditions. The carbonyl index was calculated and plotted versus incubation time to compare the carbonyl index reduction of incubated samples as it is shown in Figure 13.1

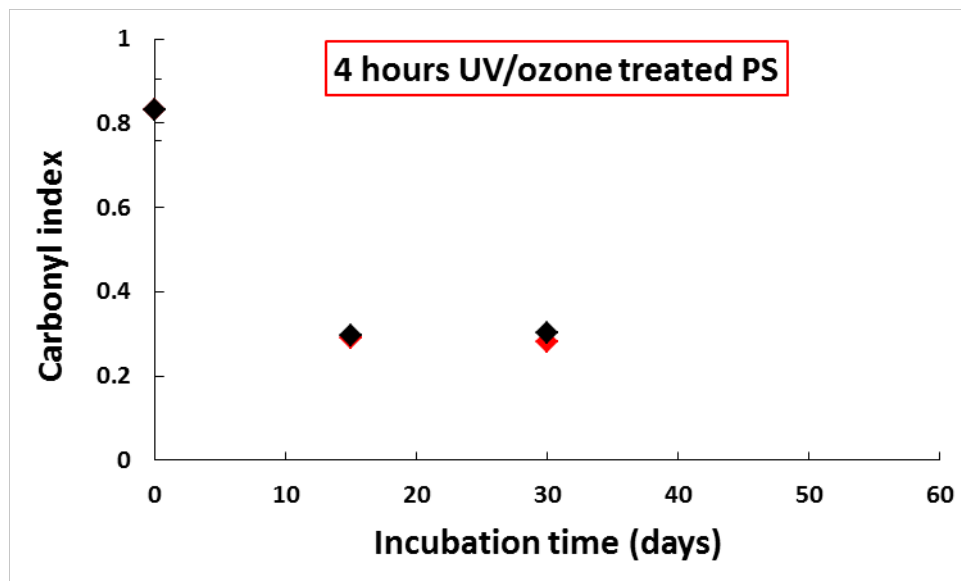


Figure 13.1 Carbonyl index versus incubation time of PS with fungal culture

UV/ozonated PS incubated under biotic conditions (red diamond) and under abiotic conditions (black diamond)

13.1.2 Weight loss measurement of PS film incubate with *Penicillium* variable

The biofilm was washed off from the surface of incubated PS samples and they were dried and weighted after incubation. The weight of the samples was compared with their initial weight and the weight loss related the biotic treatment and abiotic reaction were evaluated as it is shown in Figure 13.2.

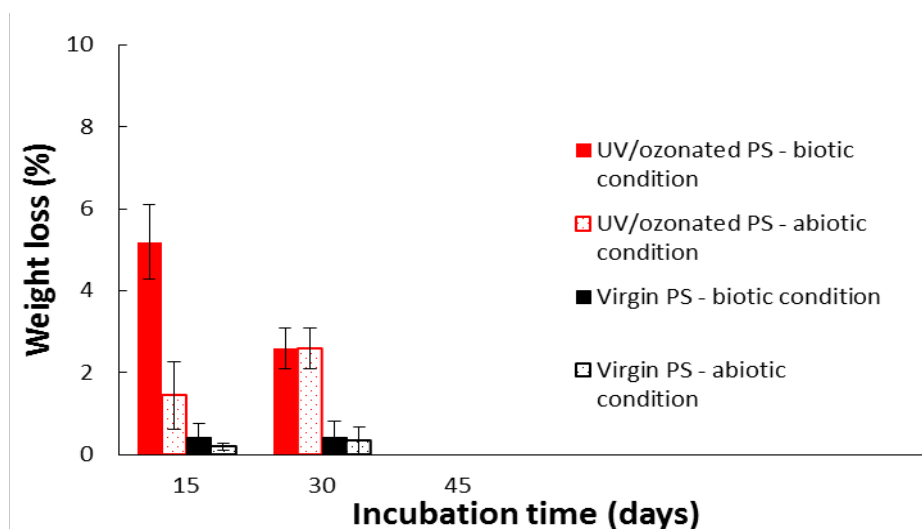


Figure 13.2 Weight loss measurements of PS films incubated with pure fungal culture.

13.1.3 Evaluation of *Penicillium variable* growth on PS films

The suspended cells and biofilm formed on UV/ozone treated and untreated PS were collected after incubation and dried. The dry weight of cells was measured and compared during incubation period as an indication of fungal growth as it is shown in Figure 13.3

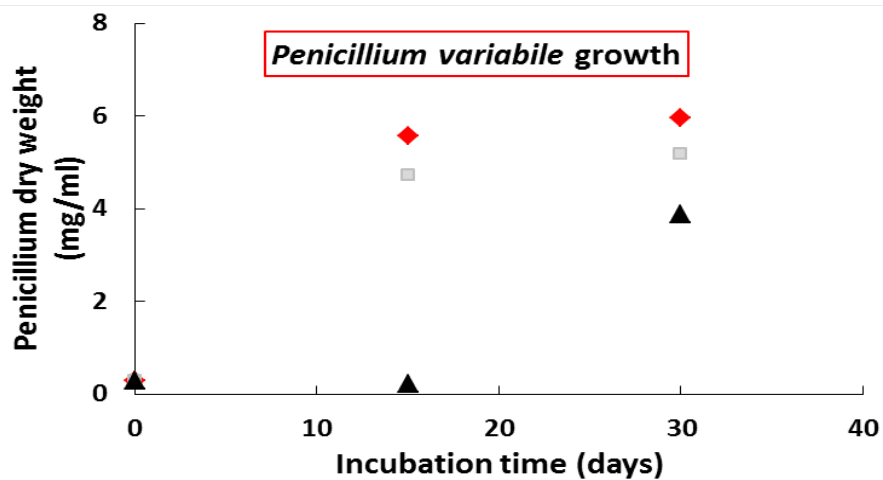


Figure 13.3 Dry weight of fungal culture versus incubation time with PS

UV/ozonated Ps (red), non-treated Ps (grey) and without polymer (black).

Preliminary test shows that co-metabolic process is a promising method for biodegradation of plastics. However, more analysis and longer incubation time is needed for evaluating the process

14 Conclusions, part 2

The main conclusions from the second part of this thesis are summarized here:

1. Conclusions regarding the chemical treatment of polymers:
 - Gaseous phase ozonation of LLDPE, PP and PS in both powder and film led to a significant formation of carbonyl groups and to structural changes in the polymers, whereas aqueous phase ozonation proved to be less effective.
 - Gaseous phase ozonation of PVC powder did not have any positive effect on formation of functional groups, while the same treatment of PVC film increased the intensity of carbonyl groups related to additives.
 - Gaseous phase UV/ozonation of LLDPE, PP and PS films was found to be more effective than gaseous phase ozonation for formation of functional groups.
2. Conclusions regarding the biodegradation of pre-treated plastics by a pure bacterial culture of *Rhodococcus ruber*:
 - A marked bacterial culture was observed for all of the incubated polymers for the first 40 days after starting the incubation. Bacterial growth on ozonated LLDPE, PS and PP was slightly higher than on those incubated with untreated polymers.
 - For PP and LLDPE, microscopic images of the surfaces of polymers surfaces showed topography changes related to surface biodegradation, and (for PP only) a decrease in decomposition temperature (evaluated through TGA) revealed changes related to biodegradation by *Rhodococcus*

ruber. On the other hand, no sign of bacterial attack was observed for PS and PVC.

3. Conclusions regarding the biodegradation of pre-treated PP by a mixed bacterial culture:

- Bacterial growth on ozonated PP was significantly higher than that observed with non-ozonated PP.
- Weight loss and melting temperature analysis (through DSC) provide clear evidence of PP biodegradation by the consortium under study.

4. Conclusions on the biodegradation of pre-treated PS films by a pure fungal culture of *Penicillium variable* in a co-metabolic process with saccharose as the co-substrate:

- Both weight loss and fungal growth were higher in the case of UV/ozonated PS, indicating a positive effect of the chemical pre-treatment and the capacity of *Penicillium variable* to biodegrade PS.

In general, a significant effect of abiotic degradation of pretreated polymers was observed during biodegradation tests of all of the polymers. This abiotic degradation needs further study.

In this study, a variety of analytical methods were used to evaluate the degradation of different polymers. The selection of the most suitable analytical methods to monitor the different aspects of the degradation process of each plastic is challenging and needs more investigation.

Overall, although the biodegradation results presented in this thesis are still very preliminary, biodegradation of the studied plastics by both bacterial and fungal cultures appears to be a promising process, worthy of further investigation.

Appendix I

List of abbreviates:

AC	Aerobic cometabolism
CAHs	Chlorinated aliphatic hydrocarbons
PBR	Packed bed reactor
TCE	Trichloroethylene
TeCA	1,1,2-Tetrachloroethane
NAPLs	Non-Aqueous Phase Liquids
DNAPLs	Dense non-aqueous phase liquids
NADH	Nicotinamide adenine dinucleotide
ATP	Adenosine triphosphate
EPS	Exocellular polymeric substances
ORC	Oxygen releasing compound
HRT	Hydraulic retention time
PE	Polyethylene
PP	Polypropylene
PVC	Polyvinyl chloride
PS	Polystyrene
LLDPE	Linear low density polyethylene
PET	polyethylene terephthalate
FTIR	Fourier transform infrared
DSC	Differential scanning calorimetry
TGA	Thermogravimetric Analysis
AFM	Atomic Force Microscopy
SEM	Scanning Electron Microscope
CFU	Colony forming unit
UV	Ultraviolet light

List of nomenclatures:

c_i	Concentration of compound i (mg L^{-1})
V	Volume of the liquid phase or gas phase (L)
H_i	Henry's constant (L atm mol^{-1})
m_i	Total mass of compound i (g)
f_{cal}	Calibration coefficient
P_i	Partial pressure of the gas on the solution (atm)
$k_{1,i}$	Pseudo first order constant of compound i ($k_1 = q_{\text{max}}/K_S$) ($\text{d}^{-1} \text{mg}_{\text{protein}}^{-1} \text{L}$)
q_i	Specific biodegradation rate of compound i ($\text{mg}_i \text{mg}_{\text{protein}}^{-1} \text{d}^{-1}$)
$q_{\text{max},i}$	True maximum specific biodegradation rate of compound i ($\text{mg mg}_{\text{protein}}^{-1} \text{d}^{-1}$)
R^2	Coefficient of determination
r_i	Initial depletion rate of compound i ($r_i = r_{i,\text{bio}} + r_{i,\text{abio}}$) ($\text{mg L}^{-1} \text{d}^{-1}$)
$r_{i,\text{abio}}$	Initial abiotic degradation rate of compound i ($\text{mg L}^{-1} \text{d}^{-1}$)
$r_{i,\text{bio}}$	Initial biodegradation rate of compound i ($\text{mg L}^{-1} \text{d}^{-1}$)
S	Substrate concentration (mg L^{-1})
K_S	Affinity constant of substrate (mg L^{-1})
I	Inhibitor concentration (mg L^{-1})
K_I	Inhibition constant (mg L^{-1})
$K_{I,\text{TCE},\text{but}}$	Constant expressing the competitive inhibition of TCE on butane uptake ($\text{mg}_{\text{inhibitor}} \text{L}^{-1}$)
$K_{I,\text{but},\text{TCE}}$	Constant expressing the competitive inhibition of butane on TCE biodegradation ($\text{mg}_{\text{inhibitor}} \text{L}^{-1}$)
V_{react}	Liquid volume in the suspended-cell tests, or bulk volume occupied by the carriers in the attached-cell tests (L)
R_i	Initial net degradation rate of compound i ($\text{mg}_{\text{but}} \text{L}^{-1} \text{d}^{-1}$)

X	Biomass concentration ($\text{mg}_{\text{prot}}\text{L}^{-1}$)
v	Interstitial velocity (m s^{-1})
$D_{L,i}$	Diffusion/dispersion coefficient relative to compound i ($\text{m}^2 \text{s}^{-1}$)
α_L	Longitudinal dispersivity (m)
ε	Effective porosity
Q	Volumetric flow rate ($\text{m}^3 \text{s}^{-1}$)
$T_{c,\text{TCE}}$	TCE transformation capacity ($\text{mg}_{\text{TCE}} \text{g}_{\text{protein}}^{-1}$)
Y_S	Biomass/substrate yield ($\text{mg}_{\text{protein}} \text{mg}_{\text{butane}}^{-1}$)
b	Endogenous decay constant (s^{-1})
$\dot{m}_{i,g}$	Mass flow rate of compound i transferred from the gas to the liquid phase, referred to the reactor volume ($\text{mg}_i \text{d}^{-1} \text{L}^{-1}$)
\bar{q}_i	Specific biodegradation rate evaluated at the average concentration of compound i ($\text{mg}_i \text{mg}_{\text{protein}}^{-1} \text{d}^{-1}$)
η_i	Conversion percentage of compound i
Pe	Peclet number
t_s^*	Fraction of the cycle time to dedicate to substrate feed in bioreactor
η^*	Complex viscosity modulus (Pa.s)
λ	Wavelength (cm)
W	Wavenumber (cm^{-1})
I_i	Intensity of absorption band relative to compound I in infrared spectroscopy

List of subscripts:

15	Refers to temperature of experiment at 15 °C
30	Refers to temperature of experiment at 30 °C
g	Refers to gas phase
l	Refers to liquid phase
but	Refers to butane
TCE	Refers to TCE

TeCA	Refers to TeCA
susp.	Refers to suspended cells
attached	Refers to attached cells
C	Refers to Chlorinated solvent
X	Refers to biomass
abio	Degradation under abiotic condition
bio	Degradation under biotic condition

References:

- [1] U.S. EPA (2000). Engineered Approaches to In-Situ Bioremediation of Chlorinated Solvents: Fundamentals and Field Applications. EPA 542-R-00-008.
- [2] ACGIH. (2001) Dichloromethane and methyl chloroform. In Documentation of the threshold limit values and biological exposure indices. 7th edn. Cincinnati, OH: ACGIH.
- [3] Tiehm A., Schmidt K. R., Pfeifer B., Heidinger M. and Ertl S. (2008). Growth kinetics and stable carbon isotope fractionation during aerobic degradation of cis-1,2-dichloroethene and vinyl chloride. *Water Research*, 42, 2431-2438.
- [4] Frascari D., Cappelletti M., Fedi S., Zannoni D., Nocentini M. and Pinelli D. (2010). 1,1,2,2-Tetrachloroethane aerobic cometabolic biodegradation in slurry and soil-free bioreactors: a kinetic study. *Biochemical Engineering Journal*, 52, 55-64.
- [5] Chang H. L. and Alvarez-Cohen L. (1995). Model for the cometabolic biodegradation of chlorinated organics. *Environmental Science and Technology*, 29, 2357-2367.
- [6] Morono Y., Unno H. and Hori K. (2006). Correlation of TCE cometabolism with growth characteristics on aromatic substrates in toluene-degrading bacteria. *Biochemical Engineering Journal*, 31, 173-179.
- [7] Hopkins G.D. and McCarty P.L. (1995). Field evaluation of in-situ aerobic cometabolism of trichloroethylene and three dichloroethylene isomers using phenol and toluene as the primary substrates. *Environmental Science and Technology*, 29, 1628-1637.

- [8] Ely R. L., Williamson K. J., Hyman M. R. and Arp D. J. (1997). Cometabolism of chlorinated solvents by nitrifying bacteria: kinetics, substrate interactions, toxicity effects and bacterial response. *Biotechnology Bioengineering*, 54, 520-534.
- [9] Frascari D., Zannoni A., Pinelli D., Nocentini M., Baleani E., Fedi S., Zannoni D., Farneti A. and Battistelli A. (2006). Long-term aerobic cometabolism of a chlorinated solvent mixture by vinyl chloride-, methane- and propane-utilizing biomasses. *Journal of Hazardous Materials*, 138, 29-39.
- [10] Frascari D., Pinelli D., Nocentini M., Baleani E., Cappelletti M. and Fedi S. (2008). A kinetic study of chlorinated solvent cometabolic biodegradation by propane-grown *Rhodococcus* sp. PB1. *Biochemical Engineering Journal*, 42, 139-147.
- [11] Ciavarelli R., Cappelletti M., Fedi S., Pinelli D. and Frascari D. (2012). Chloroform aerobic cometabolism by butane-growing *Rhodococcus aetherovorans* BCP1 in continuous-flow biofilm reactors. *Bioprocess Biosystems Engineering*, 35, 667-681.
- [12] Frascari D., Fraraccio S., Nocentini M. and Pinelli D. (2013). Aerobic / anaerobic / aerobic sequenced biodegradation of a mixture of chlorinated ethenes, ethanes and methanes in batch bioreactors. *Bioresource Technology*, 128, 479-486.
- [13] U.S. Department of Defense (2001). Environmental Security Technology Certification Program: Use of cometabolic air sparging to remediate chloroethene-contaminated groundwater aquifers. Cost and performance report. Washington DC.
- [14] Wilson J. T. and Wilson B. H. (1985). Biotransformation of trichloroethylene in soil. *Applied and Environmental Microbiology*, 29, 242-243.

- [15] Alpaslan Kocamemi B. and Çeçen F. (2009). Biodegradation of 1,2-dichloroethane (1,2-DCA) by cometabolism in a nitrifying biofilm reactor. *International Biodeterioration Biodegradation*, 63,717-726.
- [16] Shim H., Ryoo D., Barbieri P. and Wood T.K. (2001). Aerobic degradation of mixtures of tetrachloroethylene, trichloroethylene, dichloroethylenes, and vinyl chloride by toluene-o-xylene monooxygenase of *Pseudomonas stutzeri* OX1. *Applied Microbiology and Biotechnology*, 56, 265-269.
- [17] Singh R., Paul D. and Jain R. K. (2006). Biofilms: implications in bioremediation. *Trends in Microbiology*, 14, 389-397.
- [18] Soares A., Murto M., Guiesse B. and Mattiasson B. (2006). Biodegradation of nonylphenol in a continuous bioreactor at low temperatures and effects on the microbial population. *Environmental Biotechnology*, 69, 597–606.
- [19] Tziotziou G., Teliou M., Kaltsouni V., Lyberatos G. and Vayenas D. V. (2005). Biological phenol removal using suspended growth and packed bed reactors. *Biochemical Engineering Journal*, 26, 65–71.
- [20] Di Gioia D., Bertin L., Zanaroli G., Marchetti L. and Fava F. (2006). Polychlorinated biphenyl degradation in aqueous wastes by employing continuous fixed-bed bioreactors Polychlorinated biphenyl degradation in aqueous wastes by employing continuous fixed-bed bioreactors. *Process Biochemistry*, 41, 935–940.
- [21] Bertin L., Di Gioia G., Barberio C., Salvadori L., Marchetti L. and Fava F. (2013). Biodegradation of polyethoxylated nonylphenols in packed-bed biofilm reactors. *Industrial Engineering Chemistry Research*, 46, 6681-6687.
- [22] Di Gioia D., Sciubba L., Bertin L., Barberio C., Salvadori L., Frassinetti S. and Fava F. (2009). Nonylphenol polyethoxylate degradation in aqueous waste by the use of batch and continuous biofilm bioreactors. *Water Research*, 43, 2977–2988.

- [23] Halecky M., Paca J., Stiborova M., Kozliak E. I. and Maslanova I. (2013). Pollutant interactions during the biodegradation of phenolic mixtures with either 2-or 3-mononitrophenol in a continuously operated packed bed reactor. *Journal of Environmental Science and Health - Part A Toxic/Hazardous Substances and Environmental Engineering*, 48, 1609-1618.
- [24] Alpaslan Kocamemi B. and Çeçen F. (2009). Biodegradation of 1,2-dichloroethane (1,2-DCA) by cometabolism in a nitrifying biofilm reactor. *International Biodeterioration Biodegradation*, 63,717-726.
- [25] Chu K. H. and Alvarez-Cohen L. (2000). Treatment of chlorinated solvents by nitrogen-fixing and nitrate-supplied methane oxidizers in columns packed with unsaturated porous media. *Environmental Science and Technology*, 34, 1784-1793.
- [26] Fitch M. W., Weissman D., Phelps P., Georgiou G. and Speitel Jr G. E. (1996). Trichloroethylene degradation by *Methylosinus trichosporium* ob3b mutants in a sequencing biofilm reactor. *Water Research*, 30, 2655-2664
- [27] Mileva A., Sapundzhiev T. S. and Beschkov V. (2008). Modeling 1,2-dichloroethane biodegradation by *Klebsiella oxytoca* 8391 immobilized on granulated activated carbon. *Bioprocess Biosystems Engineering*, 31, 75-85.
- [28] Segar R. L., De Wys S. L. and Speitel Jr G. E. (1995). Sustained trichloroethylene cometabolism by phenol-degrading bacteria in sequencing biofilm reactors. *Water Environment Research*, 67, 764-774.
- [29] Strand S. E., Wodrich J. V., Stensel H. D. (1991). Biodegradation of chlorinated solvents in a sparged, methanotrophic biofilm reactor. *Research Journal of Water Pollution Control*, 63, 859-867.

- [30] Wahman D. G., Katz L. E. and Speitel Jr G. E. (2011). Performance and biofilm activity of nitrifying biofilters removing trihalomethanes. *Water Research*, 45,1669-1680.
- [31] Wahman D. G., Katz L. E. and Speitel Jr G. E. (2007). Modeling of trihalomethane cometabolism in nitrifying biofilters. *Water Research*, 41, 449-457.
- [32] <http://www.minotaurus-project.eu>.
- [33] Sutherland, I. W. (2001). Biofilm exopolysaccharides: a strong and sticky framework. *Microbiology*, 147(1), 3–9.
- [34] Lewandowski, Z. (2000). Structure and function of biofilms. In: Evans LV (ed.). *Biofilm: recent advances in their study and control*. Harwood academic, Amsterdam.pp. 1-17.
- [35] Donlan R. M., (2002). Biofilms: microbial life on surfaces. *Emerging Infectious Diseases*, 8(9), 881-890.
- [36] Marshall, K. Blainey, BL. (1991). Role of bacterial adhesion in biofilm formation and biocorrosion. In: Anonymous *Biofouling and Biocorrosion in Industrial Water Systems*: Springer. pp. 29–46.
- [37] Characklis, W C. (1990). Microbial fouling and microbial biofouling control. In: I.G. Characklis and K. C. Marshall (Eds.): *Biofilms*, John Wiley), New York; 523-634.
- [38] Heijnen, J.J. (1984). Biological industrial wastewater treatment minimizing biomass production and maximizing biomass concentration. Ph.D. Thesis, Delft University of Technology, Delft.

- [39] Denac, M., Uzman, S., Tanaka, H., and Dunn, I. J. **(1983)**. Modeling of experiments on biofilm penetration effects in a fluidized bed nitrification reactor. *Biotechnol. Bioengineering*. 25, 1841–1861.
- [40] Heijnen, J.J., Mulder, A., Enger, W., Hoeks, F. **(1989)**. Review on the application of anaerobic fluidized bed reactors in wastewater treatment. *Chem. Eng. J.* 41, B37–B50.
- [41] Nicolella C.M., C.M. van Loosdrecht, et al. **(2000)**. Wastewater treatment with particulate biofilm reactors. *Journal of Biotechnology*. 80 (1), 1-33.
- [42] Lowry O. H., Rosebrough N. J., Farr A. L., Randall R. J. **(1951)**. Protein measurement with the Folin phenol reagent. *J. Biol. Chem.* 193-265.
- [43] Alvarez-Cohen L., Speitel Jr. GE. **(2001)**. Kinetics of aerobic cometabolism of chlorinated solvents. *Kluwer Academic Publishers*. 12, 105–126.
- [44] Joens J. A., Slifker R. A. , Cadavid E. M., Martinez R. D., Nickelsen M. G., Cooper W. J. **(1995)**. Ionic strength and buffer effects in the elimination reaction of 1,1,2,2-tetrachloroethane. *Water Res* 29:1924-1928
- [45] Chang W., Criddle. C.S., **(1997)**. Experimental Evaluation of a Model for Cometabolism: Prediction of Simultaneous Degradation of Trichloroethylene and Methane by a Methanotrophic Mixed Culture. 54, 491-501.
- [46] Erik Arvin. **(1991)**. Biodegradation kinetics of chlorinated aliphatic hydrocarbons with methane oxidizing bacteria in an aerobic fixed biofilm reactor. *Wat. Res.* 25, 873-881.
- [47] Roberts P. V., Hopkins G. D., Mackay D. M. and Semprini L. **(1990)**. A field evaluation of in situ biodegradation of chlorinated ethenes: part 1, methodology and field site characterization. *Ground Water*, 28, 591-604.

- [48] Goltz M. N., Bouwer E. J. and Huang J. **(2001)**. Transport issues and bioremediation modeling for the in situ aerobic co-metabolism of chlorinated solvents. *Biodegradation*, 12, 127-140.
- [49] Frascari D., Cappelletti M., Fedi S., Verboschi A., Ciavarelli R., Nocentini M. and Pinelli D. **(2012)**. Application of the growth substrate pulsed feeding technique to a process of chloroform aerobic cometabolism in a continuous-flow sand-filled reactor. *Process Biochemistry*, 47, 1656-1664.
- [50] Shah A. A., Hasan F. Hameed A. and Ahmed S. **(2008)**. Biological degradation of plastics: A comprehensive review. *Biotechnology Advances*, 26(3), 246–265.
- [51] Gautam R., Bassi A. S., Yanful E. K. **(2007)**. A review of biodegradation of synthetic plastic and foams. *Applied Biochemistry and Biotechnology*, 141(1), 85–108.
- [52] Sivan A. Szanto, M., Pavlov V. **(2006)**. Biofilm development of the polyethylene-degrading bacterium *Rhodococcus ruber*. *Applied Microbiology and Biotechnology*, 72(2), 346–352.
- [53] Otake Y., Kobayashi T., Ashbe H., Murakami N. and Ono K. **(1995)**. Biodegradation of low density polyethylene, polyvinylchloride and urea-formaldehyde resin buried under soil for over 32 years. *Journal of Applied Polymer Science*. 56, 1789–1796.
- [54] Albertsson A.C., Andersson S.O., Karlsson S., **(1987)**. The mechanism of biodegradation of polyethylene. *Polymer Degradation and Stability*. 18, 73-87.
- [55] Albertsson A.C., Erlandsson B., Hakkarainen M., Karlsson S. **(1998)**. Molecular weight changes and polymeric matrix changes correlated with the formation of degradation products in biodegraded polyethylene. *Journal of Polymers and the Environment*. 6, 187-195.

- [56] (Orr) I. G., Hadar Y., and Sivan A. (2004). Colonization, biofilm formation and biodegradation of polyethylene by a strain of *Rhodococcus ruber*. *Applied Microbiology and Biotechnology*, 65(1). 1584-8
- [57] Hadad D., Geresh S., and Sivan, A. (2005). Biodegradation of polyethylene by the thermophilic bacterium *Brevibacillus borstelensis*. *Journal of Applied Microbiology*, 98(5), 1093–1100.
- [58] Amin M.U., Scott G., Tillekeratne L.M.K. (1975). Mechanism of the photo initiation process in polyethylene. *European Polymer Journal*, 11, 85-126
- [59] Yousif, E., and Haddad, R. (2013). Photodegradation and photostabilization of polymers, especially polystyrene: review. *Springer Plus*, 2, 398–460.
- [60] Wang Y., Kim J.-H., Choo K.-H., Lee Y.-S. and Lee C.-H. (2000). Hydrophilic modification of polypropylene microfiltration membranes by ozone-induced graft polymerization. *Journal of Membrane Science*, 169(2), 269–276.
- [61] Patel D., Wu J., Chan P., Upreti S., Turcotte G., Ye T. (2012). Surface modification of low density polyethylene films by homogeneous catalytic ozonation. *Chemical Engineering Research and Design*, 90(11), 1800–1806.
- [62] Chiellini E., Corti A., D'Antone S., (2007). Oxo-biodegradable full carbon backbone polymers biodegradation behaviour of thermally oxidized polyethylene in an aqueous medium. *Polymer Degradation and Stability*. 92, 1378-1383.
- [63] Bonhomme S., Cuer A., Delort A.-M., Lemaire J., Sancelme M., Scott, G. (2003). Environmental biodegradation of polyethylene. *Polymer Degradation and Stability*, 81(3), 441–452.
- [64] Sudhakar M., Doble M., Murthy P. S., Venkatesan R. (2008). Marine microbe-mediated biodegradation of low- and high-density polyethylenes. *International Biodeterioration & Biodegradation*, 61(3), 203–213.

- [65] Jakubowicz I, Yarahmadi N, Petersen H. (2006). Evaluation of the rate of abiotic degradation of biodegradable polyethylene in various environments, *Polymer Degradation and Stability*, 91(7),1556-1562.
- [66] Robin J.J., (2004). The use of ozone in the synthesis of new polymers and the modification of polymers. *Advances in Polymer Science*, 167, 35–79.
- [67] www.biocleanproject.eu
- [66] Potts J. E. (1978). Aspects of degradation and stabilization of polymers, *Biodegradation*. In: Jelinek HHG (ed), New York: Elsevier. 617–658.
- [67] Davidson M., Mitchell S., Bradley, R. (2004). UV-ozone modification of plasma-polymerised acetonitrile films for enhanced cell attachment. *Colloids and Surfaces B: Biointerfaces*, 34(4), 213–219.
- [68] http://www.ozoneapplications.com/info/ozone_properties.htm, Oct, 2010)
- [69] Restrepo-Flórez J.-M., Bassi A., Thompson M. R. (2014). Microbial degradation and deterioration of polyethylene – A review. *International Biodeterioration & Biodegradation*, 88, 83–90.
- [70] Sunthar, P. (2010). *Polymer Rheology*. In *Rheology of Complex Fluids*. Springer. Retrieved from, 10, 171–191
- [71] Smith B.C., (1996). *Fundamentals of Fourier Transform Infrared spectroscopy*, CRC press, Boca Raton
- [72] Höhne, G. (2003). *Differential scanning calorimetry: an introduction for practitioners* (2nd rev. and enl. ed). Berlin ; New York: Springer.
- [73] Duval C., (1953). *Inorganic thermogravimetric analysis*. Elsevier publishing company, Amsterdam.

- [74] Miller J. D., Veeramasuneni S., Drelich J., Yalamanchili M. R., Yamauchi G. (1996). Effect of roughness as determined by atomic force microscopy on the wetting properties of PTFE thin films. *Polymer Engineering & Science*, 36(14), 1849–1855.